ANTIBACTERIAL HYDROGEL COATINGS DERIVED FROM NOVEL CHEMICALLY RESPONSIVE VESICLES

A Thesis

presented to

the Faculty of California Polytechnic State University,

San Luis Obispo

In Partial Fulfillment

of the Requirements for the Degree

Master of Science in Polymers and Coatings

by

Emily Mobley

August 2020

COMMITTEE MEMBERSHIP

TITLE:	Antibacterial Hydrogel Coatings Derived from Novel Chemically Responsive Vesicles
AUTHOR:	Emily Mobley
DATE SUBMITTED:	August 2020
COMMITTEE CHAIR:	Sandra Ward, Ph.D. Assistant Professor, Department of Chemistry and Biochemistry
COMMITTEE MEMBER:	Raymond Fernando, Ph. D. Professor, Department of Chemistry and Biochemistry
COMMITTEE MEMBER:	Trevor Harding, Ph. D. Department Chair & Professor, Department of Materials Engineering

ABSTRACT

Antibacterial Hydrogel Coatings Derived from Novel Chemically Responsive Vesicles

Emily Mobley

In order for a drug, or any material used for the purpose of eliciting a change in an organisms' physical or chemical state, to be effective it must reach the intended target intact and for a sustained rate over time. Drug delivery systems encapsulate a drug to protect it from degradation, prevent side reactions, increase solubility, improve accumulation rates at target sites, and release drugs at a controlled rate. Controlled and sustained release of drugs is achieved by degradation of the carrier triggered by breaking dynamic chemical bonds caused by changes in the chemical environment such as pH or redox conditions. Slow, first order kinetic release of drugs increase therapeutic efficacy while also reducing side effects and other cytotoxicity issues.

Up and coming drug delivery systems include hydrogels and nanocarriers such as vesicles. Hydrogel drug delivery systems are unique three-dimensional networks of crosslinked hydrophilic polymers that contain anywhere from 50-90 wt% of water. Drugs can be loaded via encapsulation during the gelation process or may be covalently bound to the polymer backbone before gelation. Amphiphilic molecules or polymers that self-assemble in aqueous solutions to form supramolecular nanostructures, such as vesicles, can encapsulate hydrophilic drugs in the aqueous interior or hydrophobic drugs in the lipophilic bilayer membrane.

This study seeks to embed vesicles into a hydrogel to create a hybrid drug delivery system which may be applied as a coating to medical devices to prevent bacterial adhesion

and growth, injected directly to a target site, or as an additive for wound dressings. This hybrid system mitigates burst release from the hydrogel, as well as stabilizes the vesicles to afford a longer shelf life. Vesicles are prepared from a novel supramolecular amphiphile composed of thio-alkyl modified β-cyclodextrin as a macrocyclic host, and an adamantyl-dithiopropionic acid modified poly(ethylene glycol) as a linear guest. This host-guest system forms inclusion complexes that self-assemble to bilayered vesicles, which may encapsulate a payload, in aqueous solutions. These vesicles serve as three-dimensional multivalent junctions to form a hydrogel, which may encapsulate a second payload, through a dynamic disulfide exchange crosslinking reaction. This novel drug delivery system will be capable of dual and selective release of two different encapsulated payloads. A pH sensitive acid labile bond embedded in the crosslinker will cleave under acidic conditions to release the payload enclosed in the hydrogel matrix, while a disulfide bond embedded in the supramolecular amphiphile of the free vesicle can be cleaved in the presence of naturally occurring antioxidant glutathione, GSH, to release the second payload.

It has been discovered that vesicles efficaciously form, can encapsulate a payload, and are stable for several weeks, up to a month. Vesicle stability is examined in the presence of both intracellular and extracellular concentrations of GSH, and it is found that vesicles are more stable in extracellular concentrations of GSH. Crosslinking of vesicles is attempted at several molecular weights of linear thiol terminated poly(ethylene glycol) crosslinker, concentrations ratios of crosslinker: vesicle, pHs, and temperatures. It can be concluded that the crosslinking density with the linear crosslinker is not high enough to

form a hydrogel. Future studies will include 4-arm crosslinkers which are predicted to increase the number of crosslinking points and hence the crosslinking density.

ACKNOWLEDGMENTS

I would first like to give the sincerest thanks to my devoted advisor, Sandra Ward, Ph.D. She has kindly supported me through multiple research projects ever since I joined her research group as an undergraduate student at Cal Poly back in 2017, and has always been there to offer advice, guidance, and professional insight as an established organic chemist. Working with her has helped shape me into the chemist and researcher I am today, and has set me up for future success in the field. I will be forever grateful to her for believing in me, pushing past all obstacles that have come our way, and overall helping make this project come to life.

Additionally, past students in the Ward research lab have had a hand in working on this project. Kate Frischkorn, Rachel Gariepy, Maya Rieder, and Natalie Byrd, thank you for your contributions!

I would also like to thank the incredible support staff in the Chemistry and Biochemistry Department. Andrea, Kevin, Celine, Tom, Shelly, Lisa, Paul, and Candace; you have all been there on the day to day to help troubleshoot equipment, get me the supplies and resources I need in lab, fill out paperwork, share a laugh, etc. and I could not have done this project without all of your support, especially during the uncertain times the pandemic has afforded.

Last, but certainly not least, I would like to thank Raymond Fernando, Ph.D., and Trevor Harding, PhD., for serving on my thesis committee and offering their own niche insights and advice on the project. A big acknowledgement goes to the Bill Moore Fellowship, and the Bill and Linda Frost fund for their financial support as well.

TABLE OF CONTENTS

Page

LIST OF TABLES

LIST OF FIGURES

LIST OF SCHEMES

1. INTRODUCTION

1.1 Antibacterial Coatings

Polymeric coatings are an essential class of materials commonly used for substrate protection and/or functionalization, as well as aesthetics and other specialty functions. Types of coatings can range from clear to opaque, solvent to water to powder based, thermoplastic or thermoset, ambient to radiation cured, organic to inorganic, etc., and cover an expansive base of applications such as architectural paints and lacquers.[1] The complex science behind creating a successful coating depends on the material's end use goal. However, within this diverse range of possible end products lies several commonalities as demonstrated in Figure 1.[1]

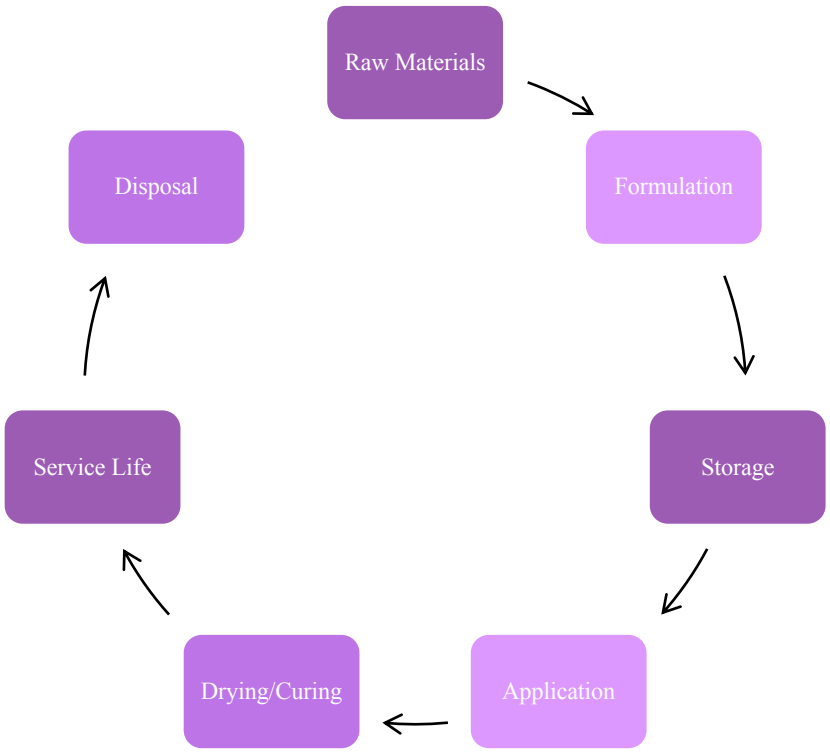

Figure 1: The process of coating formulation to application and disposal, all of which are recurring elements in all coatings' life cycles

There are numerous sub-classifications of coatings, among which is antibacterial coatings. Antibacterial coatings are becoming increasingly more significant across a wide range of industries, particularly within biotechnology and medicine.[2-7] Of the many challenges this industry faces when creating appropriate coating materials, biocompatibility and stability of biomaterials it of utmost importance for the material to attain long term use and effectiveness in order to protect the substrate and/or provide other functions.[2,5,6] Additionally, it is imperative that these materials also provide a certain level of antibacterial character in order to prevent the proliferation of bacterial infections amongst the fields of biotechnology and medicine. Bacterial related infections are currently the 6th leading cause of death in the world, with this rate being substantially higher in underdeveloped countries.[5] These infections are not only threatening from a health perspective but also from an economic perspective. Health wise, materials such as food processing equipment, medical devices, and implants are highly susceptible to bacterial infection and cause health deficits to the population; whereas economically, bacteria colonizing on industrial settings like pipelines, water treatment plants, ship hulls, etc. contribute to vast rates of decreased efficiency and increased operational costs for these essential industries.[6] The root cause of these issues can be traced back to bacterial adhesion on surfaces, which is why antibacterial coatings have become paramount in research efforts.

In terms of treating all types of bacteria-surface related infections, antibiotics have been widely used since the discovery of penicillin in 1928, and have proven to be highly effective in expelling infections caused by the growth of

pathogenic bacteria.[8] Public health efforts based on expanding antibacterial technology over time have significantly improved the quality of life across the globe by suppressing many previously problematic pathogenic bacteria related infections. Still, millions of people die annually as a result of these infections because of the rise of multi drug resistant microorganisms.[2] This is suspected to be a direct result of using antibiotics to kill bacteria, and, unfortunately, our ability to produce new antibiotics is currently vastly outpaced by these microorganisms' abilities to evolve and give rise to new resistant species.[2,5,9] Additionally, antibiotics are also subject to poor solubility, cytotoxicity, and environmental toxicity at high concentrations when used in isolation, all of which become especially problematic for biotechnology, medical, and environmental industries.[2,5,6,9] Current methods to mitigate these issues involve the development of efficient drug delivery systems that reduce the risk of bacterial resistance, as well as regulating concentrations of drug agents to avoid both cyto- and environmental toxicity.[2,5,6] Additionally, these methods also use a variety of different materials aside from traditional antibiotics, each of which has its own limitations and efficacy. Among these alternatives, include nanoparticles of metal ions, natural extracts such as chitosan and seaweed, antimicrobial peptides and enzymes, quaternary ammonium compounds, polymers, and superhydrophobic materials.[6] Ranking these different materials for coating strategies in terms of effectiveness is considered largely impossible because they are so dependent on specific clinical applications, which may vary in the need for short versus long term use, bactericidal activity, application site, etc.

Nonetheless, each of these surface coating strategies, regardless of material, is largely focused on surface modification to either prevent bacterial adherence, kill bacteria on contact with the surface, or release a drug agent to kill the bacteria as it approaches the surface, as demonstrated by Figure 2.[6.10,11]

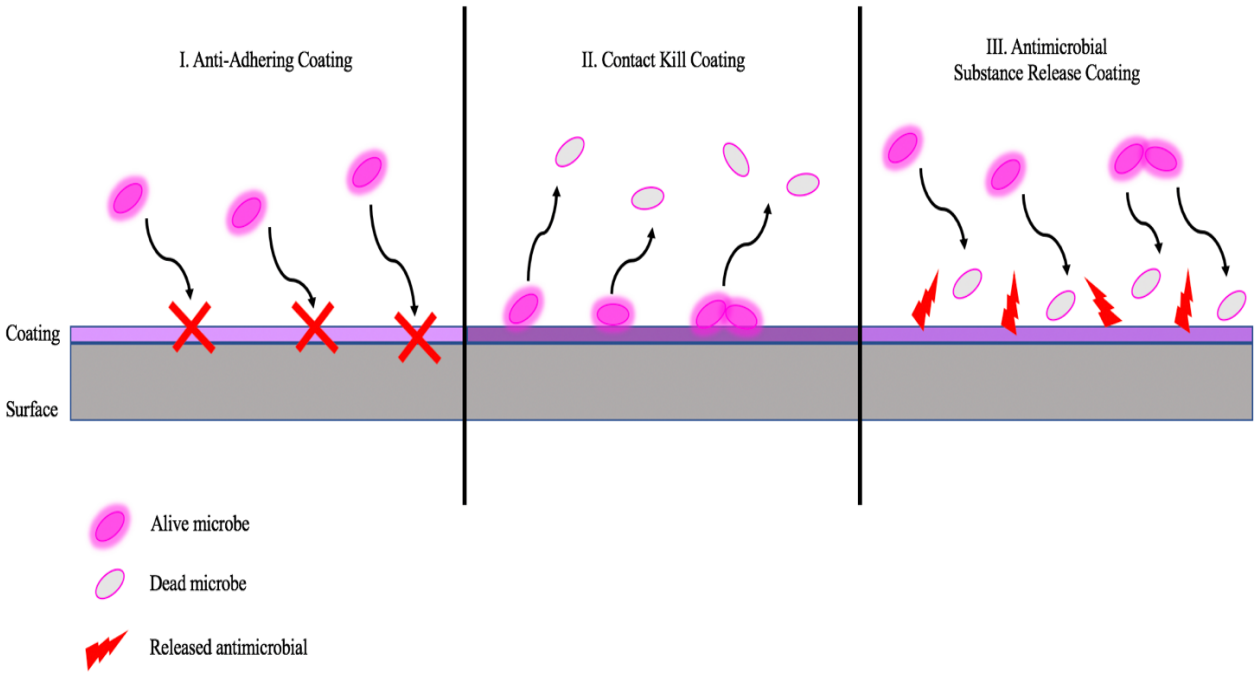

Figure 2: Three main types of antibacterial coatings being developed to prevent bacteria colonizing surfaces and subsequent infections; I. Anti-Adhering Coating- which prevents bacterial growth on surfaces, II. Contact Kill Coating- which kills bacteria that come in contact with surfaces, III. Antimicrobial Substance Release Coating- which kills bacteria that come into contact with surfaces by a stimuli responsive mechanism

Herein, in order to design effective antibacterial coatings within these categories, it becomes important to investigate the mechanisms behind bacterial adhesion to surfaces. Bacteria-surface interactions trigger certain changes in the expression of genes that influence cell morphology and behavior, including those necessary for surface mobility and attachment.[10] This ability of bacteria to adhere to surfaces is a

beneficial evolutionary trait that allows them to grow and proliferate while being protected from shear and mechanical damages.[10,12] While the phenotypes of this evolutionary advantage have been studied and are well known, the underlying mechanisms that bacteria use for sensing and responding to surfaces are not.

Current research has identified bacterial adherence to occur in two consecutive phases; one that occurs rapidly and is easily reversible, and another that occurs over several hours and is irreversible.[10-13] The first reversible "physical" phase is dependent on hydrodynamic and electrostatic interactions between the bacteria and the surface, wherein the adhesive force between them increases rapidly. The second irreversible "molecular" phase depends on non-covalent interactions between the hydrophobic region of the bacterial cell wall with the surface, and involves several proteins secreted to the surface by bacteria. While the exact molecular mechanisms of these phases are not well understood, we do know that they are heavily influenced by the laws of thermodynamics, wherein bacteria work to minimize surface energy. Bacterial cells preferentially attach to hydrophillic materials (which have high surface energy) when the surface energy of the bacterium is larger than that of the liquid surface in which they are suspended, but when the surface energy of the bacterium is lower than that of the liquid surface in which they are suspended bacterial cells preferentially attach to hydrophobic materials (which have low surface energy).[10] This is why bacteria are able to adhere to such a wide variety of surface types of varying hydrophilicity including glass, aluminium, stainless steel, teflon and other fluorinated materials, organic polymers, etc. Even with resistant surfaces, bacteria are able to trigger several mophological

changes, such as depositing layers of proteins, to make the surface more favorable for adhesion.[10-13] This creates a large challenge for antibacterial surfaces because it requires precise control over surface chemistry, strucutral properties, and the environment of a given surface.

To make matters worse, once bacteria are able to successfully adhere to a surface, they begin to synthesize a hydrated matrix of extracellular polymeric substances to form a biofilm, which, once formed, is exponentially more difficult to treat as it is highly robust and dynamic in nature.[10-13] Biofilm formation is a multistep process, as demonstrated in Figure 3, and depends on several factors including type of bacteria, type of surface, environmental conditions, and flow conditions.[11] Because biofilms are so ubiquitous in nature, it may not be possible to eliminate them from surfaces, especially because they act as a highly effective barrier from any external defenses. Specifically, biofilms act to reduce the net negative charge of bacterial cells to enhance the stability of the membrane, and also contain many dormant persister cells that are highly tolerant to any antibacterial treatment and constantly upregulate specific antibiotic resistant genes within these cells.[10] In the medical field, bacterial infection and resultant biofilm formation on medical devices or implants can begin pre- peri- or post-operatively, and may occur over the course of several years, as bacteria are known to be able to maintain a low metabolic rate for long periods of time.[12]

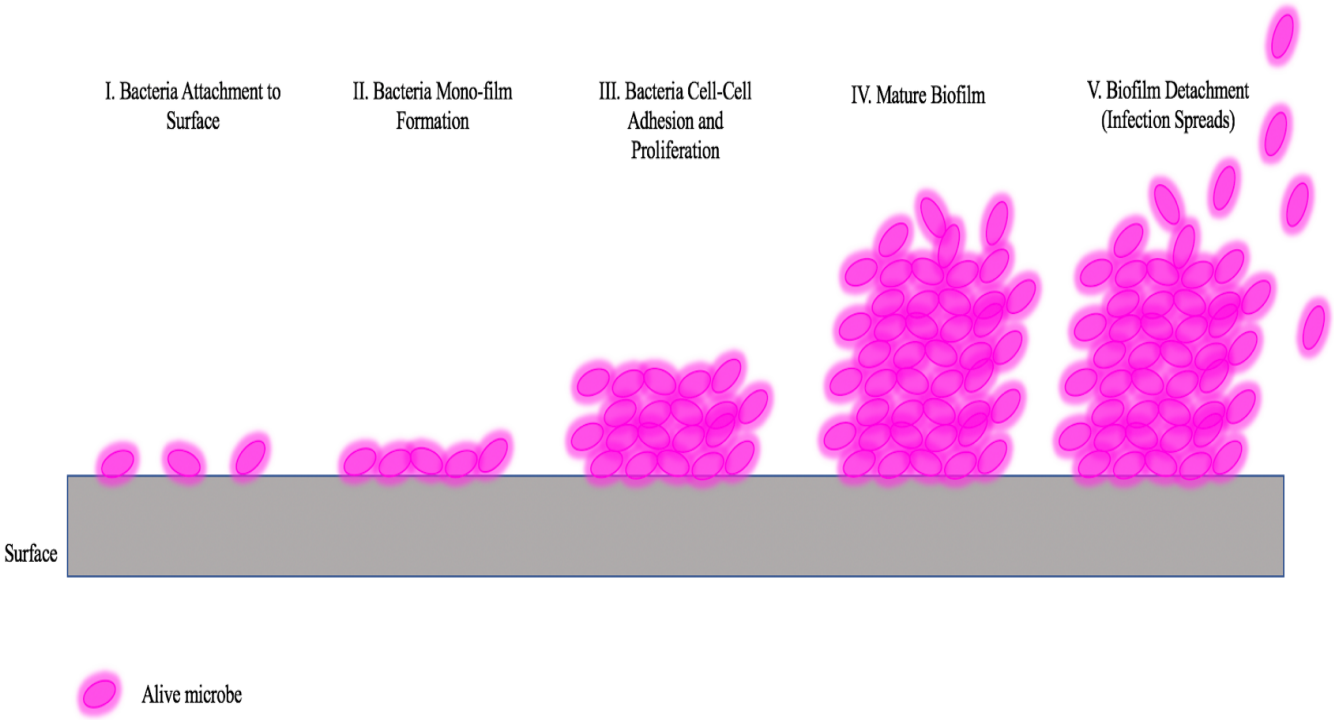

Figure 3: Generalized multistep process of biofilm formation; I. Bacteria Attachment to Surface, II. Bacteria Mono-film Formation, III. Bacteria Cell-Cell Adhesion and Proliferation, IV. Mature Biofilm, V. Biofilm Detachment

In this case, there is a direct competition between host eukaryotic cells and bacterial cells on the surface which depends on several factors- physiochemical properties of the surface, bacterial concentration and virulence, and eukaryotic cell properties.[12] In short, there is a molecular race occurring between eukaryotic and bacterial cells for integration upon indwelling surfaces of such devices and implants which invade surrounding epithelial and mucosal barriers. Common devices that are prone to these types of infections include all types of catheters, fracture fixation devices, dental implants, prosthetics, vascular grafts, pacemakers, mammary implants, mechanical heart valves, and even wound dressings.[13] Implanting devices innately impairs host defense mechanisms, so infections may rapidly become

chronic, wherein the only treatment available is to remove the associated device because destroying biofilms involves such high levels of antibacterial agents that it would cause cytotoxic effects to the host.[3,4,7,13] This is a financial drain for the medical and biotechnology industries, as devices and implants are not able to achieve their full service life before being replaced, as well as a health detriment to hosts as the infection may still persist after device removal.

Combatting these highly evolved genetic advantages of microorganisms is no small task and must focus on specific bacterial characteristics such as their mechanisms of adaptiveness to different environments. Optimizing thin film antibiotic coatings is now largely considered essential, as bulk material properties have more or less already been optimized.[5] The advantage of thin film coatings is that they are able to impart certain characteristics and functionalities to the surface without effecting those of the bulk material.[1] Relevant surface modifications with antibacterial coatings to prevent initial attachment of bacteria and subsequent biofilm formation may include altering the chemical composition of surfaces, mainly hydrophilicity and charge, as well as roughness and porosity, in order to achieve the desired bactericidal effect once applied to a given surface.[11-13] All the while, we must also take into consideration avoiding any inflammatory responses from the host immune system, specificity against cytotoxicity of eukaryotic cells, biocompatibility, solubility, long term stability and environmental sustainability of materials and processes to make them, antibiotic resistance, over/under dosing, etc.[2-13]

1.1.1 Hydrogel Coatings

One such promising material for highly effective thin film antibacterial coatings involves the use of polymeric hydrogels. Hydrogels are three-dimensional polymer networks often crosslinked by either physical interactions, ie. chain entanglements or polymer microstructure interactions, or chemical interactions such as intermolecular forces (IMFs) or covalent bonds and are distinct due to their unique physical properties.[2] One important division to make when discussing hydrogels is the difference between hydrogels and gels. Although chemically similar, the two materials are physically different in that hydrogels will swell and absorb solvent while maintaining their 3D crosslinking network, whereas a gel is already swollen to equilibrium when formed and will dissolve in solvent.[14] The former is more advantageous for coating applications because they are able to continually establish equilibrium in response to varying solvent environments.

Furthermore, as evident by Figure 4, there are truly an innumerable amount of polymer combinations that may form a hydrogel matrix. Therefore, it is important to consider specific end use goals when selecting raw materials for any hydrogel coating system; in this case, the design of a biocompatible and efficient therapeutic delivery system for broad spectrum antibacterial activity.[3] Common applications for antibacterial hydrogels include a wide range of equipment used in the medical and biotechnology industries that suffer from bacterial infections, as previously mentioned in section 1.1.

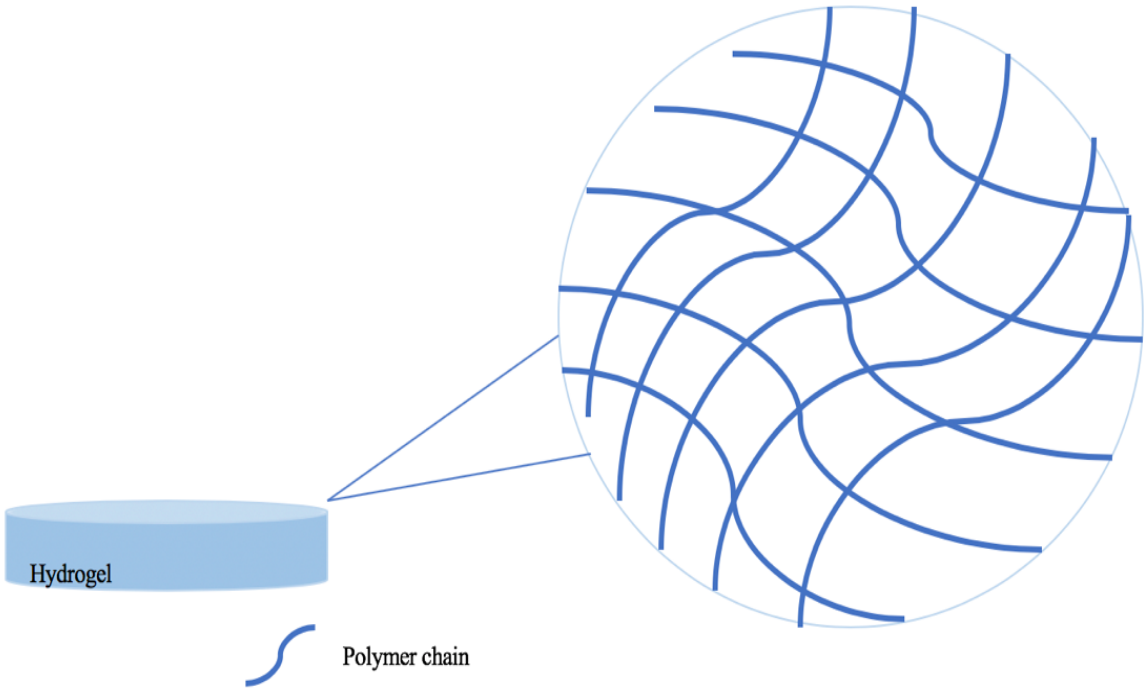

Figure 4: Generalized polymer chain entanglements/crosslinking that form thin film hydrogels, wherein mesh size may vary from micro- to nanoscale

Hydrogels inherently have varying degrees of porosity that allow them to absorb water and/or other solvents at hundreds to thousands of times their own volume, which lends itself to high swelling capacity, oxygen permeability, biocompatibility, and structural diversity.[2,6] These traits, among many others, make hydrogels highly dynamic and easily customizable materials, and has subsequently caused them to be the focus of many research efforts in the field of developing antibacterial coatings.

In the case of antibacterial coatings in the biotechnology and medical industries, hydrophilicity is of the upmost important physical properties, as it allows

the material to be biocompatible under physiological conditions.[2,3,4] Among previously mentioned physical properties, hydrogels also have a high surface area to volume ratio, which make them controllable structures than can easily mimic natural tissue, which is highly advantageous in terms of compatibility with biological systems.[6] When coupling this property with an adjustable mesh size, hydrogels have also been demonstrated to have the ability to attain controlled and prolonged release of encapsulated materials, local administration, and stimuli responsivity to certain environmental triggers such as pH, temperature, oxidation-reduction reactions, and concentrations of particular chemical species.[15] This stimuli responsiveness can be customized towards a particular end use goal by making various chemical and/or physical modifications to the underlying crosslinked polymer network structure. In some cases, this responsiveness has allowed hydrogel coatings to act as self-healing materials, which is highly desirable in terms of attaining long service life and reducing raw materials costs in the long run.[16]

1.1.1.1 Hydrogel Coatings Preparation Methods

There are a variety of preparation methods for making hydrogel coatings with antibacterial activity; each with its own strengths and limitations. These methods can be classified into a few categories which are as follows.[2]

- Inorganic nanoparticle containing hydrogels
- Antibacterial agent containing hydrogels
- Hydrogels with inherent antibacterial capabilities

Inorganic nanoparticle containing hydrogels contain nanoparticles such as metal ions and metal oxides (ex: silver, copper, gold, silica, zinc oxide, titanium

dioxide, and nickel oxide), which have inherent antibacterial character and have been demonstrated to maintain broad range antibacterial activity over long periods of time while also reducing the likelihood of antibacterial resistant species arising. Loading nanoparticles into a hydrogel matrix is a convenient and controllable platform for biofunctionalized metal nanoparticles. Although the mechanism of action isn't entirely understood, it is hypothesized that these metal nanoparticles act via attaching to the cell wall by electrostatic interactions and subsequently disrupting the cell membrane of bacterial cells and/or generating reactive oxygen species to induce oxidative stress by free radical formation.[6] However, this mechanism for antibacterial activity lacks specificity for bacterial cells, and consequently has several negative impacts on eukaryotic genes as well. This is because reactive oxygen species cause DNA damage, mitosis inhibition, and chromosomal instability in healthy eukaryotic cells as well. Hence, when making hydrogel materials embedded with metal nanoparticles, it is important to optimize biocompatibility by achieving high spatial dispersion of nanoparticles within the hydrogel matrix to avoid agglomeration, as well as overall compatibility in an organic environment, so as to avoid any damage to healthy cells. This is because agglomeration of nanoparticles in a hydrogel matrix can rapidly lead to overdosing and subsequent cytotoxicity to the host eukaryotic cells. Similarly, incompatibility in an organic environment renders the nanoparticles unstable, and subsequently unsuitable for use in biological systems due to the toxicity risk of metal nanoparticles leaching out of the hydrogel. Optimization of biocompatibility is most commonly achieved with a layer by layer coating method, wherein the layers of the hydrogel coating alternate

between containing metal nanoparticles and void of metal nanoparticles.[4] This outer layer is typically void of metal nanoparticles and acts as a shield to prevent cytotoxicity while maintaining long term antibacterial activity. However, this method does not entirely prevent damage to eukaryotic cells and therefore is not suitable for some applications.

The second type of antibacterial hydrogels are antibacterial agent containing hydrogels, wherein an "antibacterial agent" can be defined as any material that is embedded within the hydrogel matrix for the purpose of eliciting antibacterial activity. As previously mentioned in section 1.1 and visualized in Figure 5, commonly used antibacterial agents are antibiotics, antibacterial peptides, antibacterial enzymes, quaternary ammonium compounds, chitosan, and other natural extracts.[6] With any of these materials, and especially with conventional antibiotics, it is imperative to minimize the development of antibiotic resistant bacterial species arising by minimizing the concentration of antibacterial agents to that which is able to be effectively bactericidal without inducing extra systemic toxicity.

The advantage of using conventional antibiotics is that their properties are well known and easy to apply in a medical setting, but the drawback is that of the antibacterial agents, antibiotics are the most likely to lead to the development of antibiotic resistant species. With antibacterial peptides, this is not an issue, as they are already present in our immune systems which is advantageous because they are biocompatible and do not show any direct toxicity effects on mammalian cells.[6]

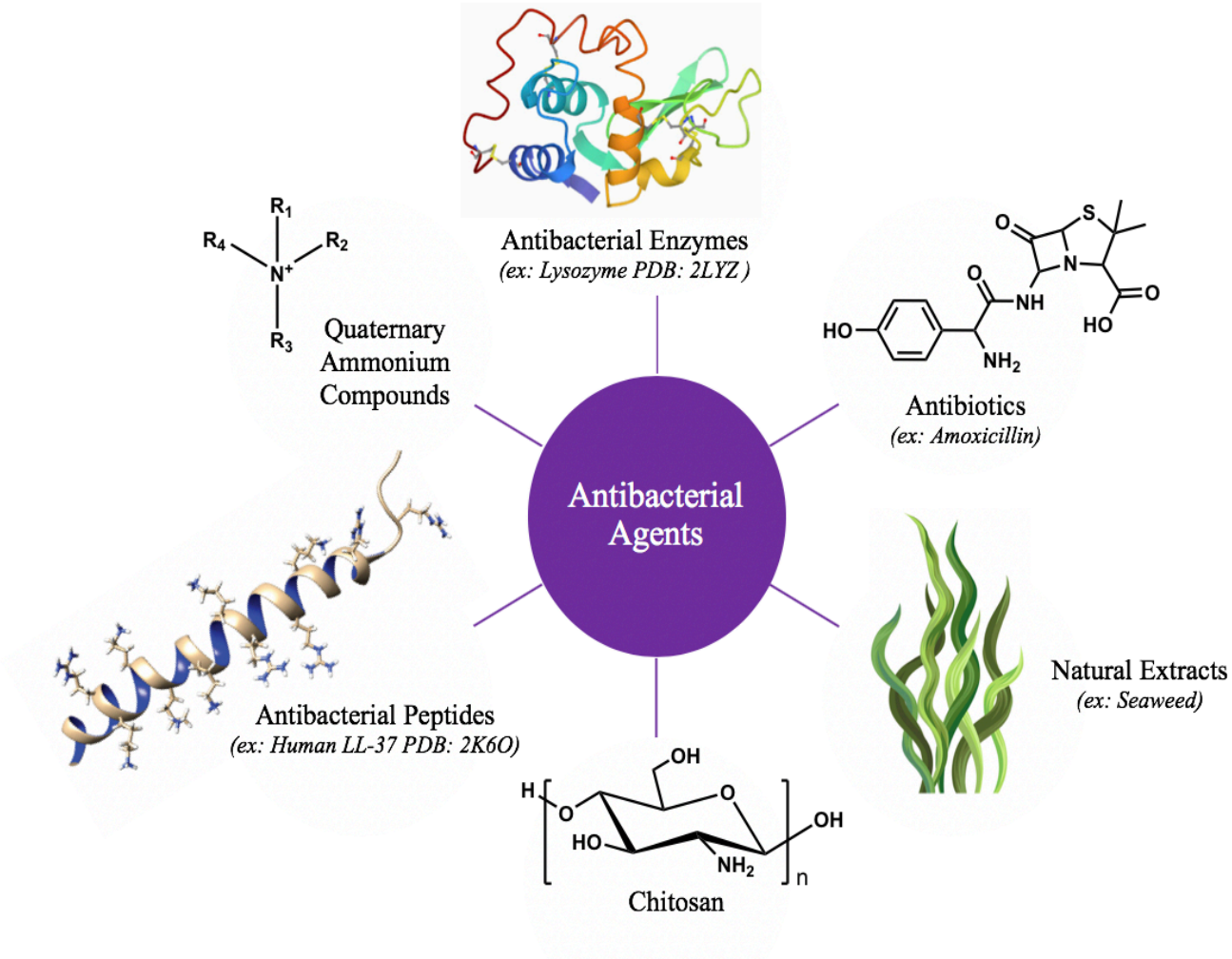

Figure 5: Different types of antibacterial agents with examples of structures

These compounds act by using their positive charges to associate with the negatively charged bacterial cell wall and disrupt it. However, they are very similar to common eukaryotic signaling peptides, so when tethered within a hydrogel matrix they have been known to cause undesirable hemolytic effects. Antibacterial enzymes are similar to antibacterial peptides in that they are largely considered non-toxic while remaining bioactive.[6] They are also commonly used in detergents, industrial processes, and the food industry and are known to achieve a bactericidal effect in hydrogel coatings by preventing bacterial adhesion due to enzymatic degradation of

molecules essential for bacterial functionality, or causing direct hydrolysis of the bacterial cell wall. The disadvantage here is that retaining enzymatic activity is very difficult, as the enzymes tend to become instable when immobilized within a hydrogel matrix or on the surface of a coating. With quaternary ammonium compounds, their bactericidal effectiveness is dependent on whether the positive charge density of the coating is able to exceed the threshold of 10^{15} N^{+} cm^{-2} with an alkyl chain length between 4-18.[6] This is because the mechanism of action involves the quaternary N atom's attraction to the phospholipid head groups of the cell wall, while the hydrophobic tail becomes incorporated into the cell membrane to lyses the bacterial cell. These compounds are also, however, limited because they require a certain degree of freedom to achieve antibacterial activity. In this case, this conformational freedom can be attained by tethering the compound to the surface of the hydrogel coating, rather than embedding it which may cause biological instability. Finally, chitosan is a naturally derived material with inherent bactericidal effects, and is also highly biocompatible and easily modifiable.[6] The limitation with this material is mainly that the bactericidal activity is low compared to other antibacterial agents as it is highly dependent on the degree of chitosan acetylation. However, a benefit of using slow release mechanisms from any type of antibacterial agent containing hydrogels is that it tends to increase the effectiveness of the antibacterial agent itself owing to targeted, minimal usage of materials.[6]

Both inorganic nanoparticle and antibacterial agent containing hydrogels generally involve the encapsulation and release of materials from the hydrogel matrix, which involves various chemical, physical, and biological triggering

mechanisms. A general structure of a hydrogel coating containing an encapsulated payload is demonstrated in Figure 6. Additionally, it should be noted that encapsulated payloads also vary in loading methods and efficiency, which is highly dependent on the compatibility of the specific polymers being used to form the initial hydrogel matrix with the encapsulated materials. Most commonly, antibacterial hydrogels are made using polyethylene glycol (PEG) or polysaccharides, because of their biocompatibility features, and then coupled with any of the bactericidal materials previously mentioned.

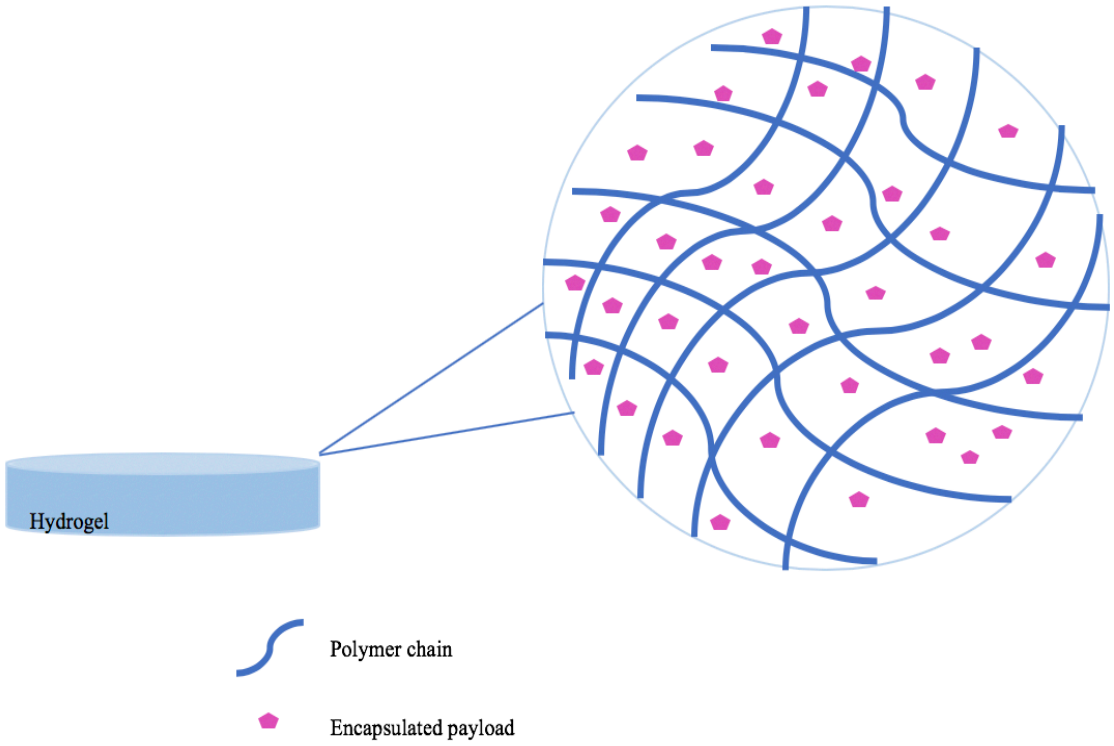

Figure 6: Generalized polymer chain entanglements/crosslinking that form thin film hydrogels that are capable of loading various payloads within the hydrogel matrix

The last type of antibacterial hydrogels are those that have inherent antibacterial activity without the incorporation of other materials. Mainly, these

hydrogels are those that are comprised of polymers with either non-stimulated or potential antibacterial activity. Here, non-stimulated polymers have inherent structural components that lend themselves to bactericidal activity, whereas potential polymers can be converted to become antibacterial under certain conditions. One such common example of this is polymer brush surfaces attached to the exterior of a hydrogel. In this case, polymers are used to prevent bacterial adhesion by occupying majority of the external surface area to create an osmotically driven steric barrier for bacterial adhesion.[6] This acts as a passive mechanism to avoid bacterial infections on surfaces. In order for this method to be effective in terms of antiadhesive properties, the polymers need to be well hydrated, which is why covalent or physisorption to the surface of thin film hydrogel coatings is so advantageous- because hydrogels are able to hold more water without collapsing than a polymer brush surface on its own.[6] Polymer brushes on the surfaces of hydrogels are, however, limited because they are unable to prevent biofilm formation over long periods of time. For this reason, polymer brushes are often combined with the loading antibacterial agents to the hydrogel matrix to increase bactericidal efficacy over longer periods of time. Similarly, superhydrophobic surfaces possess extraordinary antiadhesive properties, and hence are inherently highly effective at preventing bacterial adhesion to surfaces.[6] However, this method is seldom successful in coupling with antibacterial hydrogels because it is inherently incompatible with the hydrophilic nature of hydrogels, as well as any biological system.

Overall, the most widely utilized methods for preparing hydrogel coatings for use in the biotechnology and medical industries involve combining multiple types of antibacterial hydrogel coatings; mainly the incorporation of various antibacterial agents, which may or may not be coupled with polymer brush surfaces or layer by layer coating deposition including inorganic nanoparticles. However, current research efforts are still needed to expand upon this technology as many more developments are needed to achieve an effective and biocompatible antibacterial hydrogel coating material for widespread application. The main limitations currently are scaling up production of materials, long term stability, and efficient use of biocompatible antibacterial agents that have broad spectrum bactericidal activity without giving rise to new antibiotic resistant species or other undesirable systemic side effects.

1.1.1.2 Hydrogel Coatings Characterization Methods

Antibacterial hydrogel coatings can be characterized for a variety of physical properties such as swelling capacity, storage/loss modulus, elasticity, mesh size, hydrophilicity, stability, responsivity, encapsulation ability, level of bactericidal activity, biocompatibility, and cytotoxicity level. Some common instruments used to determine these properties include scanning electron microscopy, transmission electron microscopy, atomic force microscopy, x-ray photoelectron spectroscopy, dynamic mechanical analysis, and rheology.[7,14]

Because hydrogels can be so structurally diverse depending on the raw materials and preparation methods used, it is important to characterize the structure

of the hydrogel including porosity, mesh size, and relative uniformity of the hydrogel matrix.

Surface characterization is often accomplished with a combination of microscopy methods. X-ray photoelectron microscopy is a method based on the photoelectric effect, which describes what happens when electromagnetic radiation hits a material, and measures both the chemical composition and state of the material as well as any electronic properties. This is useful for determining the surface composition and uniformity of hydrogel coatings.[7] To obtain optical images of the surface, scanning electron microscopy or transmission electron microscopy are often used.[14] Scanning electron microscopy acts by emitting beams of electrons to the surface which interact with atoms to produce a topographical image of the surface composition with a resolution down to a few nanometers. Transmission electron microscopy has a much higher resolution due to a smaller de Broglie wavelength of electrons transmitted through the sample. These images are useful for determining the mesh size and porosity of the hydrogel matrix. Atomic force microscopy is another common method that has excellent resolution, up to fractions of a nanometer, which is more than a thousand times better than optical diffraction limit. This method can produce topographical maps of the surface by scanning with a small cantilever tip coupled with laser focusing. Results from these measurements are useful for characterizing porosity and roughness of the hydrogel coating surface.

Other physical properties are often measured using rheology and dynamic mechanical analysis. Because hydrogel coatings can absorb various solvents up to about a thousand times their own volume, it is important to characterize the flow

behavior of these materials. Rheology relates the relative stress and strain responses of the material to various shearing to uncover any viscoelastic properties. This measurement is useful because it yields information about for the storage and loss modulus of the material, which tells how it will respond to various environmental forces once applied to a surface. Similarly, dynamic mechanical analysis measurements also characterize viscoelastic properties of the material. This method applies a sinusoidal stress to the material and measures the corresponding strain that occurs at various temperatures to yield a complex modulus. These measurements are especially important when considering antibacterial hydrogels that are to be applied in biological systems, as they will be constantly exposed to shear stress from surrounding plasma and/or tissue, and must be able to remain stable in response.[5]

1.2 Drug Delivery Systems

When considering antibacterial hydrogel coatings as a functional material for biological applications, it is important to recognize that this material innately functions as a drug delivery system. Herein, a "drug" can be defined as any material either encapsulated or inherent to the bulk material for the purpose of eliciting a change in an organisms' physical or chemical state once released to the target environment.[17] Examining the current progress and methods used in upcoming drug delivery systems helps us to understand how a hydrogel coating can be customized for a variety of biological applications to achieve a therapeutic effect.

One of the issues paramount to improving the therapeutic efficacy of drugs is that the process of making new drugs is both time consuming and financially draining. This is because each new drug molecule made must go through rigorous

testing to get approved by the Food and Drug Administration (FDA) for commercial use including discovery in vitro, clinical trials in vivo, further development and optimization, and regulatory restrictions.[17] Herein, the gap from "in vitro" to "in vivo" studies is substantial. In vitro studies are typically used as a proof of concept phase, but majority of drug candidates that make it past in vitro studies will subsequently fail in vivo studies because there is an exponential increase is systemic complexity when going from physiological mimetic conditions to a true physiological system. Overall, the process of getting a new drug candidate approved typically takes an average of a decade and can end up costing over $120 million dollars.[17] Because of this largely impractical protocol for approving newly developed drugs, majority of current research efforts have been focused instead on creating better drug delivery systems to administer already approved drugs that may have issues with absorption and general biocompatibility, site specific activity, and/or systemic toxicity issues, etc. on their own.[17,18] Perhaps the biggest issue with drug delivery is the poor solubility of many pharmaceuticals. In fact, more than 40% of all currently approved drugs are nearly insoluble in water, which causes the drugs to have very poor biocompatibility and distribution since in order for a drug is to be properly absorbed, it must be in solution at the target site.[19] These features subsequently make hydrophobic drugs very problematic to deliver effectively because biological systems exist in an aqueous environment, which makes it difficult for the insoluble drug to diffuse into cell membranes, so higher concentrations of drug are needed to achieve any effect.[18] However, this often leads to unwanted side effects and/or toxicity issues.[18] Hence, some of the goals of new

drug delivery technology is to mitigate the aforementioned barriers and deliver drugs at a slow and controlled rate over time, with target specific release at the appropriate dosage, without eliciting an immunogenic response, systemic toxicity, or other harmful side effects.[17,18,20]

With any drug delivery system, there are two primary pathways in which drugs may be delivered to the target site- passively, or actively.[18] In passive drug delivery, the carrier or drug itself will circulate freely until it reaches the desired target site, which may be influenced by a variety of external factors such as pH or temperature, and then release the drug based on affinity, binding, or stimuli responsivity to the target site. In active drug delivery, specific chemical moieties are incorporated onto the drug or drug carrier, such as peptides or antibodies, which will target a specific site for expression and subsequent drug release. Each of these delivery pathways is dependent on a slew of physiochemical and environmental factors, which are quite different depending on the drug administration method. Many drug administration methods are demonstrated by Figure 7, wherein each method has its own pros and cons. Generally, oral administration is preferred whenever possible because it has the highest levels of patient cooperativity and is easy to follow. Transdermal, topical, and injection methods are also generally preferable because they are relatively simple to administer and bypass the first pass effect, wherein the concentration of a drug taken orally is greatly reduced by first pass metabolism before it reaches systemic circulation.[19,2121] This allows lower concentrations of drugs to be administered, which is advantageous because less

drug is needed to achieve the same effect. However, it is impractical to rank these drug administration methods, as they are each used for specific purposes.

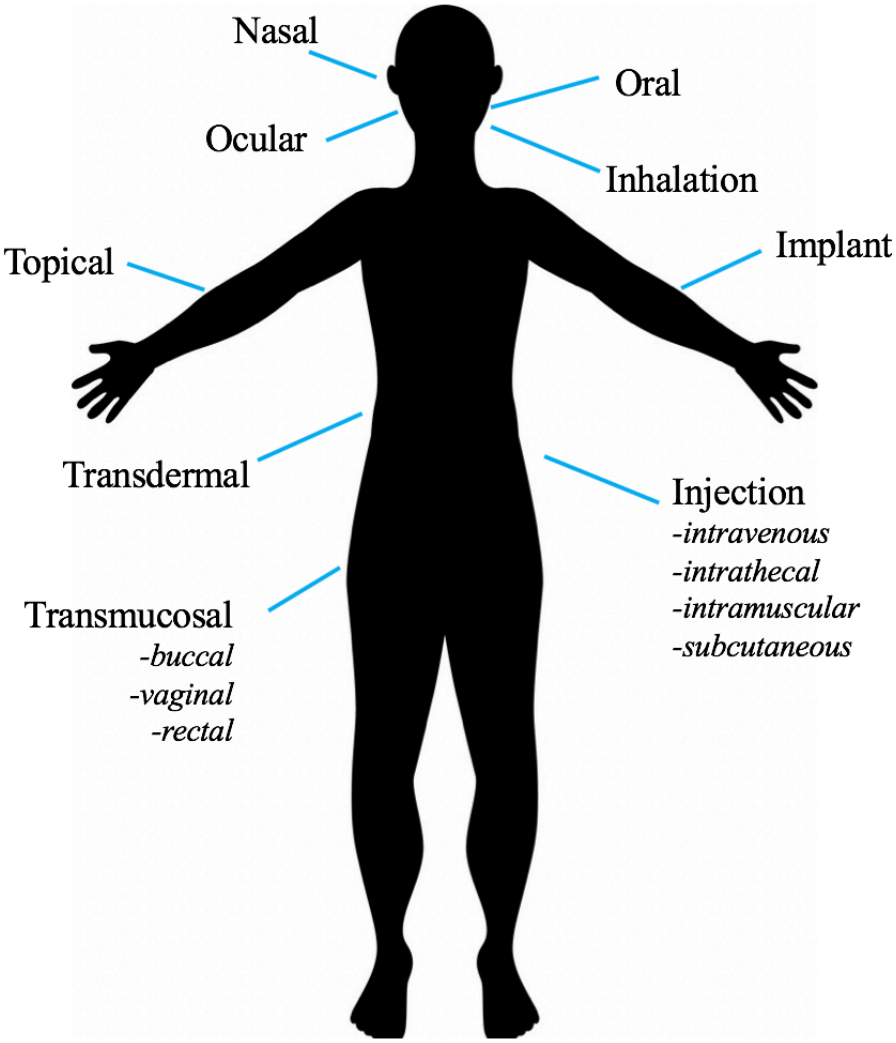

Figure 7: Routes of drug administration for all types of pharmaceuticals

Regardless of administration method, for drugs to be delivered and achieve the desired therapeutic effect, they must have adequate bioavailability. This means that the drug must have a substantial fraction of the initial dose that reaches systemic circulation and eventually its target site. Bioavailability is influenced by aqueous solubility levels, drug permeability to the target site, dissolution rate, first

pass metabolism, pre-systemic metabolism, and susceptibility to efflux mechanisms that remove solutes from cells.[19] Additionally, it is important to maximize the therapeutic index of drugs. This parameter compares the amount of drug that elicits a therapeutic effect to that which causes toxicity.[22] Therefore, the higher the therapeutic index, the safer the drug. Although increasing bioavailability and therapeutic indices of drugs are the main overarching goals of new drug delivery technology, there are a variety of different systems emerging which attempt to mitigate a range of issues related to drug delivery.

1.2.1 Types of Drug Delivery Systems

One aspect that majority of new drug delivery systems have in common is that they implement some sort of external carrier that serves to both protect the drug from the surrounding environment, and efficaciously deliver it to its target site.[20,22] Previous research in the field has established that macromolecular carriers and/or conjugates for drug molecules are highly effective tools for delivering drugs in a safe and controlled manner to their target sites in vivo. The continuing evolution of these carrier systems offers several desirable benefits to improve drug delivery such as the simplification of drug administration schemes, reducing toxicity levels of drugs in circulation, and overall improving therapeutic indices and disease outcomes.[20] There are several requirements that must be met in order for a carrier to be successful.[20] First and foremost, the carrier must be able to encapsulate a sufficient amount of hydrophobic and/or hydrophilic drug and remain in circulation in a physiological medium with tunable leakage. Additionally, the carrier must be able to target, accumulate, and distribute the drug at the desired site, as well as

increase bioavailability and biocompatibility of the drug. The carrier may accomplish this by solubilizing the drug, minimizing drug interactions with non-target cells, such as endocytosis or absorption, and minimizing elimination or degradation of the drug before it reaches its desired target site. Finally, the carrier must not illicit any immunogenic responses from the host immune system, be safe at all stages of drug delivery (ie. before, during, and after drug release), and must have a cost-effective synthetic pathway with ease of scale up.

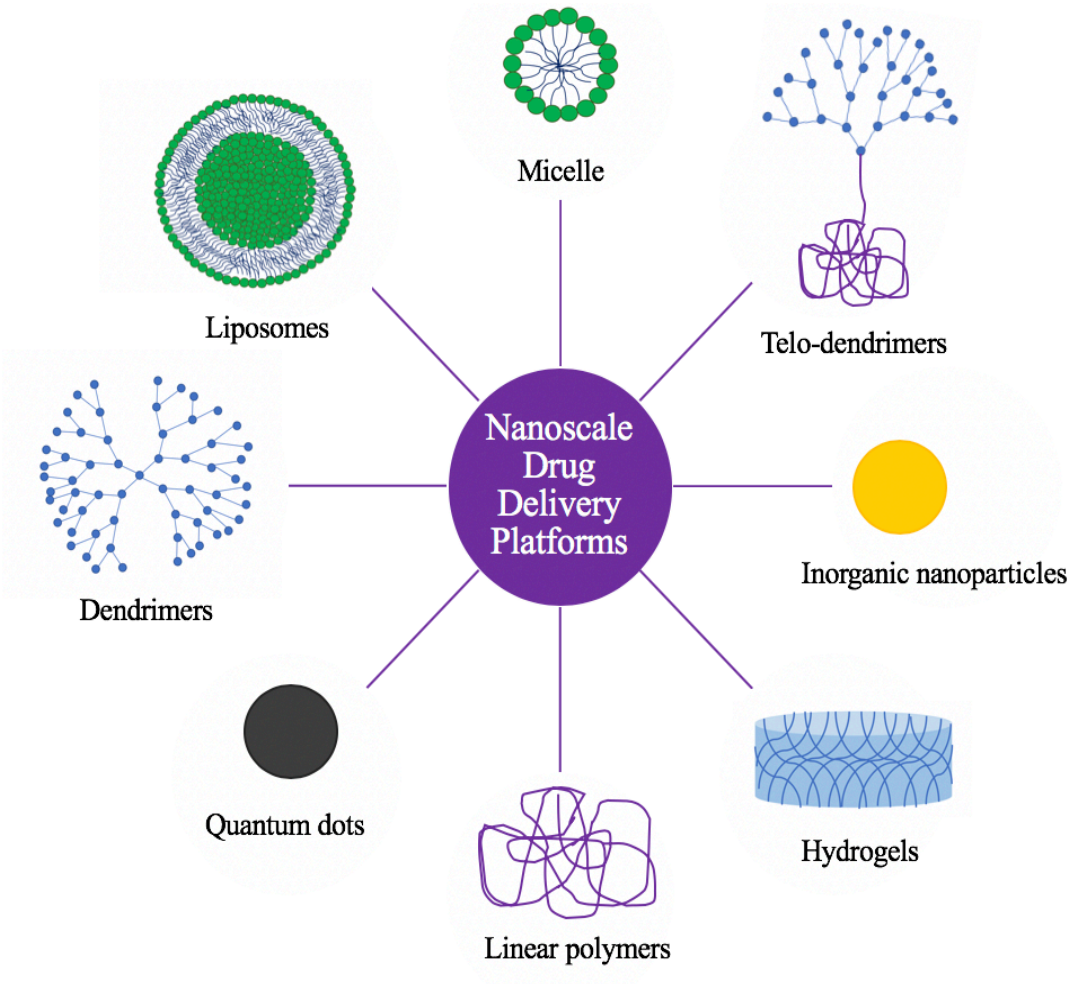

Figure 8: The most significant nanoscale drug carriers explored in current research; micelles, telo-dendrimers, inorganic nanoparticles, hydrogels, linear polymers, quantum dots, dendrimers, and liposomes

Specific carrier targeting mechanisms will be reviewed in a later section (ie.1.2.2), and here we will take a closer look at the different types of carriers currently in development, as demonstrated in Figure 8. Particularly, we will be looking at nanoscale drug carriers, as they have been shown to have significantly better uptake by cells than larger particles.

As the archetype of nanoscale drug delivery platforms, liposomes were the first to be approved for clinical use in 1995 (Doxil ®, delivers doxorubicin for the treatment of various cancers) and have since gained in popularity and technological developments.[23] Liposomes are formed by the self-assembly of amphiphiles, and consist of a bilayer membrane that is similar to that of biological cells, which makes liposomes suitable for mimicking fundamental cellular functions such as motility and shape changes in response to the extracellular environment.[20,23] This biological mimic behavior allows liposomes to go largely undetected by the host immune system as a foreign body, which is highly advantageous for a drug carrier as it prevents immunogenic responses. However, most liposomes in development are phospholipid based and tend to have poor stability and rapid clearance due to strong interactions with circulating proteins in blood plasma.[20] For this reason, it is common to use poly(ethylene glycol) (PEG) and its derivatives, as either part of the liposome itself or grafted to the exterior of the membrane in some way, to further impart stealth properties on the liposomal carriers.[24] This is because PEG is soluble in both aqueous and organic media, is non-ionic, and is subsequently known to function as an inert polymer to improve circulation time and biocompatibility of liposomal drug carriers.[20,23,24]

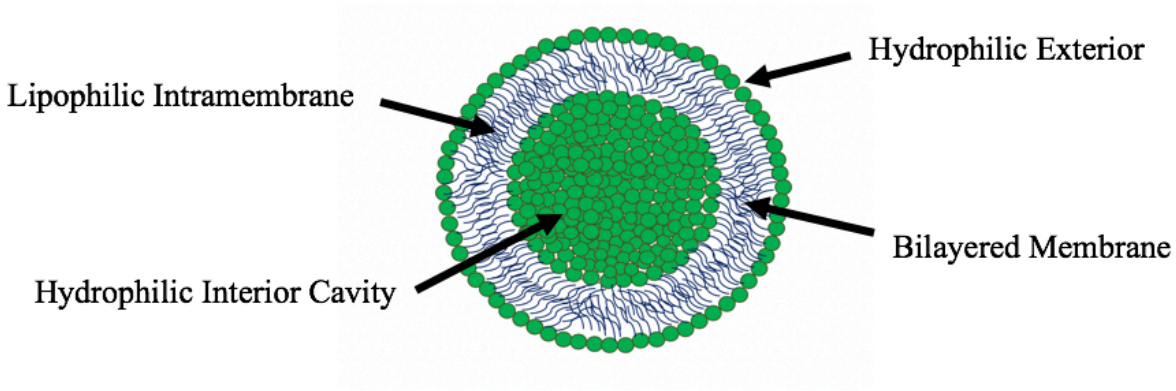

Figure 9: A closer look at general the structure of liposomes

Taking a closer look at the general structure of liposomes in Figure 9, we see multiple sites for drug encapsulation (ie. within the lipophilic intramembrane, or within the hydrophilic interior cavity). This is highly advantageous because it allows liposomes to encapsulate both hydrophobic and hydrophilic drug molecules, which also makes for better cell penetration for hydrophilic drugs and improved solubility for hydrophobic drugs.[20] Another feature of these types of carriers is that the physiochemical properties are easily customizable for a variety of target sites and improving biodistribution, circulation times, loading capacity, etc.[20,23] Being such, there are several different classifications of liposomes. Liposomes may be classified according to lamellarity (ie. uni, bi, or multi), size (ie. small <100nm, intermediate 100-250nm, large >250nm, or giant >1μm), surface charge (ie. anionic, nonionic, or cationic), etc.[20] Typically, the type of preparation method will have a large impact on these factors. For example, using the common thin film hydration method on its own usually results in oligolamellar and polydisperse liposomes, whereas coupling this method with extrusion as a purification method will exclude larger aggregates and results in a more monodisperse, unilamellar

liposome solution. Generally, monodisperse and unilamaller are preferred because they tend to behave more uniformly and predictably, which is useful for creating statistical models to predict how they will interact with eukaryotic cells.[20] Furthermore, there have been several sub-classifications of liposomes for improving various features such as transferosomes for improving elasticity, ethosomes for improving skin cell penetration, pharmacosomes for improving the delivery of poorly soluble drugs, niosomes, virosomes, nebulized, stimuli responsive, and specific cell targeted liposomes.[21,23] However, majority of these modifications have largely been unsuccessful thus far due to a variety of factors ranging from instability to difficulties with industrial production and storage, apart from stimuli responsive and specific cell targeted liposomes, which will be further discussed in section 1.2.2.

Another type of drug nanocarrier like liposomes are micelles. These are also formed from the self-assembly of amphiphiles and hence also have both hydrophobic and hydrophilic moieties capable of encapsulating both hydrophobic and hydrophilic drugs.[25] They are much smaller than liposomes, on the order of approximately 1-10nm, which makes for improved cell penetration. However, these carriers aren't as successful as liposomes because they are much less stable in physiological media and hence tend to suffer from early drug release and degradation.[20]

Still, there are other polymeric nanocarriers such as dendrimers, telo-dendrimers, linear polymers, and hydrogels. Linear polymers are the most simplistic model, and yet possess innumerable possibilities for chemical and

physical modifications. These materials can be either natural or synthetic, and typically function by forming either a drug-polymer conjugate colloid suspension or the aforementioned nanostructures (ie. liposomes or micelles).[20] Dendrimers, on the other hand, are highly branched polymers made from either convergent or divergent reaction schemes that generate several generations of branching. These materials are globular in shape, well defined, monodisperse, and multivalent structures with large surface area functionality capable of encapsulating a variety of drug molecules at a high loading capacity for controlled delivery and enhanced cell permeation which results in overall better distribution physiologically.[20,21] Telo-dendrimers combine a linear polymer chain with a dendritic segment to enhance the self-assembly and mobility properties of the linear polymer chain, with the uniformity and multivalence of dendrimers.[20] In theory, this system should function ideally for controlled encapsulation and release of drug molecules, but these materials are still in the very early stages of development so there are not many successful examples to speak of yet.[24] Conversely, polymeric hydrogels have been widely explored for applications as nanocarriers in drug delivery technology. As previously mentioned in section 1.1.1, hydrogels have numerous advantageous and easily tunable physical, chemical, and mechanical properties which make them ideal for interacting with biological systems. In fact, hydrogels are the closest mimic to biological tissues of any of the current nanoscale drug delivery platforms. This is because of their high water content and soft rubbery texture, which makes for very low interfacial tension with surrounding tissues and subsequently a low tendency to absorb proteins from blood and other bodily fluids.[14,26,27] Possibly the

most unique feature of hydrogels that make them ideal for drug delivery is that they have been demonstrated to have self-regulating capabilities. Herein, the hydrogel matrix has a seemingly elastic memory which allows it to respond to changing metabolic states in the body by swelling, altering network structure, permeability, and/or mechanical strength, and then alter their release profile accordingly before returning to their original state.[14] Hydrogels are also ideal for implantable localized drug delivery, which maximizes therapeutic efficacy and minimizes side effects when compared to systemic approaches.[27] However, like other nanocarriers, hydrogels have a few drawbacks which are limiting their clinical viability such as a limited ability to load hydrophobic drugs, and burst release of drug molecules.[26,27]

Alternative to polymeric nanocarriers, there are also quantum dots and inorganic nanoparticles. These systems deliver drugs by coupling drug-ligand conjugates to the surface, and accumulate successively at the target site by an external magnetic field, but it is important that they are combined with another delivery system, as they suffer from chronic uncontrolled release and clearance on their own.[21]

1.2.2 Stimuli Responsive Delivery Mechanisms

Considering the issues with current nanocarriers as drug delivery systems, mainly burst release of drug molecules at sites other than the target site, rapid physiological clearance, and general instability, it becomes clear that these nanocarriers could benefit from stimuli responsive delivery mechanisms. Smart materials, as they are often termed, are of increasing interest for a variety of industries, including biotechnology and medicine, because they are able to receive,

transmit, or process a stimulus and respond by producing a useful effect.[14,26,28,29] There have been many research efforts made to try to understand stimuli responsive mechanisms in biological systems so that we may create effective mimics of our own. Polymer based systems (ie. liposomes, micelles, linear polymers, dendrimers, telo-dendrimers, and hydrogels) are exceptional materials for this purpose as they are able to be made at large scales with a wide range of functionalities and post-synthetic modifications, and can be processed into a variety of different forms.[24,28]

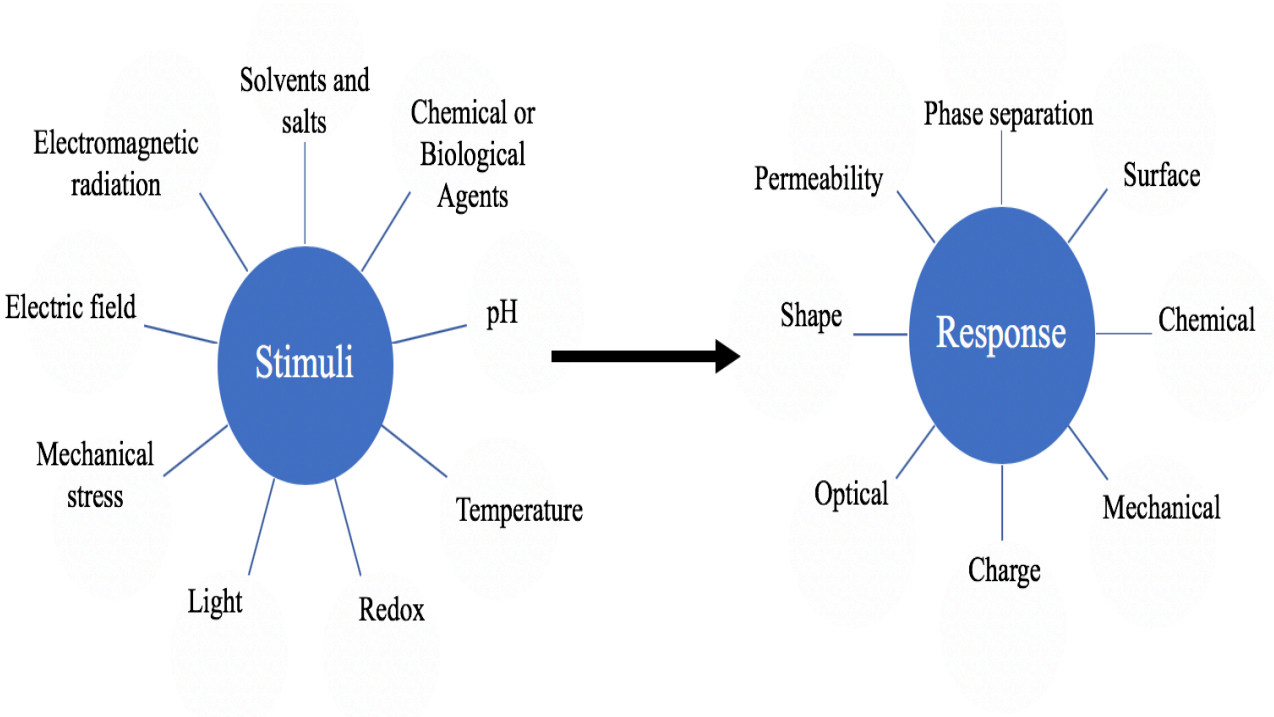

Figure 10: Various potential stimuli and responses for nanocarrier drug delivery systems

Several potential stimulus and responses are demonstrated by Figure 10, but not all of these are viable for physiological applications because once the nanocarrier enters the body, it is limited in the amount of stimuli present. Those that are of the most interest for these systems are pH and temperature, because physiological systems consist of many different organs, organelles and other

compartments that vary in both pH and temperature.[28,.29] Specific organ and cell targeting has been a dream of pharmaceutical companies ever since the industry began, because when a drug is targeted to a specific site either by affinity, charge, etc. it eliminates potentially harmful side effects and toxicity to the system as a whole. Coupling this targeting with stimuli responsive controlled release mechanisms furthers this beneficial effect and makes for even more specific drug delivery pathways.

For example, cancer tissue and chronic wounds are known to have a lower pH, which makes pH sensitive linkages a target that can be used to elicit a response (ie. release of the drug molecule) from a nanocarrier. Incorporating acid sensitive moieties, such as acid labile bonds, on any of the previously mentioned polymeric materials is useful for triggering controlled release of a drug from nanocarriers at an acidic target site as the change in pH will elicit a conformational and/or chemical change in the nanocarrier which causes it to release the active drug.[29] As another example, glutathione, a natural antioxidant found in higher concentrations intracellularly than extracellularly, is also a suitable trigger which elicits a dynamic covalent reaction between its thiol group and any disulfide modified polymer on a nanocarrier to produce a dynamic covalent reaction which could cause the nanocarrier drug release at a sustained and controlled rate.[29] Overall, these are just a few examples, as there are a wide variety of potential stimuli that can be installed onto nanocarriers, and there has been an abundance of research into this area that has shown various methods to be successful in improving circulation times, stability, and controlled and targeted delivery mechanisms for drug molecules.[26-29]

Furthermore, researchers have also been able to combine different types of nanocarriers together with stimuli responsive moieties installed, which highlights how truly innumerable the possibilities are for customizing the properties of nanocarriers for drug delivery.[28]

1.3 Supramolecular Chemistry

Another key factor amongst biological systems- supramolecular chemistry, although somewhat recently a discrete field of interest for biologists, chemists, and physicists, has been a fundamental aspect of life since its origin. This is because supramolecular chemistry is the ubiquitous factor that controls many biological functions such as signal transduction, membrane transport, enzymatic reactions, binding antibodies to macrophages, cell-cell recognition, protein folding, etc.[30-34]. Contrary to covalent bond formation to form molecules, supramolecular chemistry takes advantage of non-covalent interactions to form molecules. Although non-covalent interactions are individually weak compared to covalent bonds, taken collectively they are quite powerful.[31] These non-covalent interactions include a variety of intermolecular forces such as hydrogen bonding, dipole-dipole, van der waals, electrostatic attraction, π-π stacking, metal coordination, charge transfer, etc.[31,35-38] Nature provides us with one of the most prolific examples of supramolecular chemistry in action- the deoxyribonucleic acid (DNA) double helix structure. These polymeric strands are held together primarily through π-π stacking and hydrogen bonding and are able to store, receive, and process vast amounts of information all while being both responsive and adaptive to the external environment.[31,32] Structures, such as DNA, that are held together through non-

covalent interactions are commonly called supramolecules. Supramolecules are complex structures made up of many smaller building blocks held together very precisely by non-covalent interactions.[31] Studying biological building blocks such as nucleic acids for DNA, proteins for protein folding, and lipids for cell membranes that each create sophisticated hierarchical structures that are held together by non-covalent interactions helps researchers understand how they can mimic this molecular recognition behavior synthetically. The first synthetic supramolecules on record were crown ethers, for which the Nobel Prize in Chemistry was awarded in 1987 to Lehn, Pederson, and Cram for their design and development of cryptans, crown ethers, and cavitands, respectively.[30,31] These complex structures have many interactive properties and are easily customizable for a variety of applications such as sensors, luminescence, gels, biological and cell imaging probes, liquid crystals, etc.[31] The possibilities are truly endless with these dynamic materials, which makes them very attractive for research and development across many fields of study.

Over the years since their synthetic journey began, supramolecules have evolved to even more complex and larger architectures such as macromolecules, multimetallic helicates, rotaxanes, coordination polymers, etc.[31] Continuously evolving and inspired by several biological systems and processes, supramolecular chemistry primarily relies on the programmed self-organization of its building blocks. This self-organization has been termed self-assembly, wherein the building blocks spontaneously yet controllably organize themselves into complex and sophisticated architectures, driven by non-covalent interactions.[32] This type of non-

covalent synthesis is superior to traditional covalent synthesis in that it is simplified, the bonds form spontaneously without any harsh conditions or chemical reagents, are reversible under thermodynamic equilibrium, conditions, and do not produce any undesired side products.[30,35] The bottom up assembly style allows for highly specific control over properties of the resultant complex structure because it begins with the simplest building blocks and as they bind together increase in complexity which results in highly homogenous chemical assemblies with less defects and better short- and long-range ordering.[30] For example, stereo-control (ie. controlling which stereoisomers are formed by a reaction) over covalent synthesis is difficult but possible, whereas with non-covalent synthesis it is exponentially more difficult in theory because bonds of the individual building blocks are kinetically labile and are continuously breaking and reforming. However, in practice, stereo-control with self-assembly is not an issue because of the amplification of chirality, wherein the achiral building blocks seem to follow the chiral building blocks in their self-assembly pattern regardless of the relevant concentrations.[30] Overall, self-assembly of supramolecules requires precise control at the molecular level, which then influences the macroscopic level and bulk material properties.

1.3.1 Amphiphiles as Building Blocks for Self-Assembly

Perhaps the most powerful self-assembly building blocks are amphiphiles, which are also called surfactants (ie. surface active agents) interchangeably. Amphiphiles are characteristic in that they contain both a hydrophobic and a hydrophilic moiety, which may be linked together covalently or non-covalently.[25,34-38] When they are linked non-covalently the amphiphile is then

referred to as a supra-amphiphile. Regardless of how bonds are formed, there are a variety of different types of amphiphiles which are classified based on structural components. Topologies can range from any combination of hydrophilic "head" groups and hydrophobic "tail" groups. For example, one hydrophilic head with one hydrophobic tail, two tails one head, etc. Two unique topologies are termed bolaform, in which two hydrophilic groups are covalently linked to a single hydrophobic chain, and gemini, in which two different amphiphiles are linked at their charged head groups.[35]

One property that makes these molecules particularly unique and powerful tools for self-assembly and supramolecular chemistry is that when they are suspended in water, the hydrophilic moiety prefers the aqueous phase, while the hydrophobic moiety prefers an organic phase. Depending on the particular amphiphile topology, self-assembly behaviors and subsequent physical properties will differ because a different structure means different interactions in solution which leads to different aggregations. Typically, amphiphiles will first form a monolayer at air-water interfaces with the hydrophobic moiety facing the air and the hydrophilic moiety facing the aqueous solution, but when the concentration of amphiphile in solution is high enough they are driven to self-assemble based on the repelling and coordinating forces between the hydrophobic and hydrophilic moieties and the surrounding environment, as visualized in Figure 11.[36]

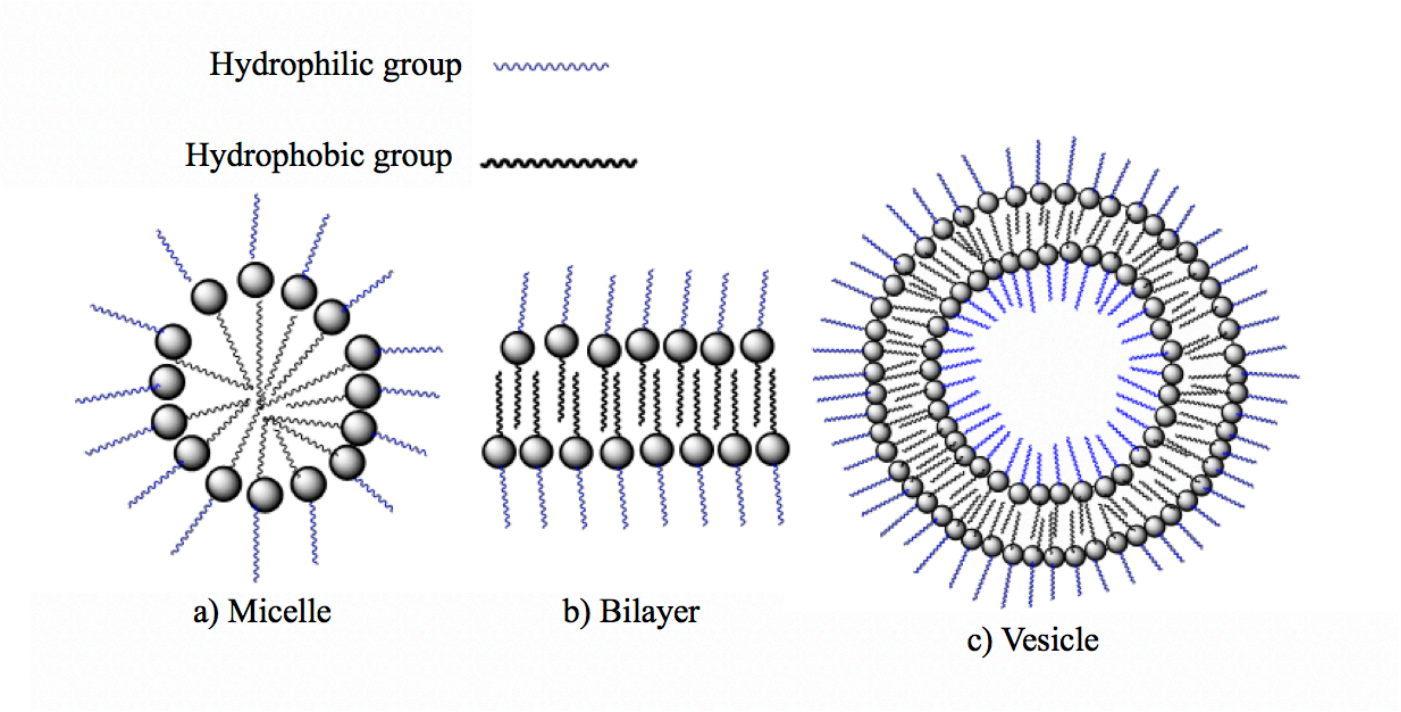

Figure 11: Amphiphiles containing a hydrophobic and hydrophilic moiety may self-assemble into a variety of nanostructures in aqueous media including but not limited to a) Micelle b) Bilayer c) Vesicle

This phenomenon is driven by the hydrophobic effect, and will occur at or above the critical micelle concentration (CMC) (ie. the concentration at which amphiphiles form micelles in solution). Further increasing the concentration of amphiphile beyond this point will result in nanostructures of increasing complexity, such as bilayers and vesicles.[39]

Herein, the hydrophobic effect can be defined as the tendency for hydrophobic segments of molecules to exclude themselves from the surrounding aqueous media by forming aggregates in solution where the hydrophobic segments of amphiphiles interact with each other, while the hydrophilic segments interact with the surrounding aqueous environment.[40] The hydrophobic effect is a thermodynamic phenomenon which is effected by both enthalpy and entropy, and

is overall thermodynamically favorable and hence spontaneous. Although it may seem counterintuitive at first, the hydrophobic effect is primarily driven by entropy, except at high temperatures where enthalpy is the driving force.[40-43] This is because of the relationship between the free energy required for hydrophobic hydration and the strength of the water mediated attraction between pairs of solute molecules. When a hydrophobic molecule is dissolved in water, the water molecules form highly ordered networks around the molecule. In order to minimize the surface area exposed to the aqueous environment, the hydrophobic molecules will aggregate with each other to exclude water and the water molecules involved in the highly order network are then free and the entropy of the water increases. When compared to the entropy loss of hydrophobic moieties creating ordered structures in solution, this gain in entropy from freeing water molecules is orders of magnitude higher.[42] Therefore, the entropy loss of forming ordered structures is significantly less in magnitude than the entropy gained from the freeing of water molecules.[40-43] Hence, forming ordered nanostructures in aqueous environments is actually highly entropically favorable. The hydrophobic effect is central to the self-assembly of amphiphiles into highly ordered nanostructures, in which the function of the whole is much greater than the sum of its parts.[31]

1.3.2 Inclusion Complexes with a Host-Guest Based System

One particularly unique class of supramolecular amphiphile non-covalent assembly is driven by host-guest interactions, which refer to the forming of a supramolecular amphiphile in which one component includes within the other, as demonstrated by Figure 12.

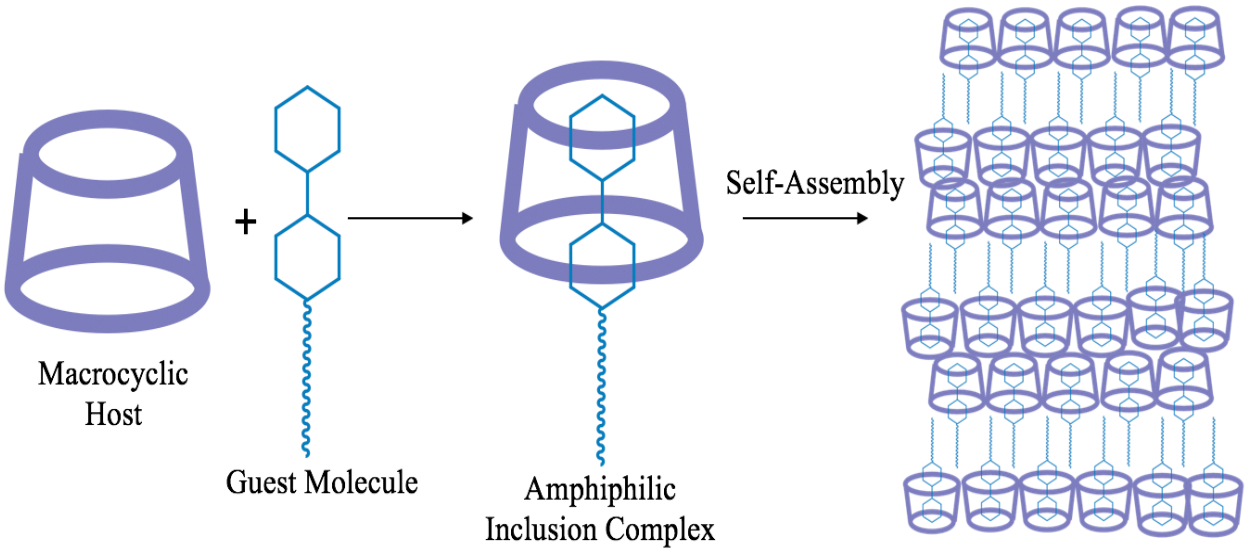

Figure 12: Inclusion complex formation reaction involves the combination of a compatible host and guest molecule, which will then self-assemble

Typically, a small organic molecule will include within the hydrophobic cavity of a macrocyclic host. The host and guest molecule can be functionalized with one component possessing hydrophobic tail and the other functionalized with hydrophilic moieties. Then, instead of covalently linking the hydrophilic and hydrophobic portions of the molecules, a supramolecular amphiphile will spontaneously self-assemble in aqueous solutions. This type of host- guest chemistry is driven by the hydrophobic effect and favorable non-covalent interactions. The combination of these forces can form a stable complex, which may be comparable in strength to a covalent bond.[35, 44] This non-covalent synthesis forms an inclusion complex which, dependent on the degree of amphiphilicity, will self-assemble into a variety of nanostructures in aqueous media. Herein, the inclusion complex is typically formed by the evaporation of solvent to create a thin film, and subsequent hydration of this film will give rise to self-assembly.[39] The

binding ability of the host-guest can be mainly attributed to the hydrophobic interactions and the complementary character of both size and shape in the molecular components.[31, 44] Therefore, host and guest combinations will form inclusion complexes based on binding affinity with stronger affinity resulting in more robust inclusion complexes and subsequent supramolecular architectures.

One of the principle advantages of supramolecular assemblies, and particularly inclusion complexes, is that they are dynamic, easily reversible, and can be customized to be responsive to various environmental and chemical stimuli such as pH, light, temperature, voltage, etc.[35, 44] Macrocyclic hosts are especially attractive for this purpose because they offer a cavity with multiple recognition sites for inclusion of a guest molecule, and can be tailored to promote self-assembly into well-defined architectures by the addition of hydrophilic and/or hydrophobic chains on either side of the macrocyclic framework.[34]

1.3.2.1 Cyclodextrin Hosts

There are several different classes of macrocyclic hosts such as calixarenes, crown ethers, and cucurbiturils, but by far the most widely used hosts are cyclodextrin (CD) derivatives.[44] These macrocyclic oligosaccharides are composed of several D-glucose rings with α-1,4 linkages, where αCD has six repeat units, βCD has seven, and γCD has eight.[34, 44, 45] The truncated toroidal cone shape of these molecules possess a hollow, tapered cavity of 0.79 nm in depth, where the top and bottom diameters are influenced by the number of repeat units, as demonstrated by Figure 13.[45]

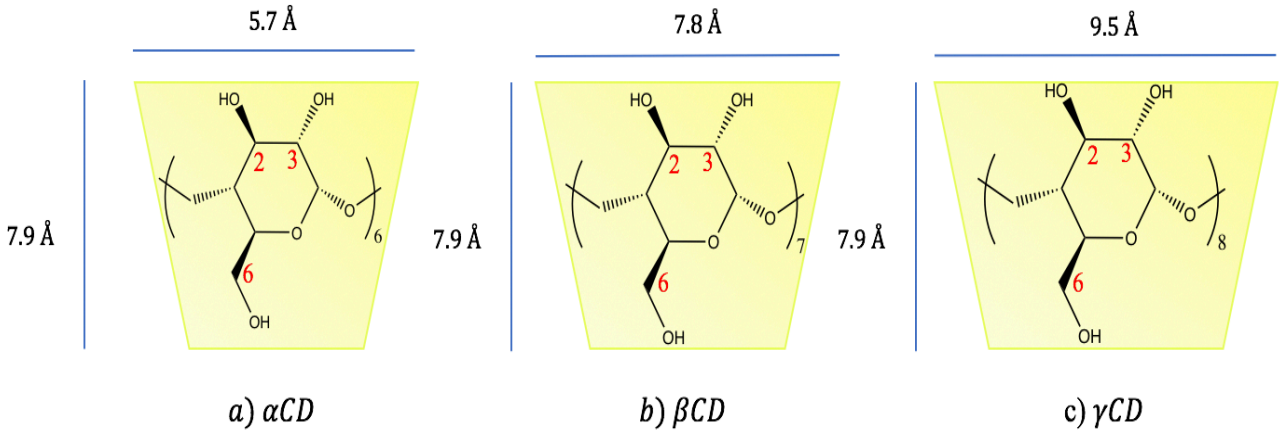

Figure 13: A closer look at the structure of cyclodextrin derivatives a) αCD, b) βCD, and c) γCD where the wider side of the cavity measures 0.57 nm, 0.78 nm, and 0.96 nm, respectively, while the depth remains constant at 0.79 nm. Positions 2, 3, and 6 are indicated accordingly

This hollow interior cavity is hydrophobic, which is ideal for encapsulating guest molecules of the appropriate size and shape for inclusion complexation, while the exterior is hydrophilic, which is ideal for interacting with surrounding aqueous media.[44-46] Here, the CD itself may be amphiphilic based on synthetic modifications, or the inclusion complex may create a supramolecular amphiphile through non-covalent interactions. Inclusion complexation with a variety of guest molecules and synthetic modifications of CDs have been extensively studied, and perhaps the most powerful inclusion capacity is βCD with adamantane, with a binding association constant of around $1x10^5$ M^{-1} in water.[34, 45, 46] It is important to note that inclusion complexation innately alters the amphiphilicity of the CD, which subsequently alters both the chemical and physical properties of self-assembled bulk materials to make for advantageous easily customizable systems.

Among the principle benefits of using CDs and their derivatives as hosts is their excellent biocompatibility, unique inclusion complex formation capabilities, powerful functionalization capacity with ease of synthetic modification, stability across a wide range of pH (ie. 1-11), and negligible toxicity.[34, 44-46] These properties also make CDs ideal candidates for developing new drug delivery systems and other materials used in biological systems. In fact, CDs have been utilized extensively in this field with more than 30 CD based pharmaceuticals currently marketed, and many others undergoing phase I/II trials.[45] These supramolecular assemblies have been shown to increase drug solubility and stability, enhance drug absorption and permeability, control drug release profiles, decreasing toxicity, etc.[45] Because of the abundant hydroxyl groups on native CDs, chemical modifications offer infinite opportunities to further improve upon the aforementioned physiochemical properties and molecular recognition abilities for specific applications. It is common to install charged groups, and either hydrophilic or hydrophobic moieties at position(s) 2, 3, and/or 6 to achieve specific functionality in bulk materials.[44-46] Overall these synthetic modifications give rise to three main classes of CDs- amphiphilic, hydrophobic, and polymer containing; all of which have multiple recognition sites for binding molecules of varying hydrophobicity/hydrophilicity. These hierarchical self-assemblies are especially interesting when combined with polymers, since their unique characteristics depend on individual molecules' properties and polymers are known to possess extremely useful properties on their own, which can be amplified using supramolecular assemblies with CDs.[45, 46]

1.3.3 Self-Assembly Features

Specifics of the numerous interactions that govern self-assembly of amphiphiles is, in part, related to the amphiphilicity of individual molecules. The degree of amphiphilicity is often termed the hydrophilic lipophilic balance, or HLB.[47] The HLB describes the size of the hydrophilic moiety relative to that of the hydrophobic. This determines the mean radii of curvature of the hydrophobic-hydrophilic interface, which relates to the individual components' radii of curvature and the relevant Gaussian curvature to give the overall packing parameter that determines what kind of nanostructures may form.[47] For example, in order for an amphiphile to form bilayers and/or bilayered vesicles in solution the product of the hydrophobic-hydrophilic interfacial area and the alkyl chain length must approach uniformity with the hydrophobic volume, which yields a packing parameter of 1.[47] However, the HLB of amphiphiles not only determines what type of inclusion complex and supramolecular architecture they may self-assemble into. Chemical linkages may provide a triggered degradation mechanism for nanostructures which is highly advantageous for developing stimuli responsive materials.[44]

Besides relevant size and shape of amphiphiles, thermodynamics also govern the self-assembly of amphiphiles, as previously discussed in part in section 1.3.1, as these molecules aim to lower interfacial energy.[40-43, 47, 48] Additionally, concentration of amphiphile in solution also plays a part.[49] Typically, the first aggregates observed in solution are monolayers, and then some form of micelles. Further increasing the concentration results in several more complex aggregates, depending on the HLB and shape of the amphiphile, as demonstrated by Figure 14.

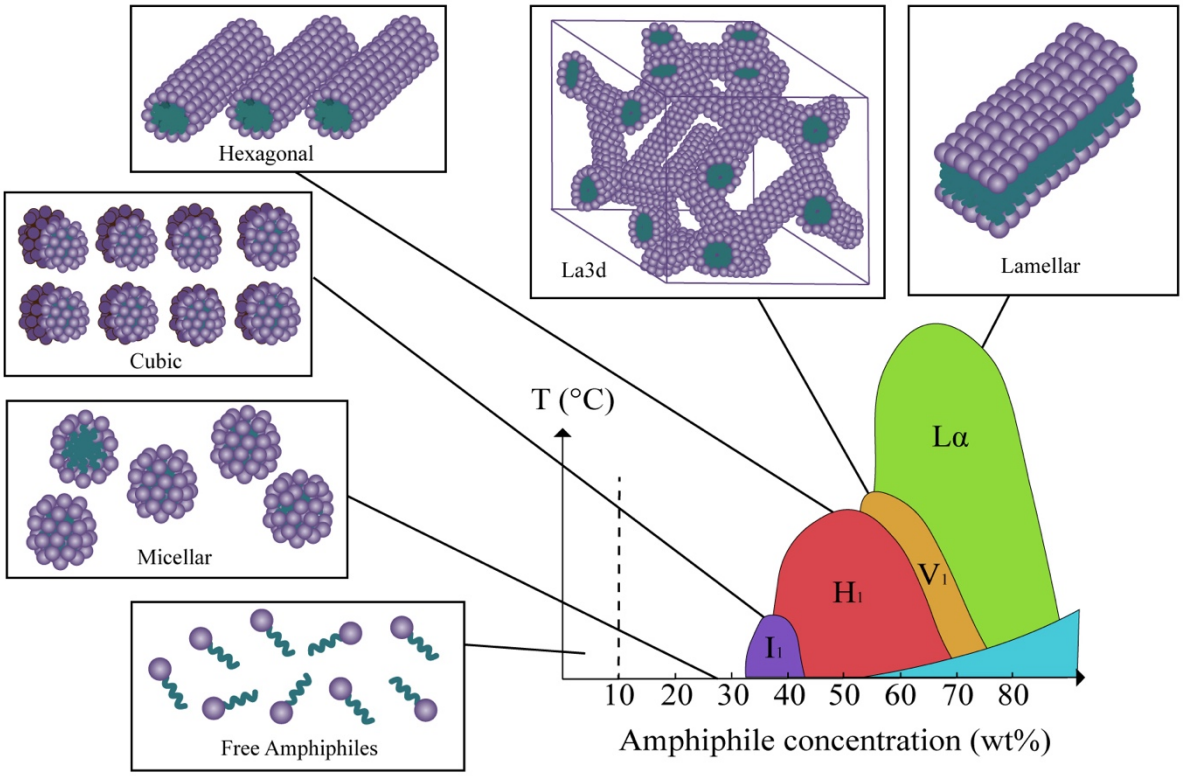

Figure 14: The relationship between amphiphile concentration and temperature gives rise to a variety of nanostructures of self-assembled supramolecular complexes

1.3.3.1 Vesicles

One particular aggregate omitted from Figure 13 is vesicles. Liposomes, previously discussed in section 1.2.1, although sometimes termed interchangeably with vesicles, are not the same on a molecular level. Liposomes refer to vesicles formed from lipids, most commonly, phospholipids. Therefore, all liposomes are a type of vesicle, specifically self-assembled from lipids, while vesicles may be self-assembled from all types of amphiphiles, including small molecules and polymers, that exhibit the appropriate size, shape, HLB, etc. for bilayer, and subsequent vesicle formation.[47] Here, the lamellar bilayer observed in Figure 13 will begin to fold upon itself to form a spherical vesicle in a two-step process.

Although liposomes and vesicles possess the same overall macromolecular shape that forms an aqueous interior separated from the bulk solution by one or more bilayers of self-assembled amphiphiles, their physical and chemical properties can vary quite dramatically.[48] For example, their abilities to encapsulate and release a payload in a sustained and controlled manner at a designated target site varies based on the particular amphiphilic building blocks' strength of non-covalent interactions and thickness of the bilayer membrane.[47, 48] Because the membrane is a semi-permeable barrier, both nanostructures tend to suffer from premature leakage of either hydrophobic or hydrophilic encapsulated payloads, and yet vesicles tend to suffer less so than liposomes owing to their superior adaptability to external environments.[47-49] This is because phospholipids tend to hydrolyze easily and so their liposomes have shorter shelf lives in aqueous solutions. In general, compared to liposomes, vesicles tend to show superior dynamic stability and mechanical strength/flexibility, and also offer much more numerous opportunities for customizing physiochemical properties such as stimuli responsiveness, and self-healing.[47, 49] Particularly, polymeric vesicles demonstrate excellent capability here, owing to the highly dynamic nature of polymers.

Characterization of vesicles typically includes measurements of hydrodynamic radius, encapsulation ability, stability, stimuli responsivity, controlled release kinetics, and overall shape and surface functionality.[49] Hydrodynamic radius is most easily measured using dynamic light scattering, wherein the size distribution of small aggregates suspended in solution are analyzed as an intensity/photon autocorrelation function to account for fluctuations in

aggregate distribution due to Brownian motion. Encapsulation ability can be probed with a variety of methods which may include using a fluorescent small molecule as a proof of concept, or a sample drug molecule for more specific measurements. Herein, in order to determine whether vesicles have encapsulated a payload, they must be destroyed, and the concentration of the encapsulated payload is then measured. Stability measurements can be taken over time using dynamic light scattering. The typical hydrodynamic radius of vesicles is on the order of 50-100 nm. When vesicles degrade, they may form micelles in solution which typically have hydrodynamic radii of around 1-10 nm, or they may form even larger aggregates with radii >>100 nm. Stimuli responsivity and controlled release kinetics are often measured collectively, as it is of interest to see the controlled release profile of vesicles in response to external stimuli. Herein, a particular stimulus is applied and released concentration of encapsulated payload can be measured using a variety of techniques including dialysis, UV spectroscopy, etc. Finally, to get a morphological view of vesicles, scanning electron microscopy, x-ray photoelectron spectroscopy, transmission electron spectroscopy, etc. are used, as previously discussed in section 1.1.1.3.

1.4 Dynamic Covalent Chemistry

While supramolecular chemistry has revolutionized the bottom-up assembly of functional nanoscale materials with the dynamic reversibility of self-assembly that takes advantage of non-covalent interactions, dynamic covalent chemistry exploits reversible covalent bonds to generate covalent systems that, like supramolecular systems, can adapt, respond, and degrade in a controlled manner.[50-

[51] Both allow the modification of molecular components; where supramolecular chemistry provides molecular recognition and directed self-assembly in a controlled manner beyond molecules, dynamic covalent chemistry imparts the dynamic feature on the molecular level by breaking and forming covalent bonds within molecules that may be used as building blocks in supramolecular self-assembly.[52] Dynamic covalent chemistry has primarily been explored in the fields of materials science, biotechnology, and medicine to create functional responsive sensors, adaptive membranes, drug delivery systems, etc.[50] By combining the multivalent error correction and proofreading mechanisms of supramolecular chemistry with the robustness and innate strength of covalent bond formation dynamic covalent chemistry has evolved to offer potential improvement upon the stimuli responsivity of supramolecular architectures.[51] The key feature of these reactions is the thermodynamically controlled product distribution at equilibrium. Herein, the exchange of molecular components at equilibrium achieves a thermodynamic minima of the system that is adaptable to the surrounding environment, in which the most stable product will predominate.[51, 52]

Typically, reversible covalent reactions are undesirable and tedious compared to supramolecular reactions because the breaking and forming of covalent bonds has much slower kinetics, may require the use of a catalyst, and result in low yields and low conversation rates.[50, 51] Therefore, dynamic covalent reactions with fast kinetics under mild conditions are preferable. In general, there are a few requirements for dynamic covalent reactions to be useful for modifying nanostructures on the molecular level.[52, 53] First, the lifetime of the reversible

covalent bond should be on the order of 1 ms < τ < 1 min, where τ is the bond lifetime, to ensure that they are stable enough to bond molecular structures and yet have dynamic behavior. The reaction must also be able to proceed under mild reaction conditions, and the exchange mechanism should have a functional trigger (ie. temperature, pH, light, removal of catalyst, redox), much like an on/off switch, to isolate particular products.

Although dynamic covalent chemistry is a relatively new and insufficiently explored field as of yet, there are numerous dynamic covalent reactions that have been discovered and more or less optimized.[50-52] Mostly, these reactions proceed as exchange types, where one component is exchanged for another and the products will have the same type of bonding as the reactants, or formation types, where new types of bonds are formed.[52] So far, dynamic covalent bonds that have been heavily researched include C-C, C-O, C-N, C-S, B-O, and S-S (ie. carbon to carbon, carbon to oxygen, carbon to nitrogen, carbon to sulfur, boron to oxygen, and sulfur to sulfur, respectively). These dynamic covalent bonds and their subsequent reaction possibilities are summarized in Table 1.[50-52]

Table 1: Types of dynamic covalent chemistry reactions according to bond type

Type of Bond	Possible Dynamic Covalent Reactions
C-C	Aldol Reaction
	Diels-Adler Reaction
	Phenol/Aldehyde Condensation
	Friedel-Crafts Reaction
	Strecker Reaction
	Olefin Metathesis
	Alkyne Metathesis
	Carbene Coupling
	[2+1] Cycloaddition
C-N	C=N Formation/Exchanges
	Aminal Formation
	Amide Formation/Exchanges
C-O	Ester Formation/Exchanges
	Acetal Formation/Exchange
	Nicholas Ether-Exchange
	Hemiaminal Ether Exchange
	Alkyoxyamine Exchange
C-S	Thioacetal Exchange
	Thiazolidine Exchange
	Thia-Michael Reaction
B-O	Boronic Acid Condensation
S-S	Disulfide Exchange

1.4.1 Thiol-Disulfide Exchange

Of the types of dynamic covalent reactions listed in Table 1, the disulfide exchange is of particular interest because of the biological significance it holds. Disulfide bonds play an important role as part of the building blocks utilized in protein folding (ie. the formation of secondary and tertiary structures) with both intra and inter subunit crosslinking reactions.[54, 55] Additionally, disulfides are the major products of thiol oxidation, which is a biological process that's primary role is defense mechanisms against oxidative stress, as well as redox controlled cell-cell

signaling.[54] Disulfides are also key dynamic bonds responsible for many enzymes' functionalities.[54] This reaction is known to be highly robust, easily controllable, and dynamic, and may proceed in the presence of any supramolecular structure to create a reversible chemical system that is perhaps the most widely studied of any dynamic covalent reaction.[55]

This disulfide exchange reaction proceeds as a three-step mechanism that proceeds spontaneously, as demonstrated by Scheme 1.[54, 55]

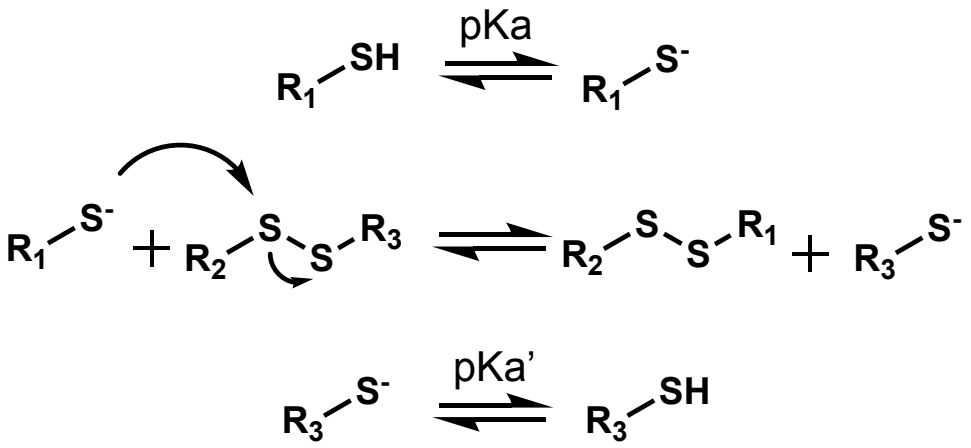

Scheme 1: Three step thiol-disulfide exchange reaction begins with a thiol deprotonated to form the nucleophilic thiolate anion which attacks a sulfur atom to form a new disulfide and thiolate anion. The former is then protonated to complete the mechanism

This reaction proceeds by a simple SN_2 type nucleophilic substitution with a single transition state, and no intermediate formation. There have been some studies that indicate this transition state is a linear trisulfide with the negative charge largely delocalized, but most abundant on the attacking and leaving sulfurs.[54] This transition state can easily become too crowded and sterically hindered, so bulky

functional groups will not work for this reaction. However, sterics may also introduce strain on the disulfide bond which makes it more labile. Recent studies suggest that the reaction is kinetically controlled, not thermodynamically, which indicates that redox potentials and equilibrium constants will only indicate whether the process is favorable, while the partitioning of particular pathways is rate dependent.[54] There are several factors that influence the rate of disulfide exchange reactions, which are mainly focused on the pKa and nucleophilicity of the attacking thiol group, but anything that may affect the stability of the leaving group or the electrophilicity of the central disulfide sulfur are also important factors for decreasing the activation energy barrier.[54] Examining the rate law and kinetic behavior of the reaction, it becomes clear that it cannot be fit to a simple first order exponential equation that yields the apparent rate constant (k_{app}).[54] This is because disulfide exchanges will usually not reach completion, but rather a dynamic equilibrium in which both products and reactants are present.

Instead, the reaction is easily controlled by adjusting the pH.[54-56] Although the reaction may proceed with an attacking thiol, the thiolate anion is a much stronger nucleophile, and so deprotonating the thiol (ie. pH > pKa) is an easily controllable molecular trigger to initiate the reaction which occurs quickly under aqueous conditions.[54-56] This molecular trigger is especially advantageous for creating responsive functional materials for applications in biotechnology and medicine because as previously mentioned in section 1.2.2, biological systems naturally vary in pH. For example, the tripeptide glutathione (GSH), for which the structure is shown in Figure 15, is a natural antioxidant found in both cytosolic fluid

of cells and plasma. It has been demonstrated that the concentration range of intracellular GSH is an order of magnitude higher than extracellular GSH (ie.approximately 1-10 mM, and 1-10 μM, respectively).[57, 58] Additionally, in tumor tissues, GSH concentration is even higher than that typically found in normal cell tissues.

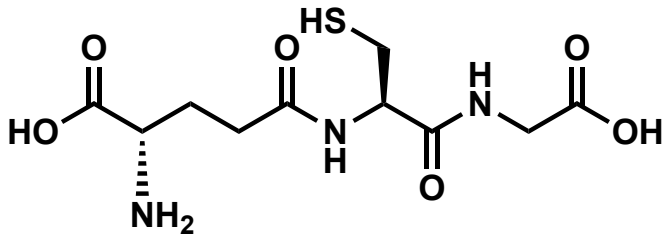

Figure 15: Chemical structure of glutathione (GSH) tripeptide structure in its reduced form is composed of y-glutamate, cysteine, and glycine amino acid residues and may serve as a nucleophile in disulfide exchange reactions

This appreciable difference in concentration makes GSH a suitable trigger to stimulate release of an encapsulated payload in any nanocarrier, equip with a disulfide bond, that is taken up into cells.[56-58] Triggered release is predicted to be more efficient in tumor cells than normal cells, as the higher GSH concentration in tumor cells makes the disulfide exchange reaction more favorable. Although the disulfide exchange reaction could theoretically occur at both intra- and extracellular GSH concentrations, it has been proven that disulfide bonds are quite stable in extracellular fluids, which is likely because the concentration of thiol is too low to elicit a reaction.[58]

1.5 Nanomaterials

From antibacterial coatings for drug delivery to supramolecular and

dynamic covalent chemistry, nanomaterials (ie. materials with dimensions of approximately ≤100 nm) have been of heavily researched over the last century.[59, 60] This is, in part, due to the broad availability of nanoscale materials and the technological advances for characterizing them, but more so, controlling materials properties on the nanoscale is highly advantageous.[59] Atoms do not behave the same way on the nanoscale as they do on the macroscopic scale. Hence, as the size of materials decreases, the scalability of the principles that govern macromolecular control over materials properties becomes quite challenging.[60] However, the use of nanomaterials has enhanced bulk material properties in ways that were never before possible, which is why they are so exhaustively studied and applied in diverse applications. The main challenges with developing new nano-based macromaterials are specialized and financially draining characterization requirements, as well as concerns over health and safety.[59, 60] New technology is making the former issue much more manageable, while the latter is still quite ambiguous. This is because the physiochemical effects of nanomaterials on human physiological systems and the environment is difficult to measure.[59] It is presumed that since a very small change in intricacies such as size, shape, surface functionality, charge, etc on the nanoscale can elicit a large change in bulk material properties, that the same would be true of living beings and their surrounding environment. Therefore, thorough nanotoxicology studies are considered essential for the development of newly developed nanomaterials to ensure their safety with widespread use, especially in biotechnology and medicine.[59]

1.5.1 Vesicle Loaded Gel Networks

Previous sections (ie. 1.1-1.4) have addressed recent advances and issues in some select topics of nanomaterials applications (ie. antibacterial coatings for drug delivery, supramolecular chemistry, and dynamic covalent chemistry), and although there have been remarkable developments in these fields individually, a multidisciplinary approach may offer even more. Individually, perhaps the two most promising candidates to create antibacterial coatings for drug delivery are hydrogels and vesicles. Taking a look at their advantages, as previously mentioned in sections 1.1.1 and 1.3.3.1, respectively, hydrogels demonstrate superior biocompatibility, mechanical strength, and adaptability to the external environment, largely owed to their porous crosslinking networks that allows them to absorb water up to hundreds of times their own volume. Likewise, vesicles demonstrate excellent encapsulation ability for both hydrophobic and hydrophilic drugs, controlled release in response to certain stimuli, and overall biocompatibility and stability. However, vesicles tend to suffer from rapid clearance in vivo while hydrogels tend to suffer from limited encapsulation ability and rapid release of encapsulated payloads.

Therefore, it is of interest to combine these two platforms to mitigate their individual issues and combine their advantages. In fact, there has been a lot of up-and-coming research done in this field that has demonstrated that the mechanical strength and adaptability of hydrogels tends to stabilize the vesicles and prevent rapid physiological clearance, while the vesicles tend to further stabilize the hydrogel matrix and prevent rapid released of encapsulated payloads.[61-74] This

hybrid system also offers opportunities for implementing dual release mechanisms, one for the hydrogel and one for the vesicles, as well as encapsulation of more than one payload. The combination of supramolecular chemistry forming vesicles and dynamic covalent bonds for triggered release mechanisms and/or crosslinking network formation takes advantage of the programmed multivalent self-assembly of supramolecular amphiphiles with the robustness of dynamic covalent bonds to extend the applicability of both vesicles and hydrogels in drug delivery and coatings.

1.6 Motivation and Research Plan

This study aims to create a novel antibacterial hydrogel coating by embedding vesicles into a hydrogel coating, as visualized in Figure 16.

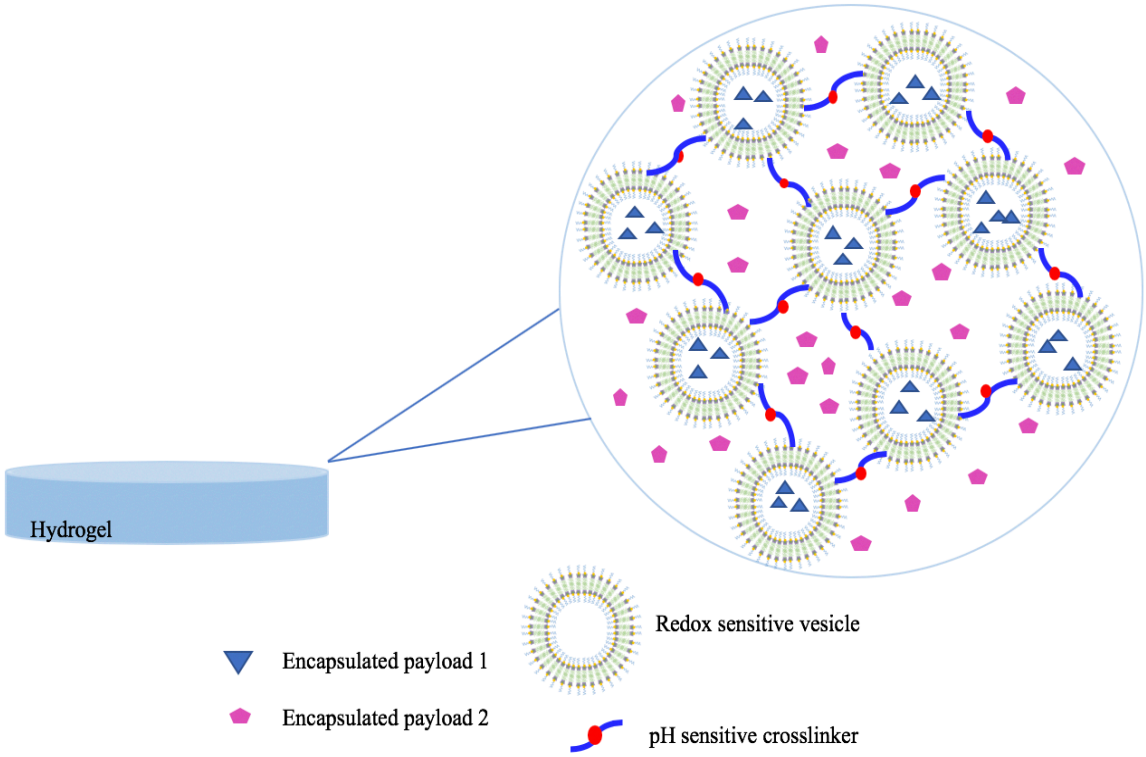

Figure 16: Schematic illustration of novel vesicle embedded hydrogel coating capable of encapsulating two different payloads, with dual sustained release mechanisms

This will mitigate burst release of encapsulated payload in the hydrogel, as well as stabilize the vesicles for a longer shelf life. Vesicles will be prepared from a novel supramolecular amphiphile composed of thio-alkyl modified βCD of varying chain lengths (ie. 12 and 14 carbon) as the macrocyclic host (ie. βCD-C12, βCD-C14), and an adamantyl-dicarboxylic acid-disulfide modified PEG (ie. AdSSPEG) with an average degree of polymerization (DP) of 22 as the linear guest, as demonstrated by Figure 17. This host-guest system will form inclusion complexes that self-assemble spontaneously to bilayered vesicles in aqueous solutions, which decreases the number of synthetic steps to simplify preparation.

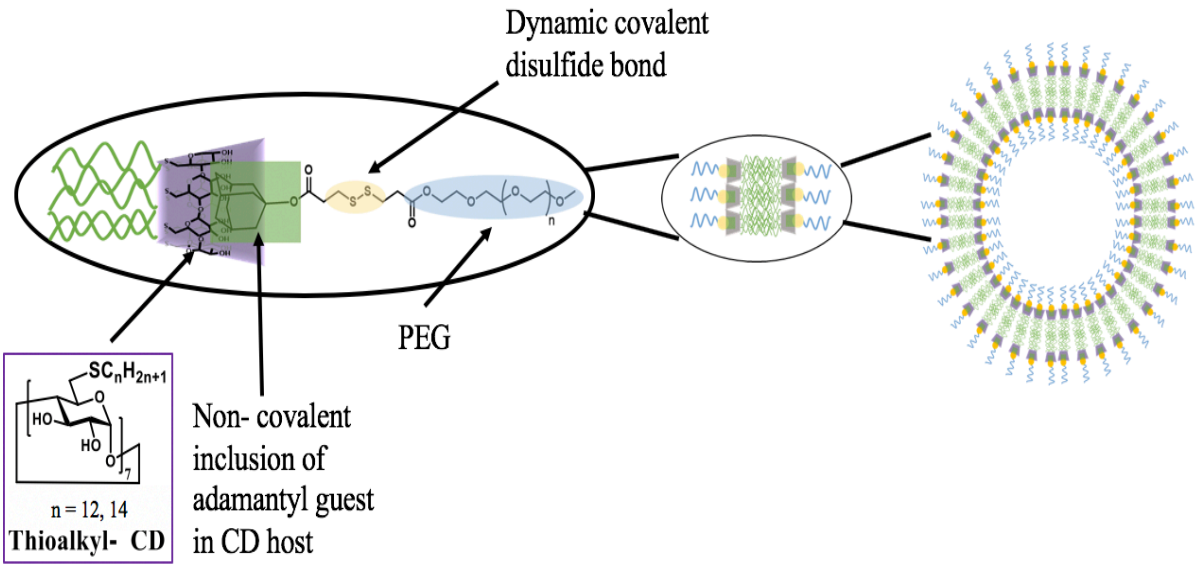

Figure 17: Schematic illustration of thioalkyl modified βCD-Cn host including the adamantyl group of the AdSSPEG guest, which self assembles to form bilayers and then bilayered vesicles in aqueous solutions

These vesicles will serve as three-dimensional multivalent junctions to form a hydrogel through crosslinking of thiolated PEG through a dynamic disulfide exchange reaction and will be capable of dual and selective release of two different

encapsulated payloads. Herein, the vesicles are capable of encapsulating hydrophobic or hydrophilic drugs in either its lipophilic bilayer membrane or aqueous interior cavity, respectively, while the hydrogel may also encapsulate a second drug during the crosslinking reaction. A pH sensitive acid labile bond embedded in the thiolated PEG (PEGdiSH) crosslinker will cleave under acidic conditions to release the payload enclosed in the hydrogel matrix, while a disulfide bond embedded in the supramolecular amphiphile of the free vesicle can be cleaved in the presence of GSH to release the second payload.

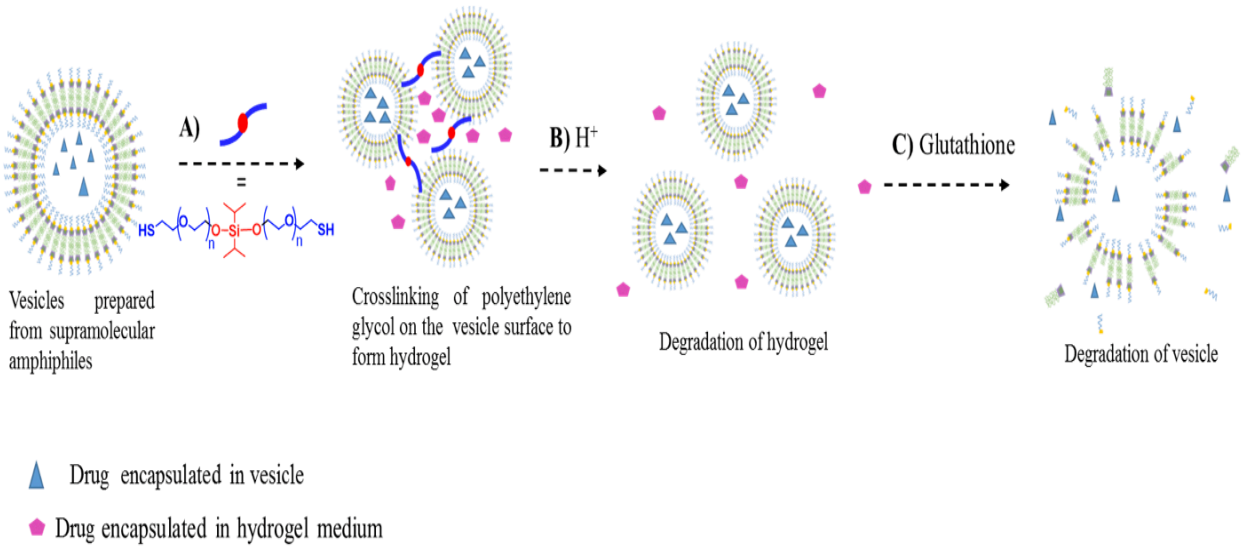

Figure 18: AdSSPEG and βCD-Cn inclusion complexes form a supramolecular amphiphile that self-assembles to bilayered vesicles in aqueous solution. A) Vesicles are crosslinked by PEGdiSH to form a hydrogel coating with two payloads encapsulated within each of the vesicle and hydrogel during preparation B) Acidic environment will trigger the cleavage of acid labile silyl-ether bond to release encapsulated payload from the hydrogel medium C) Intracellular concentrations of glutathione will cleave the disulfide bond in the AdSSPEG guest and remove the hydrophilic PEG to disrupt the ideal HLB and cause release of encapsulated payload in the vesicle

In this study, we will determine the ideal conditions for preparing the vesicle loaded hydrogel coating and fully characterize the individual components as well as the end product(s). The overall schematic is demonstrated by Figure 18.

2. EXPERIMENTAL METHODS AND MATERIALS

2.1 Materials

All materials were used as received, unless otherwise stated. β-Cyclodextrin (βCD), triphenylphosphine (PPh_3), 1-tetradecanethiol, 1-dodecanethiol, poly(ethylene glycol) (PEG; molecular weights 2000, 3400, 4000, 10000, and 20000 g/mol), anhydrous dichloromethane (DCM), anhydrous tetrahydrofuran (THF), poly(ethylene glycol)-methyl ether (PEGOMe; molecular weight 1000 g/mol), triethylamine (TEA), and nile red were purchased from TCI Chemicals. Anhydrous dimethylformaldehyde (DMF), potassium-tert-butoxide (K-*t*-butoxide), acetyl chloride, 3,3-dithiopropionic acid (DTDP), 4-dimethylaminopyridine (DMAP), 1-adamantol, and 5,6-carboxyfluorescin were purchased from Acros Organics. Triton X-100, sephadex G-50, PEG (molecular weights 200, and 1000 g/mol), and liquid bromine ($Br_{2\ (l)}$) were purchased from Sigma Aldrich. L-glutathione (reduced), N,N'-dicyclocarbodiimide (DCC), and p-toluenesulfonyl chloride (TsCl) were purchased from Alfa Aesar. Anhydrous pyridine was purchased from DriSolv. Thiourea was purchased from MCB. Magnesium sulfate ($MgSO_4$), and tris base were purchased from Fisher Chemical. Polycarbonate 200 nm pore size membrane was purchased from Avanti Polar Lipids, Inc. All other solvents and materials were received and/or prepared from the Cal Poly Organic Chemistry Stockroom.

2.2 Synthesis of Thioalkyl Modified β-Cyclodextrins (βCD-C12, βCD-C14)

2.2.1 Synthesis of Heptakis(6-bromo)- βCD

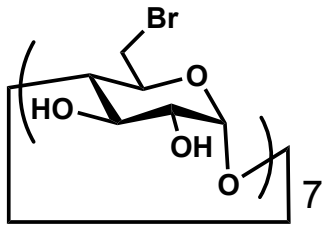

[1]

Figure 19: Chemical structure of **[1]** Heptakis(6-bromo)- βCD

Native β-CD (4.0 g, 3.5 mmol) was dried over molecular sieves with anhydrous DMF (≈20 mL) overnight (≈18 hours). The solution was transferred to a round bottom flask, and solvent along with any residual water was removed under reduced pressure. PPh_3 (20 eq.) was added to a round bottom flask, dissolved in anhydrous DMF (≈20 mL), and purged under nitrogen three times. $Br_{2\,(l)}$ (20 eq.) was then added dropwise to the PPh_3 solution via nitrogen purged syringe and stirred at 60 ℃ for 30 minutes. Dry β-CD was dissolved in anhydrous DMF (≈10 mL) and was then added to the reaction mixture dropwise and stirred overnight (≈18 hours) at 80 ℃. Approximately half the solvent volume was then removed under reduced pressure, and the resulting reaction mixture was added to methanol (≈100 mL). The pH was adjusted to 10-12 with K-*t*-butoxide and the resulting reaction mixture was stirred at room temperature for 30 minutes. This reaction mixture was then precipitated in rapidly stirring ice-cold deionized water (DI water). The precipitate was isolated via vacuum filtration, transferred to a falcon tube, and then dissolved in methanol. The resulting solution was centrifuged

(Eppendorf, Centrifuge 5810) three times in 5-minute intervals at 7500 RPM. Methanol was decanted and the precipitate was transferred to a round bottom flask and dissolved in a minimal amount of DMF. The solvent was then removed under reduced pressure. Product was dried under high vacuum pump overnight (≈18 hours) to obtain a white powder [1].

2.2.2 Synthesis of Heptakis(6-dodecylthiol)- βCD (βCD-C12), Heptakis(6-tetradecylthiol)- βCD (βCD-C14)

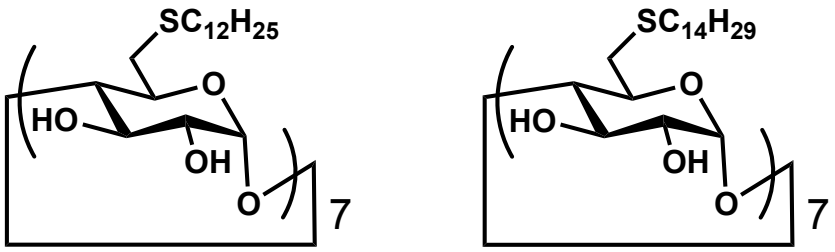

[2a] **[2b]**

Figure 20: Chemical structure of **[2a]** Heptakis(6-dodecylthiol- βCD, and **[2b]** Heptakis(6-tetradecylthiol)- βCD

Brominated β-CD [1] (350 mg, 0.22 mmol), either 1-dodecanethiol (for [2a]) or 1-tetradecanethiol (for [2b]) (20 eq.), and K-*t*-butoxide (20 eq.) were combined and purged under nitrogen three times. Anhydrous DMF (≈20 mL) was added via nitrogen purged syringe to dissolve all reagents, and was allowed to stir for 72 hours at 80 ℃. The reaction mixture was then precipitated in rapidly stirring ice cold DI water. The precipitate was isolated via vacuum filtration, and transferred to a round bottom flask. The precipitate was then refluxed (65 ℃) in methanol (≈20 mL) for 1 hour. The resulting precipitate was isolated by vacuum filtration and washed with hot methanol. The product was dried under high vacuum pump overnight (≈18 hours) to obtain a white powder (n = 12) [2a] ^{1}H NMR (400

MHz, Chloroform-d) δ 6.71 (s, 1H), 5.24 (s, 1H), 4.98 (s, 1H), 3.99 (t, 1H), 3.92 (t, 1H), 3.74 (t, 1H), 3.49 (t, 1H), 3.05 (d, 1H), 2.88 (m, 1H), 2.60 (t, 2H), 1.57 (m, 12H), 1.26 (m, 51H), 0.88 (t, 8H), or (n = 14) [2b] ^{1}H NMR (400 MHz, Chloroform-*d*) δ 6.71 (s, 1H), 5.24 (s, 1H), 4.97 (s, 1H), 3.99 (t, 1H), 3.91 (t, 1H), 3.74 (t, 1H), 3.49 (t, 1H), 3.04 (d, 1H), 2.88 (m, 1H), 2.60 (t, 2H), 1.55 (m, 15H), 1.25 (m, 29H), 0.88 (t, 4H).

2.3 Synthesis of Adamantyl-Dithiopropionic acid Modified Poly(ethylene-glycol) / Poly(ethylene glycol)-methyl ether (AdSSPEG / AdSSPEGOMe)

2.3.1 Synthesis of Dithiopropionic Anhydride

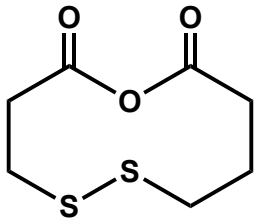

[3]

Figure 21: Chemical structure of **[3]** Dithiopropıonıc anhydride

DTDP (2.10 g, 10 mmol) was added to a round bottom flask and refluxed (65 ℃) in acetyl chloride (10 eq.) for 2 hours. The reaction mixture was cooled to room temperature, and acetyl chloride was removed under reduced pressure. The resulting residue was precipitated in rapidly stirring ice-cold diethyl ether. Precipitate was then isolated via vacuum filtration and washed with ice cold diethyl ether. The product was dried under high vacuum pump overnight (≈18 hours) to obtain an off-white powder [3].

2.3.2 Synthesis of Dithiopropionic acid Modified Poly(ethylene glycol) / Poly(ethylene glycol)-methyl ether

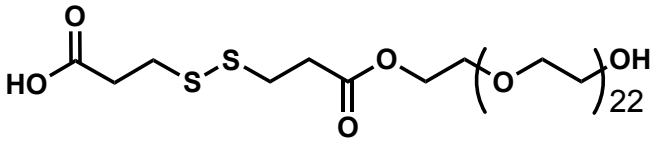

[4a]

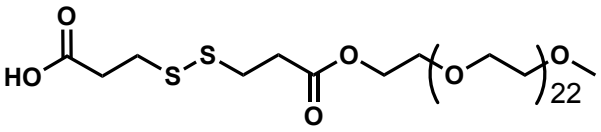

[4b]

Figure 22: Chemical structure of **[4a]** Dithiopropionic acid-Poly(ethylene glycol), and **[4b]** Dithiopropionic acid-Poly(ethylene glycol)-methyl ether

Either PEG (for [4a]) or PEGOMe (for [4b]) (6.5 g, 6.5 mmol) was dried over molecular sieves with anhydrous DMF (≈20 mL) overnight (≈18 hours). The solution was transferred to a round bottom flask, and solvent along with residual water was removed under reduced pressure. Dithiopropionic anhydride [3] (2 eq.), and DMAP (1 eq.) were added to the round bottom flask and all reagents were dissolved in anhydrous DMF (≈20 mL). TEA (2 eq.) was added dropwise. The resulting solution was purged under nitrogen three times and allowed to stir at 35 ℃ for 36 hours. The reaction mixture was then precipitated in rapidly stirring ice-cold diethyl ether. The precipitate was isolated via vacuum filtration and washed with ice cold diethyl ether. The product was then dried under high vacuum pump overnight (≈18 hours) to obtain a brown powder [4a] or [4b].

2.3.3 Synthesis of Adamantyl-Dithiopropionic acid Modified Poly(ethylene-glycol) / Poly(ethylene glycol)-methyl ether (AdSSPEG / AdSSPEGOMe)

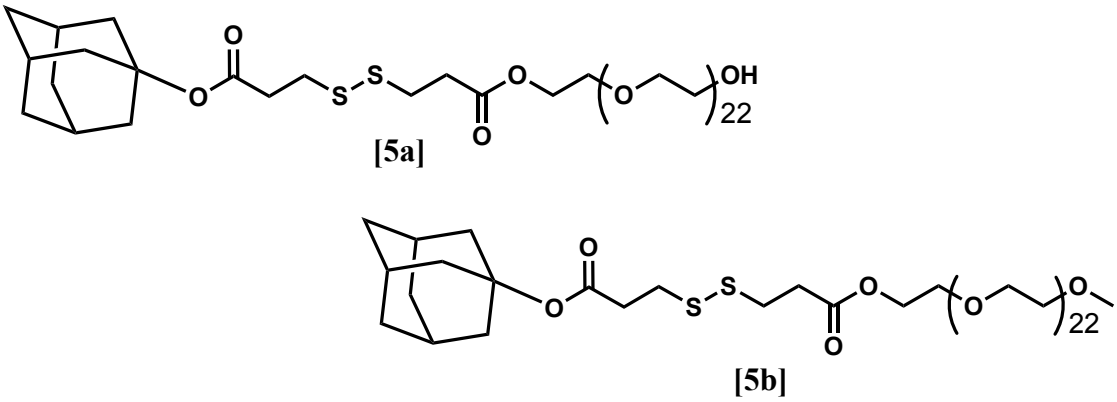

Figure 23: Chemical structure of **[5a]** Adamantyl-Dithiopropionic acid-Poly(ethylene-glycol) (AdSSPEG), and **[5b]** Adamantyl-Dithiopropionic acid-Poly(ethylene-glycol)-methyl ether (AdSSPEGOMe)

Dithiopropionic acid-PEG [4a] or dithiopropionic acid-PEGOMe [4b] (7 g, 5.87 mmol) was co-dissolved with 1-adamantol (2 eq.) in anhydrous DCM (≈20 mL) at 0 ℃. In a separate round bottom flask, DCC (2 eq) was also dissolved in anhydrous DCM (≈ 5 mL) at 0 ℃. Both solutions were then purged under nitrogen three times. DCC solution was added to the initial solution dropwise and stirred for 2 hours at 0 ℃. The reaction mixture was then allowed to stir for 22 hours at room temperature. By product N,N'-dicyclourea (DCU) was removed by gravity filtration. The filtrate was washed three times with 10% hydrochloric acid (HCl). The aqueous layer was extracted with DCM until the organic layer appeared clear (≈6 times). The organic layer was then washed three times with brine and dried over $MgSO_4$. The solvent was then removed under reduced pressure. The resulting

residue was precipitated in rapidly stirring ice-cold heptane, isolated via vacuum filtration, and washed with ice cold ether. The product was further purified in DI water via dialysis (Float-A-Lyzer G2) with a 0.1-0.5 kDa pore membrane. The resulting solution was flash-frozen with liquid nitrogen and left on the lyophilizer (Labconco, FreeZone 4.5) overnight (≈18 hours) to remove water and obtain a yellow-orange powder [5a] ^{1}H NMR (400 MHz, DMSO-d_6) δ 5.62 (s, 4H), 3.49 (s, 3H), 3.43 (s, 2H), 3.34 (s, 38H), 2.88 (s, 4H), 2.62 (s, 4H), 2.03 (s, 11H), 1.73 (s, 10H), 1.58 (s, 62H), or [5b] ^{1}H NMR (400 MHz, Chloroform-*d*) δ 3.82 (s, 1H), 3.71 (s, 6H), 3.65 (s, 199H), 3.56 (s, 5H), 3.38 (s, 6H), 2.92 (s, 4H), 2.77 (s, 3H), 2.14 (s, 15H), 1.71 (s, 18H), 1.63 (s, 27H).

2.4 Synthesis of Thiol Modified Poly(ethylene-glycol) (PEG-diSH)

2.4.1 Synthesis of Poly(ethylene glycol)-di(p-toluenesulfonic acid) (PEGdiOTs)

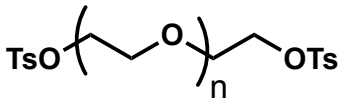

[6]

Figure 24: Chemical structure of **[6]** Poly(ethylene glycol)-di(p-toluenesulfonic acid) (PEGdiOTs) (n = 22 **[6a]**, 45 **[6b]**, 77 **[6c]**, 90 **[6d]**, 227 **[6e]**, 454 **[6f]**)

PEG (n = 22 [6a], 45 [6b], 77 [6c], 90 [6d], 227 [6e], 454 [6f], 1.5 mmol) was dried over molecular sieves with anhydrous DMF (≈20 mL) overnight (≈18 hours). The solution was transferred to a round bottom flask, and solvent along with any residual water was removed under reduced pressure. TsCl (4 eq.) was added and the resulting mixture was purged under nitrogen three times. Anhydrous

pyridine (10 eq.) was then added at 0 ℃, and all reagents were dissolved in anhydrous DCM (≈20 mL). The reaction mixture was stirred overnight (≈18 hours) at 0 ℃. Three pieces of 7 cm diameter cellulose-based filter paper were cut up into small pieces and added to the solution. The reaction mixture was then sonicated (Ultrasonic Cleaner, GB-928) at 40 kHz for 1 hour to remove excess TsCl. The filter paper was removed, and the reaction mixture was washed three times with 10% HCl. The aqueous layer was extracted with DCM until the organic layer appeared clear (≈6 times). The organic layer was washed three times with brine and dried over $MgSO_4$. The solvent was removed under reduced pressure, and the product was dried overnight (≈18 hours) under a high vacuum pump to obtain a slightly yellow oil (n = 22 [6a]), or a slightly yellow powder (n = 45 [6b], 77 [6c], 90 [6d], 227 [6e], 454 [6f]).

2.4.2 Synthesis of Poly(ethylene glycol)-dithiol (PEGdiSH)

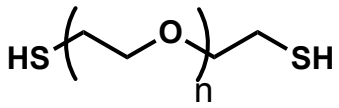

[7]

Figure 25: Chemical structure of **[7]** Poly(ethylene glycol)-dithiol (PEGdiSH) (n = 22 **[7a]**, 45 **[7b]**, 77 **[7c]**, 90 **[7d]**, 227 **[7e]**, 454 **[7f]**)

PEGdiOTs (n = 22 [6a], 45 [6b], 77 [6c], 90 [6d], 227 [6e], 454 [6f], 1 mmol) was co-dissolved with thiourea (6 eq.) in anhydrous THF (≈ 15 mL) in a round bottom flask. The resulting solution was purged under nitrogen three times and allowed to reflux (66 ℃) overnight (≈18 hours). The reaction mixture is cooled to room temperature and 10% NaOH (≈ 10 mL) was added through the top of the condenser. The reaction mixture was again allowed to reflux (66 ℃) overnight (≈18

hours). Once the layers separated, the organic layer solvent was removed under reduced pressure and the aqueous layer was extracted three times with DCM. The organic residue was dissolved in DI water, and the pH is adjusted to 7 with 10% HCl. The organic layer was then extracted three times with DCM. All organic layers were combined and washed three times with brine before drying over $MgSO_4$. Solvent was removed under reduced pressure and the product was dried under high vacuum pump overnight (≈18 hours) to obtain a slightly yellow oil (n = 22) [7a] ^{1}H NMR (400 MHz, Chloroform-d) δ 3.81 (q, J = 4.6 Hz, 4H), 3.65 (s, 551H), 3.51 – 3.43 (m, 4H), 2.88 (s, 4H), 1.89 (s, 43H), or a slightly yellow powder (n = 45) [7b] ^{1}H NMR (400 MHz, Chloroform-d) δ 3.85 – 3.79 (m, 17H), 3.64 (s, 2567H), 3.51 – 3.43 (m, 18H), 2.88 (s, 4H), 1.80 (s, 451H), (n = 77) [7c] ^{1}H NMR (400 MHz, Chloroform-d) δ 3.85 – 3.79 (m, 17H), 3.66 (s, 2483H), 3.49 – 3.44 (m, 18H), 2.88 (s, 4H), 1.43 (s, 4H), (n = 90) [7d] ^{1}H NMR (400 MHz, Chloroform-d) δ 3.82 (dd, J = 5.8, 4.1 Hz, 4H), 3.64 (s, 995H), 3.47 (dd, J = 5.7, 4.1 Hz, 6H), 2.82 (s, 4H), 1.65 (s, 150H), (n = 227) [7e] ^{1}H NMR (400 MHz, Chloroform-d) δ 3.85 – 3.78 (m, 15H), 3.65 (s, 2206H), 3.50 – 3.43 (m, 16H), 2.79 (s, 4H), 1.43 (s, 1H, (n = 454) [7f]) ^{1}H NMR (400 MHz, Chloroform-d) δ 3.85 – 3.79 (m, 16H), 3.65 (s, 6453H), 3.49 – 3.44 (m, 71H), 2.69 (s, 4H), 1.43 (s, 1H).

2.5 Nuclear Magnetic Resonance (NMR) Measurements

NMR (Bruker Ascend, 400 mHz) samples were prepared with approximately 10 mg of compound dissolved in an appropriate solvent. Compounds [2a, 2b, 5a, 5b, 7a-f] were analyzed via ^{1}H NMR to confirm that final

products were formed as expected. Novel compounds [5a, 5b] were also analyzed via ^{13}C NMR, and HSQC. MestreNova software was used to process all raw data.

2.6 Fourier-Transform Infrared (FTIR) Measurements

The FTIR (Perkin Elmer, Spectrum 100) crystal was cleaned with 2-propanol and allowed to dry under ambient conditions. A background spectrum was then recorded. Samples were deposited onto the crystal in order to cover it. Novel compounds **[5a, 5b]** were analyzed for %Transmittance.

2.7 Inclusion Complex Formation

Host and guest (ie. thioalkyl modified βCD [2a, 2b] host, and adamantyl-dithiopropionic acid modified PEG / PEGOMe [5a, 5b] guest) were combined in equimolar amounts (5 μmol) in a round bottom flask with DI water (≈ 2 mL) and sonicated (Ultrasonic Cleaner, GB-928) at 40 kHz for 30 minutes. The solvent was removed under reduced pressure to afford a thin film. The film was hydrated with 1:1 chloroform: DI water (≈ 2 mL total) and were again sonicated (Ultrasonic Cleaner, GB-928) at 40 kHz for 30 minutes. The solvent was removed under reduced pressure to afford the thin film inclusion complex. Inclusion complexes were stable and stored in the fridge.

2.8 Vesicle Formation

Thin film inclusion complex was rehydrated with Tris buffer (10 mM Tris base, 10 mM NaCl, pH 7.40, ≈ 1 mL) and allowed to sit for 30 minutes at room temperature. This buffer solution was subjected to five freeze-thaw (liquid nitrogen-55 ℃ water bath) cycles to form vesicles, and was then probe sonicated (QSonica Sonicators, Ultrasonic Processor) at 20 kHz for 2 minutes to break up

larger aggregates. The solution was pushed through a 450 nm filter and then extruded (Avanti Polar Lipids, Inc.) ten times with a 200 nm pore size polycarbonate membrane (Avanti Polar Lipids, Inc.). Purified vesicles were stable for several weeks to a month and stored in the fridge.

2.9 Fluorescent Vesicle Formation

Thin film hydration method from section 2.8 was used with 5,6-carboxyfluorescin (CF) buffer (50 mM CF, 10 mM Tris base, 10 mM NaCl, pH 7.40, ≈ 1 mL) instead of Tris buffer. After extrusion, fluorescent vesicles were further purified with size exclusion chromatography using a sephadex G-50 column. The column was prepared in a 5 mL syringe with 1:10 sephadex G-50: Tris buffer. Sephadex G-50 was allowed to settle to the 3 mL mark before adding vesicle containing CF buffer solution. The column was then eluted with Tris buffer, and a fraction was collected for each colored band. Vesicles were in the orange band. Vesicles with encapsulated CF were stored in the fridge. The column was reused once all fluorescent dye had been eluted from the column.

2.10 Fluorimeter Measurements

Fluorimeter (Horiba Scientific, Fluorolog-QM) was set to the appropriate experimental parameter and run at room temperature. Sample was loaded into a quartz cuvette with a stir bar and stirred at speed 5 during all measurements. FluorEssence™ software was used for all data analysis.

2.10.1 Fluorescent Vesicle Encapsulation and Lysing via Fluorimetry

Fluorimeter (Horiba Scientific, Fluorolog-QM) was set to kinetics acquisition with λ_{em} = 517 nm with a slight width of 1 nm, and λ_{ex} = 492 nm with

a slit width of 1 nm for fluorescent probe CF. Total run time was 90 seconds with data collection every 0.1 seconds. Fluorescent vesicles prepared according to the method in section 2.9 were diluted with Tris buffer (25 μL vesicles, 2000 μL Tris buffer) and pipetted up and down to mix. Sample was then allowed to equilibrate for 30 seconds before measurements were taken. The kinetics acquisition was initiated, and a baseline was established for 30-40 seconds before adding 250 μL of 10% Triton X-100 detergent to lyse the vesicles. The percent change in fluorescence intensity (%ΔFluorescence Intensity) was calculated using Equation 1, where I_t = Fluorescence Intensity (CPS) at time *t*, and I_0 = Fluorescence Intensity (CPS) at time *0*.

$$\%\,\Delta Fluorescence\ Intensity = \frac{(I_t - I_0)}{I_0} * 100 \qquad \text{EQ. 1}$$

Results from this calculation determine whether vesicles were formed and whether they encapsulated CF in their interior. A high %ΔFluorescence Intensity comparing inclusion complexes, and host and guest molecules on their own (treated with the same fluorescent vesicle formation method in section 2.9) was indicative of successful vesicle formation and CF encapsulation.

2.10.2 Critical Aggregation Concentration (CMC) via Fluorimetry

Fluorimeter (Horiba Scientific, Fluorolog-QM) was set to spectra acquisition with λ_{ex} = 515 nm with a slit width of 7 nm and λ_{em} = 530 – 670 nm with a slit width of 7 nm for fluorescent probe nile red. Samples were prepared at a broad range of supramolecular amphiphile (ie. thioalkyl modified βCD [2a, 2b]

host, and adamantyl-dithiopropionic acid modified PEG / PEGOMe [5a, 5b] guest inclusion complexes) concentrations (0 – 500 μM) with nile red concentration held constant at 0.156 μg/mL. Nile red stock solution (5 μg/mL) was prepared in DCM and was added to 5 mL volumetric flasks. Solvent was evaporated from the flasks before amphiphile addition. Amphiphile was then added at the appropriate amount and the sample was diluted to volume with nanopure water (Thermo Scientific, Barnstead GenPure, 18.20 MΩ*cm). Each sample was sonicated (Ultrasonic Cleaner, GB-928) at 40 kHz for 10 minutes and was then stored in vials for a few hours before fluorimeter measurements were taken to allow for equilibration. Fluorimeter measurements were taken in triplicate for each sample, and λ_{max} and the Fluorescence Intensity (CPS) at λ_{max} were recorded.

Nile red behaves differently in aqueous environments versus lipophilic environments, so when amphiphiles begin to form micelles the nile red will be encapsulated in the hydrophobic interior and fluoresce at a higher wavelength and intensity than in aqueous solutions.[75] Therefore, by plotting fluorescence intensity (CPS) at λ_{max} against amphiphile concentration (μM), the slope approaches 0 at the critical micelle concentration (CMC). Two linear fits can be made before (0) and after (f) the CMC. Finding the intersection of these lines via Equation 2 will give CMC (x).

$$(mx + b)_f = (mx + b)_0 \qquad \text{EQ. 2}$$

2.11 Dynamic Light Scattering (DLS) Measurements

Dynamic light scattering (DLS) (Wyatt Tech, DynaPro NanoStar) measurements were taken in disposable cuvettes in a dust free environment. The cell temperature was set to 25 ℃ and the solvent was set to water for all samples. If samples were clear, 100 μL was loaded into the cuvette without scratching the sides, the cap was placed, and measurements were taken after a 30 second equilibration time. If samples were not clear, they were diluted with nanopure water (Thermo Scientific, Barnstead GenPure, 18.20 MΩ*cm) until clear and loaded as previously mentioned. For all samples, the average of 20 scans was used for data collection and %Intensity, %PD (polydispersity), and hydrodynamic radius (nm) were recorded. The sample was then aspirated out of the cuvette, and the cuvette was rinsed several times with nanopure water (Thermo Scientific, Barnstead GenPure, 18.20 MΩ*cm) before re-use.

2.11.1 Vesicle Particle Size via DLS

Vesicles prepared according to section 2.8 were measured on DLS (Wyatt Tech, DynaPro NanoStar) according the method previously mentioned in section 2.11. To determine relative stability of vesicles, all vesicle samples were measured repeatedly over the course of several weeks.

2.11.2 Vesicle Glutathione (GSH) Degradation via DLS

Vesicles prepared according to section 2.8 (with the modification of Tris buffer pH = 8.5) were measured on DLS (Wyatt Tech, DynaPro NanoStar) according the method previously mentioned in section 2.11. Initial measurements were recorded, and then vesicle particle size stability was tested first with 10%

Triton X-100, and then intracellular and extracellular concentrations of glutathione (GSH). For 10% Triton X-100 degradation experiments, a 25 μL aliquot of vesicles was added to a vial with 2000 μL of Tris buffer and 250 μL 10% Triton X-100. Sample was mixed by hand and measurements were taken immediately according to the method previously mentioned in section 2.11. For intracellular [GSH] degradation experiments, a GSH buffer (500 mM GSH, 10 mM Tris base, 10 mM NaCl, pH 8.5) was prepared. A 25 μL aliquot of vesicles was added to a vial with 2000 μL of Tris buffer and 50 μL of GSH buffer to give a final [GSH] = 12 mM, which is just above the intracellular GSH range.[57, 58] Samples were orbit mixed for 1 hour, and then overnight (≈18 hours), and measurements were taken at each time increment according to the method previously mentioned in section 2.11. For extracellular [GSH] degradation experiments, a GSH buffer (1 mM GSH, 10 mM Tris base, 10 mM NaCl, pH 8.5) was prepared. A 25 μL aliquot of vesicles was added to a vial with 2000 μL of Tris buffer and 40 μL of GSH buffer to give a final [GSH] = 20 μM, which is just above the extracellular GSH range.[57, 58] Samples were orbit mixed for 1 hour, and then overnight (≈18 hours), and measurements were taken at each time increment according to the method previously mentioned in section 2.11. Initial measurements were compared to the measurements with 10% Triton X-100, intracellular, and extracellular [GSH] to determine if any vesicle degradation had occurred.

2.12 Hydrogel Formation

Hydrogel formation was attempted with all vesicles prepared according to section 2.8, and all PEGdiSH [7a-f] crosslinkers of varying molecular weight (ie. 1000, 2000, 3400, 4000, 10000, and 20000 g/mol).

Initial experiments were done at pH 7.4 at room temperature and PEGdiSH wt/wt% 0.5, 1.0, 2.5, and 5.0 where PEGdiSH wt/wt% was calculated according to Equation 3. Vesicle amount was held constant at 250 μL.

$$PEGdiSH\ wt/wt\% = \frac{weight\ of\ PEGdiSH\ buffer}{weight\ of\ total\ buffer} * 100 \qquad \text{EQ. 3}$$

Samples were prepared by combining vesicles in Tris buffer and PEGdiSH buffer (1 mM PEGdiSH, 10 mM Tris base, 10 mM NaCl, pH 7.4) in the appropriate amounts. Samples were vortex mixed for 30 seconds, and then orbit mixed overnight (≈18 hours). Samples were checked every hour for 3 hours, and then again after 24 hours, for hydrogel formation by inverting the vial to see if it can hold its own weight.

Additional experiments were done at pH 8.5 at room temperature at PEGdiSH wt/wt% 1.0, 2.5, 5.0, 10, and 20 where PEGdiSH wt/wt% was calculated according to Equation 3. Vesicle amount was held constant at 250 μL. Samples were prepared by combining vesicles in pH modified Tris buffer (pH 8.5) and PEGdiSH buffer (1 mM PEGdiSH, 10 mM Tris base, 10 mM NaCl, pH 8.5) in the appropriate amounts. Samples were vortex mixed for 30 seconds, and then orbit mixed overnight (≈18 hours). Samples were checked every hour for 3 hours, and

then again after 24 hours, for hydrogel formation by inverting the vial to see if it can hold its own weight.

Further experiments were done with the aforementioned 20 wt/wt% PEGdiSH containing samples. These samples were incubated at temperatures 30, 35, 40, 45, and 50 ℃ for 2 hours each, and checked for hydrogel formation every 30 minutes by inverting the vial to see if it can hold its own weight.

Final experiments were done at pH 8.5, temperatures 25, 35, 45 and 55 ℃, and PEGdiSH wt/wt% 10 and 20, where PEGdiSH wt/wt% was calculated according to Equation 4. Vesicle amount was gradually increased after each temperature incubation from 10, 20, 40, 60, 80, 100, to 250 μL. PEGdiSH amount was held constant at 250 μL.

$$PEGdiSH\ wt/wt\% = \frac{weight\ PEGdiSH}{weight\ of\ Tris\ buffer} * 100 \qquad \textbf{EQ. 4}$$

Samples were prepared by combining vesicles in pH modified Tris buffer (pH 8.5) and PEGdiSH in pH modified Tris buffer (pH 8.5) in the appropriate amounts. Samples were vortex mixed before being allowed to incubate at each of the previously mentioned temperatures for 1 hour each and are checked for hydrogel formation every 30 minutes by inverting the vial to see if it can hold its own weight.

3. RESULTS AND DISCUSSION

3.1 Synthesis of Thioalkyl Modified β-Cyclodextrins (βCD-C12, βCD-C14)

Thioalkyl modified βCDs [2a, 2b] were synthesized according to Scheme 2 and were characterized via ^{1}H NMR to confirm that the macrocyclic host molecules were formed as expected.

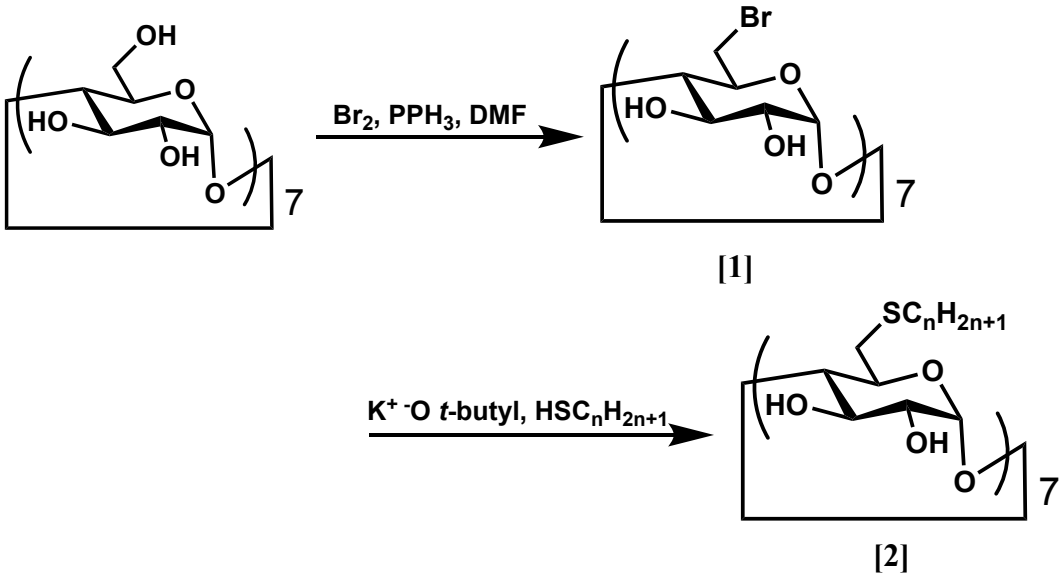

Scheme 1: Synthesis of **[1]** Heptakis(6-bromo)- βCD, and **[2]** Heptakis(6-thioalkyl)- βCD (n= 12 **[2a]**, 14 **[2b]**)

After the initial bromination at position 6 of the native βCD, the thioalkyl chain was covalently attached via an S_N2 substitution reaction. Products [2a, 2b] were then isolated via a hot methanol reflux, filtration, and centrifugation to remove excess unreacted free thiol from the precipitate. It was found that increasing reaction times increased the overall yield from this synthetic pathway, and persistent centrifugations in addition to vacuum filtrations were effective methods

to purify the final products [2a, 2b]. Hot methanol filtration and washing in the final step was essential in removing free unreacted alkyl thiol.

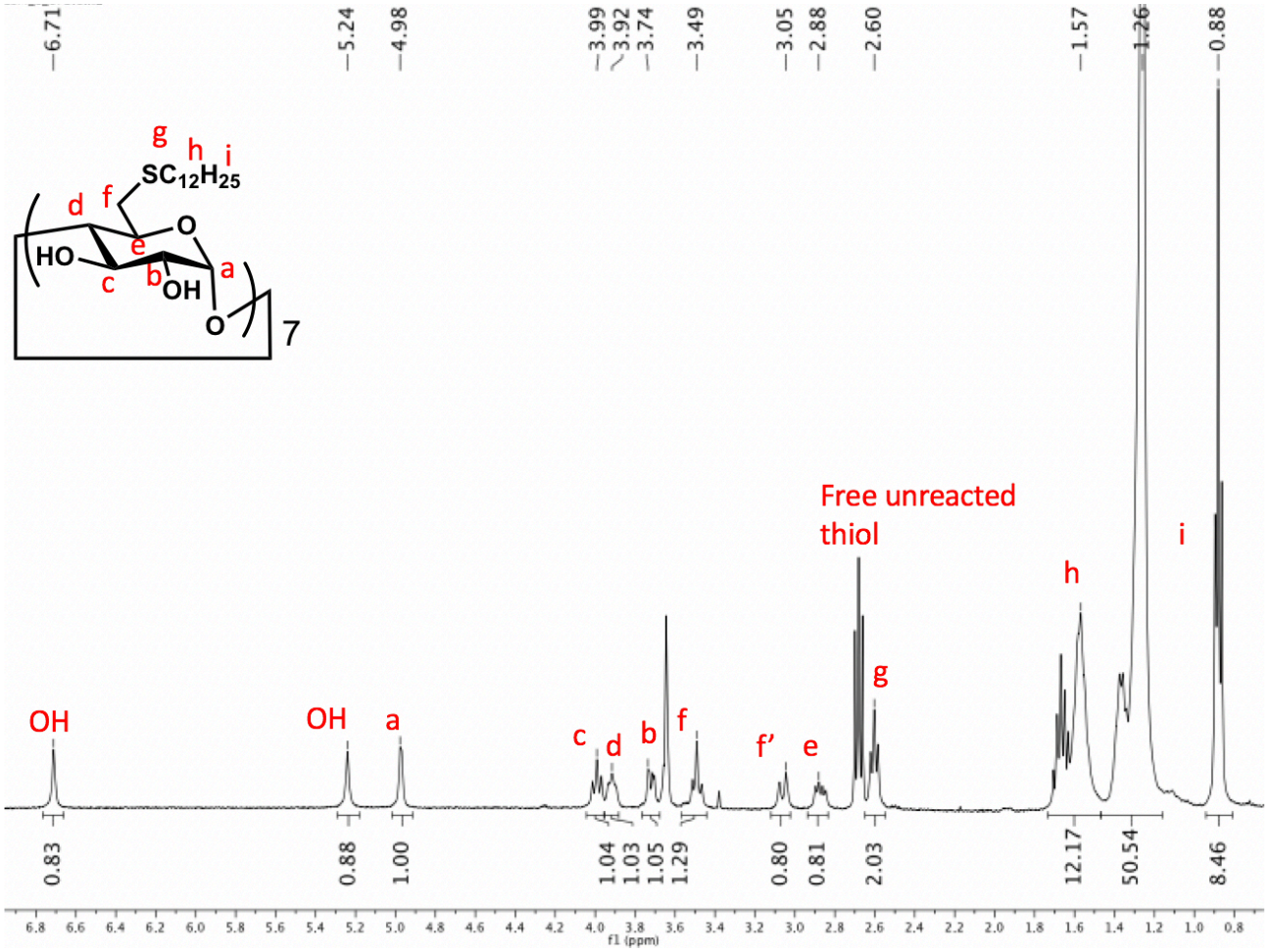

Figure 26: ^{1}H NMR of βCD-C12 [2a] in deuterated chloroform ($CDCl_3$)

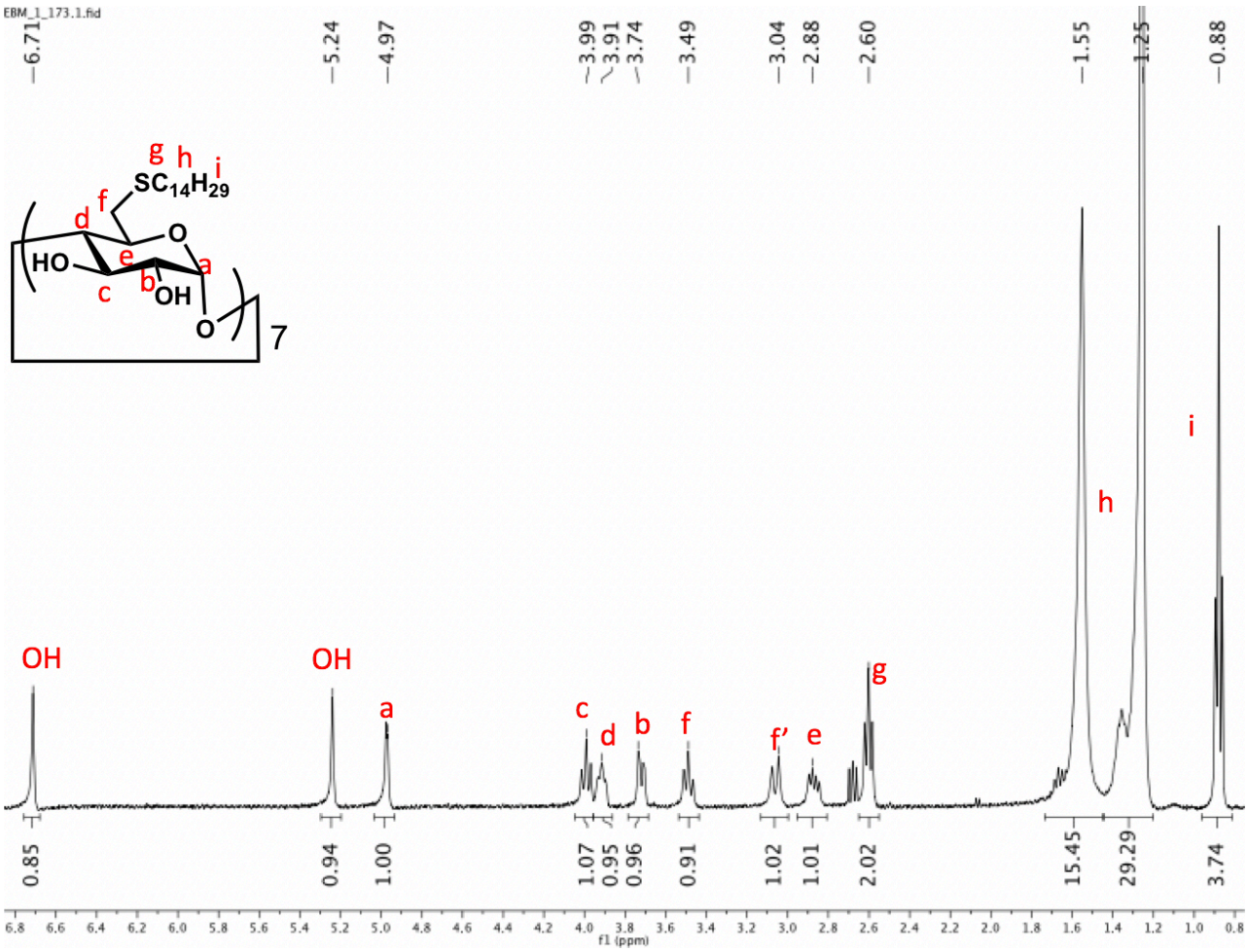

Figure 27: ^{1}H NMR of βCD-C14 [2b] in deuterated chloroform ($CDCl_3$)

Proton NMRs in Figures 26 and 27 correspond to *β*CD-C12 [2a] and *β*CD-C14 [2b], respectively. Here, peaks labeled a, b, c, d, and e correspond to protons within the core glucose structure. Peak f corresponds to protons at position 6 where the thioalkyl chain has been covalently bound. The triplet peak g corresponds to the protons directly besides the sulfur atom, as they are downfield due to deshielding effect from the sulfur. The appearance of this peak at 2.60 ppm was used to confirm final product formation. Peak h corresponds to the rest of the protons on the thioalkyl chain, while peak i corresponds to the terminal methyl protons. Overall,

both βCD-C12, βCD-C14 [2a, 2b] were synthesized successfully and in good yield (78-86%).

In Figure 26, excess free unreacted alkyl thiol was still present in the final product, but it is in such a small amount compared to the βCD-C12 [2a] product that the material was deemed pure enough for use in subsequent experiments. Additionally, the excess alkyl thiol does not have the necessary amphiphilicity and geometry needed to form inclusion complexes or self-assemble on its own, so it is not a concern for interfering with subsequent experiments. The βCD-C12, and βCD-C14 [2a, 2b] products on their own have very poor water solubility which can be attributed to the hydrophobic thioalkyl modification along with the hydrophobic core of the truncated cone structure. However, the exterior of the truncated cone structure is hydrophilic due to the stereochemistry of the abundant hydroxyl groups on the core glucose structure facing outwards, which overall makes these macrocyclic host molecules amphiphilic on their own.

3.2 Synthesis of Adamantyl-Dithiopropionic acid Modified Poly(ethylene-glycol) (AdSSPEG, AdSSPEGOMe)

Novel adamantyl-dithiopropionic acid modified poly(ethylene glycol)s (AdSSPEG, AdSSPEGOMe) [5a, 5b] were synthesized according to Scheme 3 and 4 and characterized via ^{1}H NMR, ^{13}C NMR, HSQC, and FTIR to confirm that linear guest molecules were synthesized as expected.

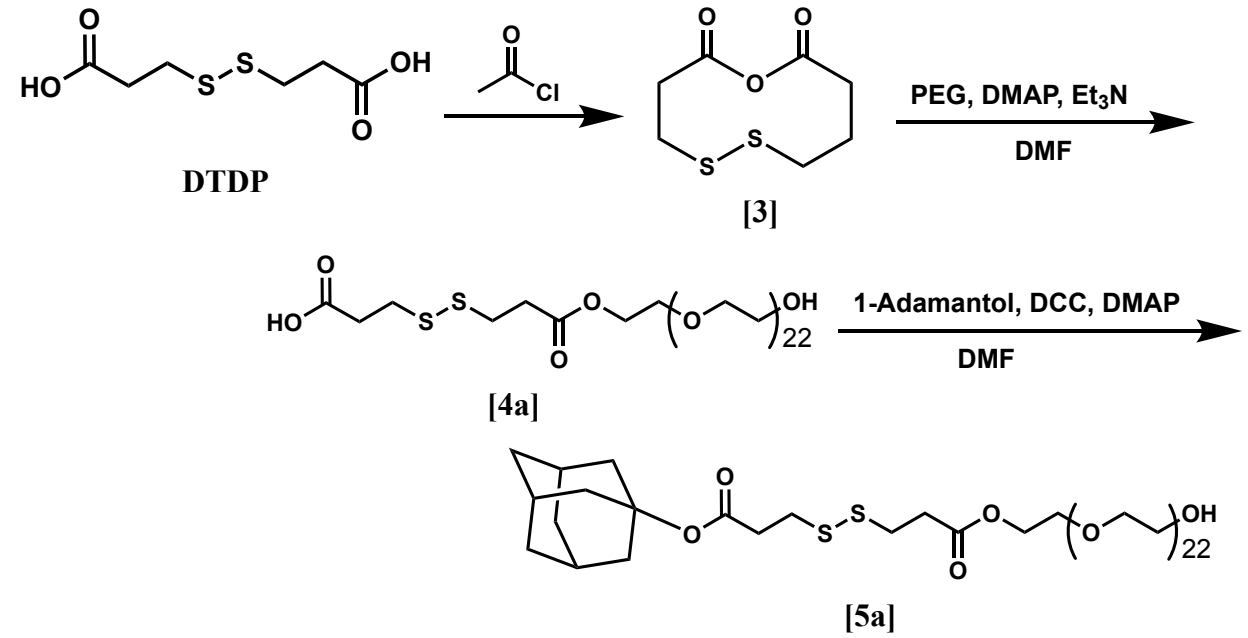

Scheme 2: Synthesis of **[3]** Dithiopropionic anhydride, **[4a]** Dithiopropionic acid-poly(ethylene glycol), and **[5a]** Adamantyl-dithiopropionic acid-poly(ethylene glycol) (AdSSPEG)

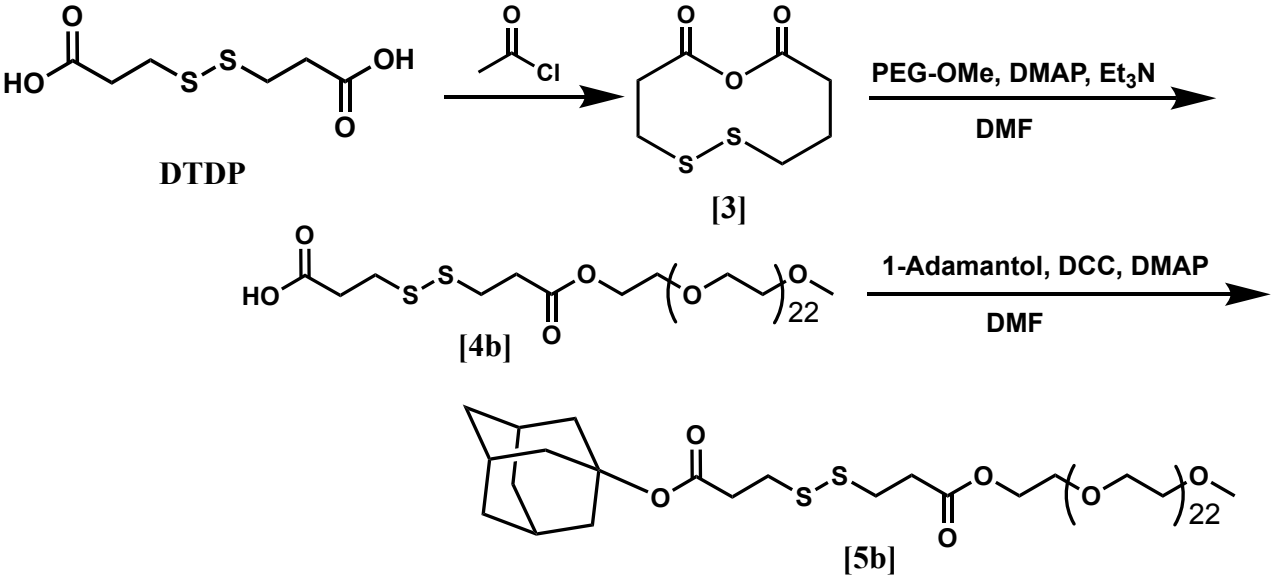

Scheme 3: Synthesis of **[3]** Dithiopropionic anhydride, **[4b]** Dithiodipropionic acid-poly(ethylene glycol)-methyl ether, and **[5b]** Adamantyl-dithiopropionic acid-poly(ethylene glycol)-methyl ether (AdSSPEGOMe)

Initially, DTDP was cyclized to form an anhydride. The anhydride ring was then opened via alcohol addition to covalently attach PEG (for [5a]) or PEGOMe (for [5b]). DCC was used as a coupling agent to attach an adamantane group to the terminal carboxylic acid of [4a] or [4b] to form the final product [5a] or [5b]. The first two steps of this synthetic pathway were simple and straightforward to execute in practice, while the final step required much more effort to isolate a pure final product due to the strong amphiphilicity of the linear guest molecules creating solubility challenges. PEG / PEGOMe molecules of 1000 g/mol were used because PEG with lower molecular weights are much more soluble in diethyl ether, and hence much more difficult to isolate via precipitation as a purification method. Additionally, lyophilizing the final product after dialysis was instrumental in removing all excess water and obtaining a pure product. Due to the amphiphilicity of the products, water was unable to be completely removed via rotary evaporation. Lyophilization was preferable because it converts water straight from the solid phase to the gas phase, while rotary evaporation converts water from the liquid phase to the gas phase. This is because the solid to gas transition occurs at a much lower temperature than the liquid to gas transition which decreases the amphiphilic molecules' ability to hold onto water molecules.

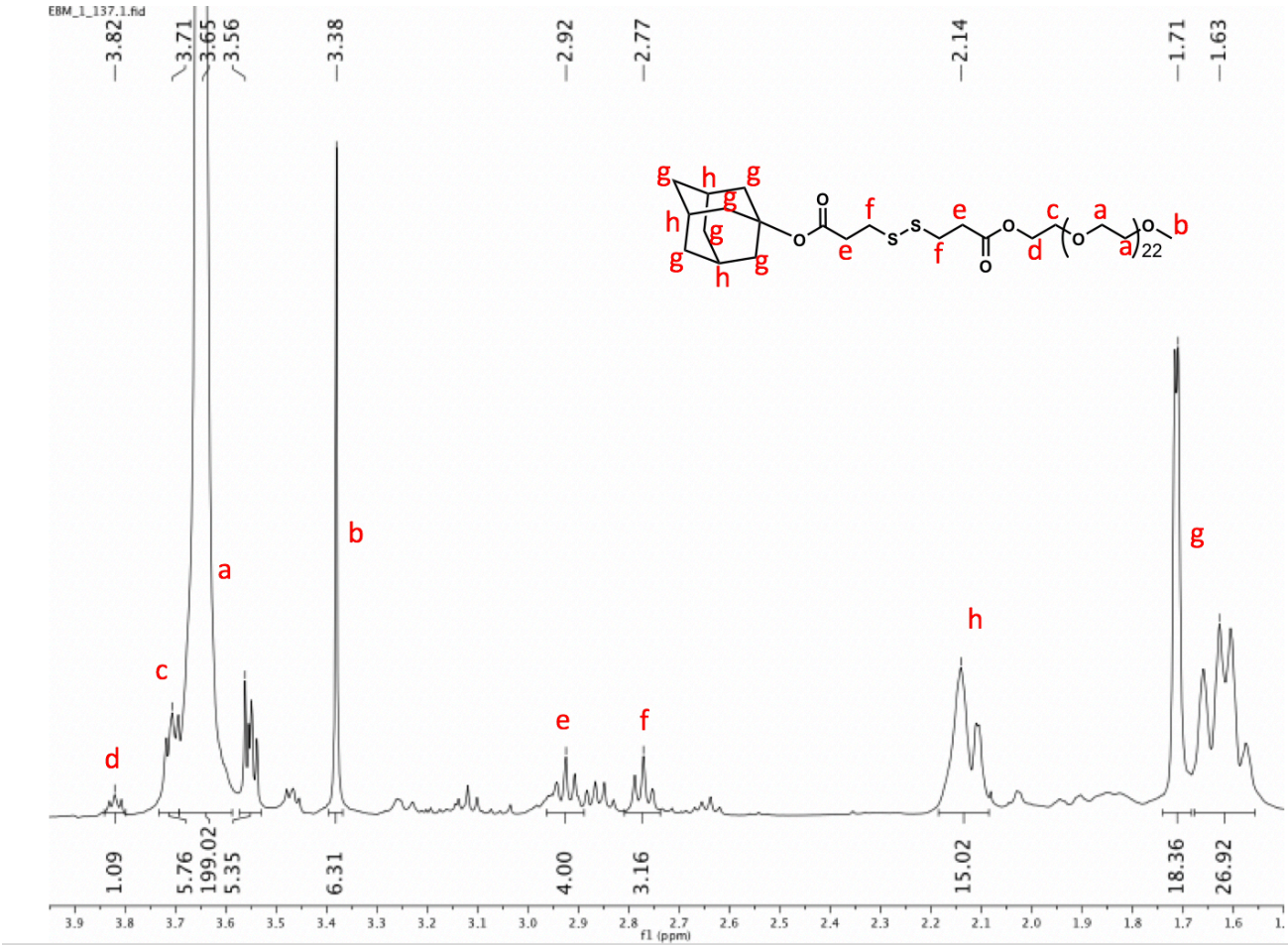

Figure 28: ^{1}H NMR of AdSSPEGOMe **[5b]** in deuterated chloroform ($CDCl_3$)

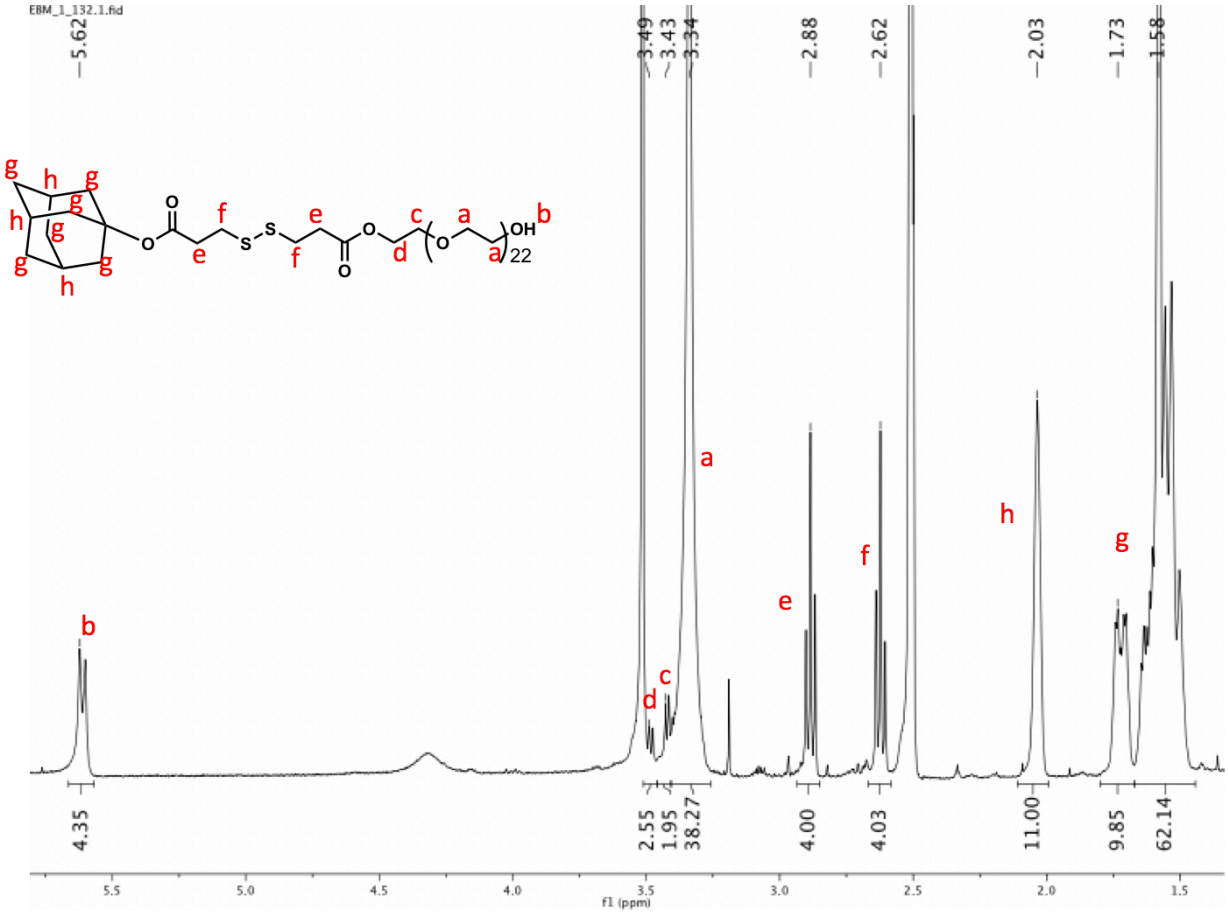

Figure 29: ^{1}H NMR of AdSSPEG **[5a]** in deuterated dimethylsulfoxide (DMSO)

Proton NMRs in Figures 28 and 29 correspond to AdSSPEGOMe and AdSSPEG [5b, 5a], respectively. Here, peaks labeled g and h correspond to protons within the adamantane group structure. Peak a corresponds to protons within the ethylene glycol repeat group, while peak b corresponds to the end group. For AdSSPEGOMe, this is three methyl protons, while for AdSSPEG this is one hydroxyl proton. Hydroxyl protons are known to have unreliable and broad chemical shifts (if they show up at all), so although the integration for the hydroxyl proton indicates four protons, it is actually just one. Peaks c and d correspond to the protons between the repeat group and the ester linkage, which were used to

confirm that the final product formed. The nearby oxygens on the ester group deshield these protons which pushes them slightly downfield of the rest of the PEG protons. Similarly, peaks f and e correspond to protons between the ester and disulfide linkages, where the disulfide group is less deshielding than the surrounding oxygens which results in these triplet peaks being upfield the PEG protons.

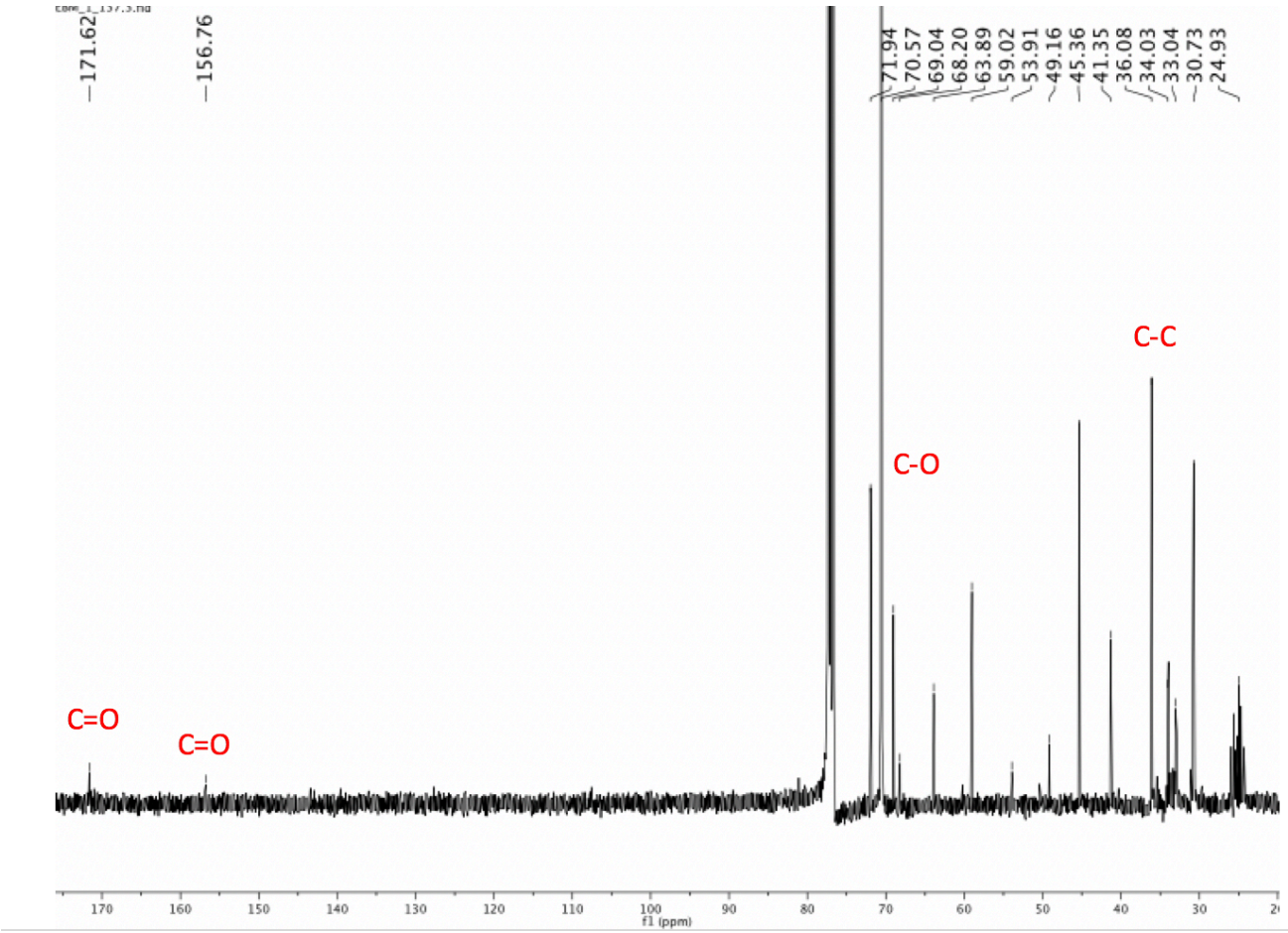

Figure 30: ^{13}C NMR of AdSSPEGOMe **[5b]** in deuterated chloroform ($CDCl_3$)

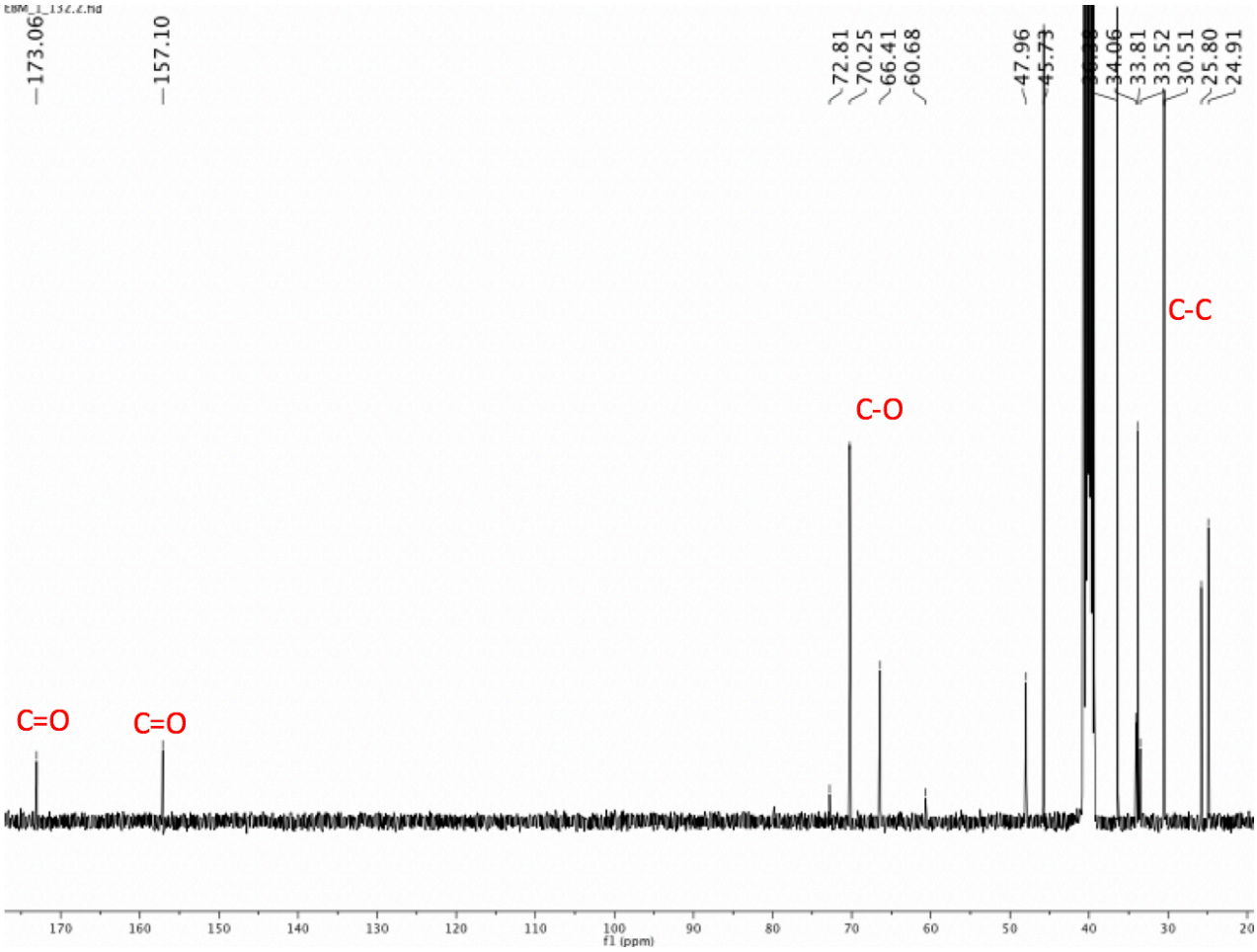

Figure 31: ^{13}C NMR of AdSSPEG **[5a]** in deuterated dimethylsulfoxide (DMSO)

Carbon NMRs in Figures 30 and 31 correspond to AdSSPEGOMe and AdSSPEG [5b, 5a], respectively. Here, carbonyl peaks labeled C=O correspond to the two ester peaks in the core of the guest molecule structure. They exhibit different chemical shifts as they are not equivalent due to the adamantyl linkage on one and PEG linkage on the other having different electron densities. The PEG group electron density is much lower than that of the adamantane group, which

causes the ester carbon attached to the PEG group to be more deshielded and appear slightly downfield from the ester carbon attached to the adamantane group.

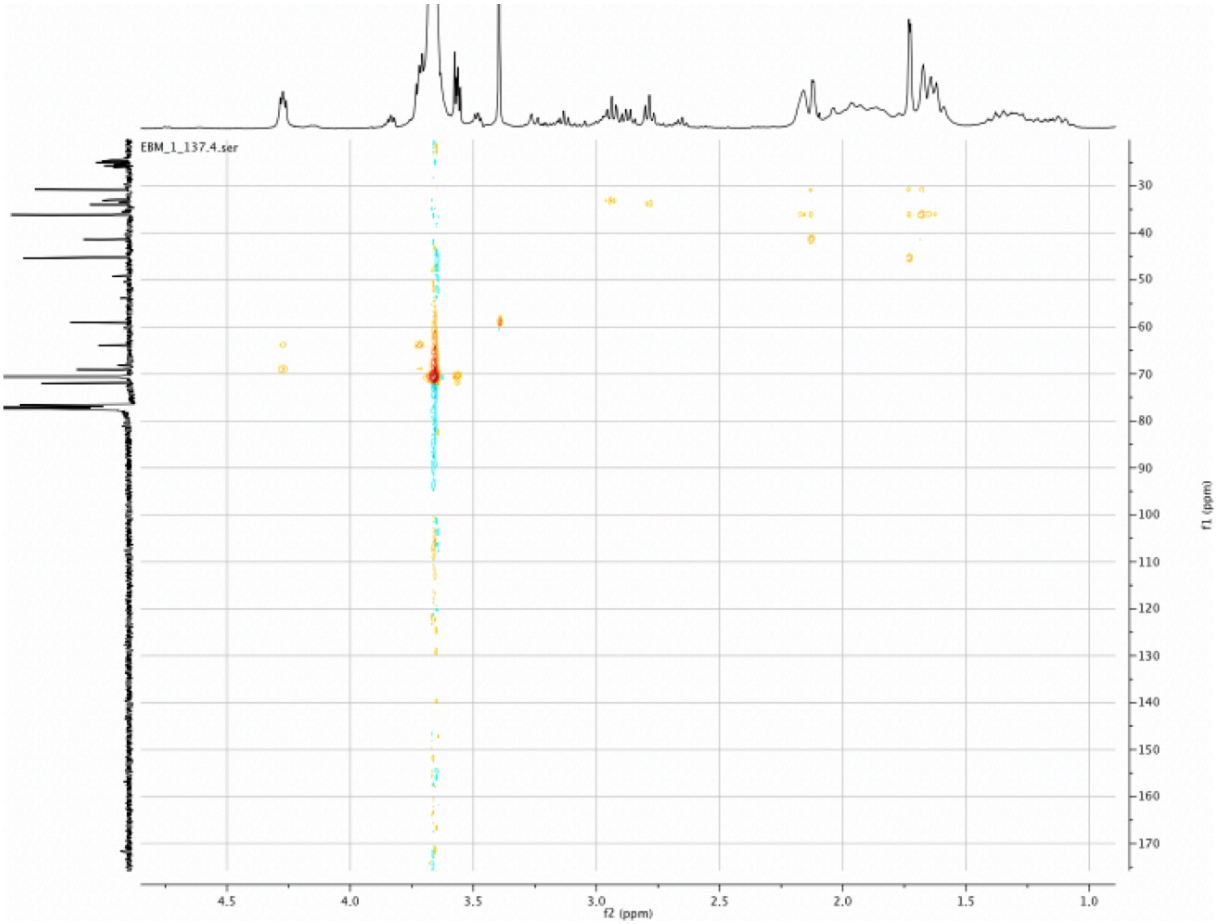

Figure 32: HQSC two-dimensional NMR of AdSSPEGOMe [5b] in deuterated chloroform ($CDCl_3$) shows correlations between ^{13}C NMR and ^{1}H NMR peaks

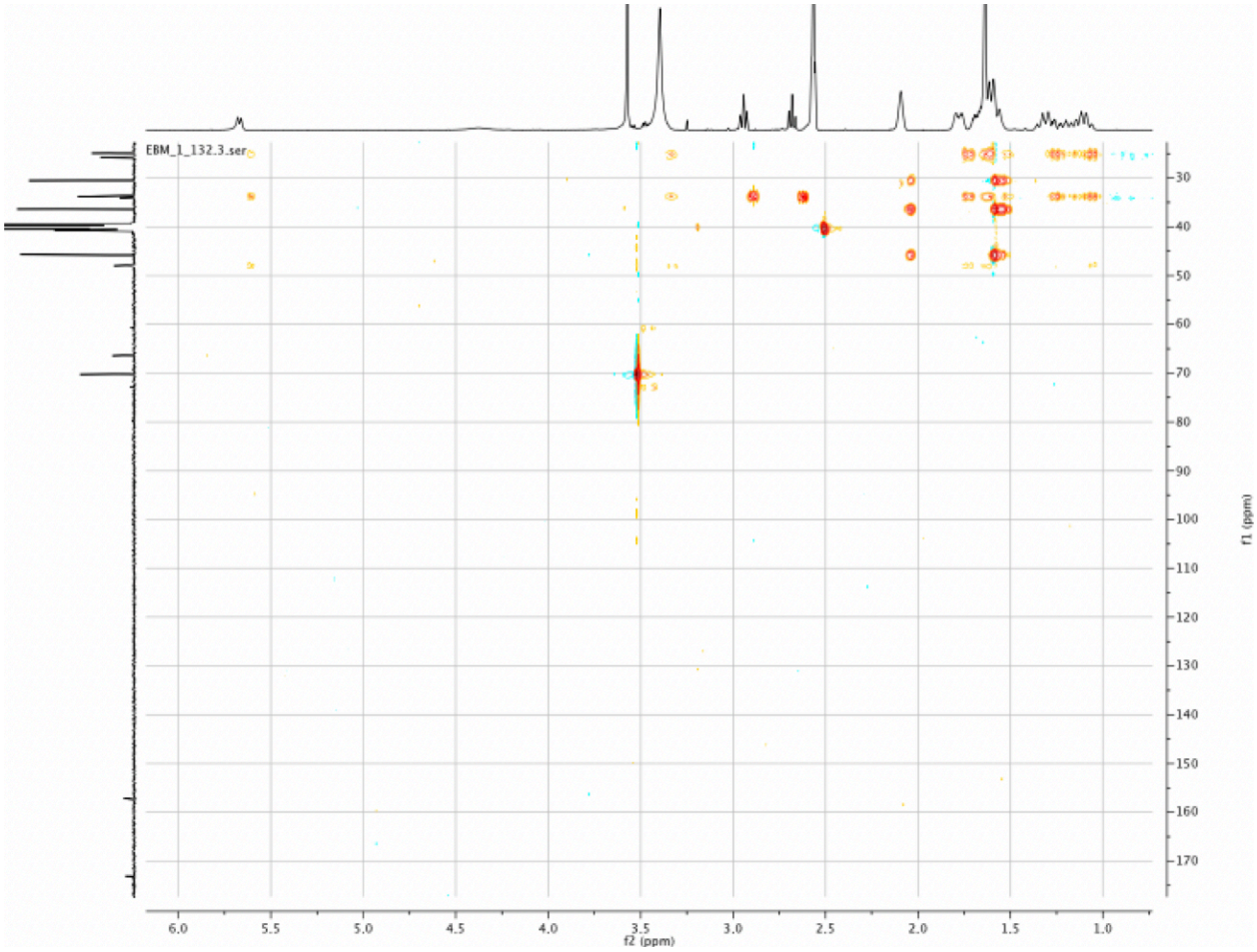

Figure 33: HQSC two-dimensional NMR of AdSSPEG **[5a]** deuterated dimethylsulfoxide (DMSO) shows correlations between ^{13}C NMR and ^{1}H NMR peaks

HSQC two-dimensional NMRs in Figures 32 and 33 correspond to AdSSPEGOMe and AdSSPEG [5b, 5a], respectively. They both show strong correlations between the proton and carbon NMR peaks.

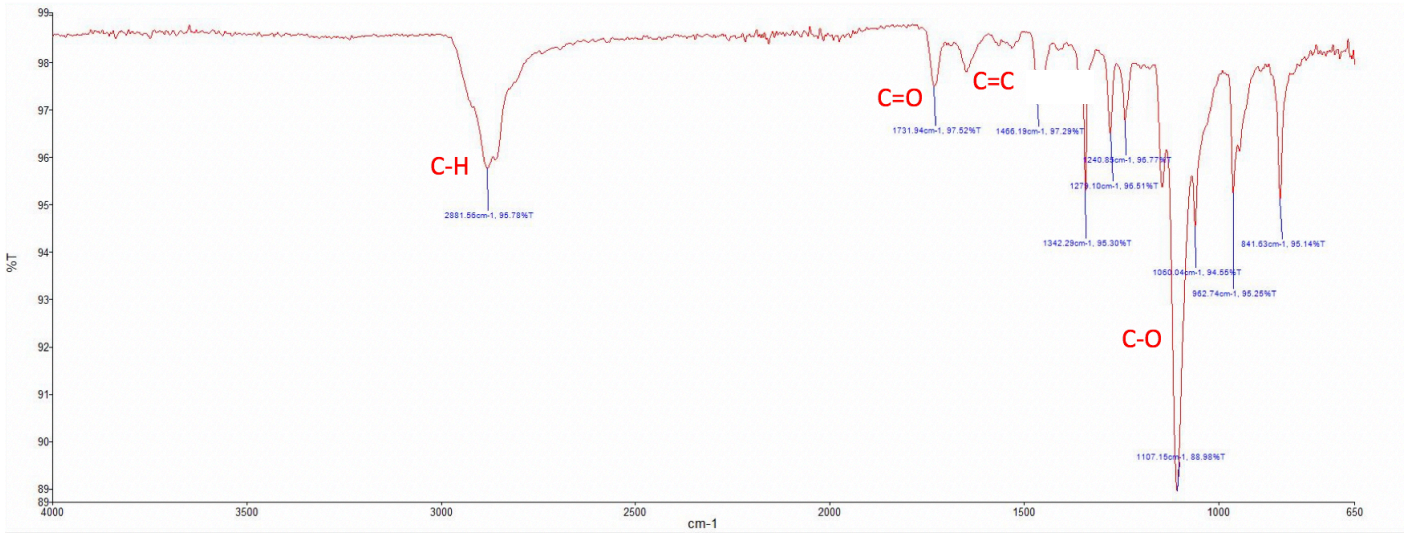

Figure 34: FTIR of AdSSPEGOMe **[5b]**

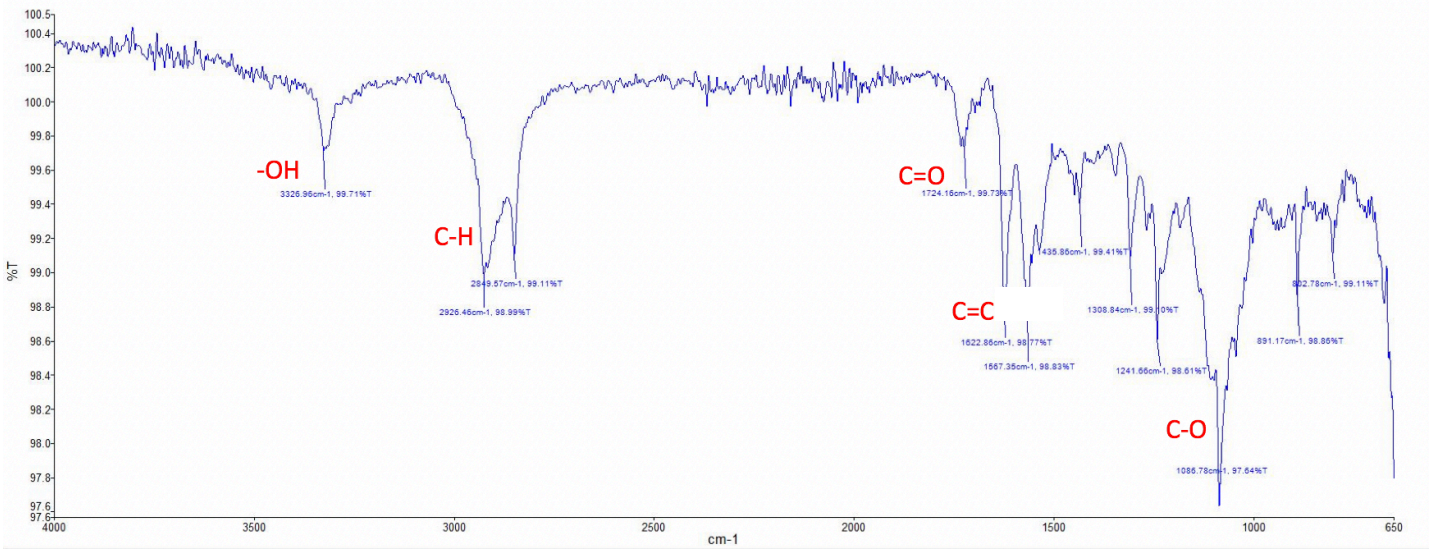

Figure 35: FTIR of AdSSPEG **[5a]**

FTIR spectra in Figures 34 and 35 correspond to AdSSPEGOMe and AdSSPEG [5b, 5a], respectively. Here, we can see a clear difference between the two structures which confirms singular substitution was achieved on the hydroxyl terminated AdSSPEG [5a], as we can see a clear hydroxyl peak around 3300 cm^{-1} in Figure 35, which is absent in Figure 34 with the methyl terminated

AdSSPEGOMe [5b], as expected. Typically, hydroxyl peaks on an FTIR spectra are broad but with AdSSPEG [5a] the peak is sharp. This is likely due to the other functional groups present in the polymer providing a shielding effect and decreasing the hydroxyl signal. Overall, both AdSSPEG and AdSSPEGOMe [5a, 5b] were synthesized successfully and in good yield (69-74%).

Synthetically, the AdSSPEGOMe [5b] derivative is much easier to synthesize as di-substitution of the PEG molecule does not have to be considered. Final products AdSSPEG and AdSSPEGOMe [5a, 5b], although structurally very similar, exhibit much different behavior in aqueous solutions. Dialysis with the AdSSPEG [5a] derivative required ethanol addition as a co-solvent to get the guest molecule to go into solution, which was not necessary with the AdSSPEGOMe [5b] derivative as it was water soluble on its own. This is due to the hydroxyl versus methyl groups terminating the PEG chain. Here, the hydroxyl group pulls electron density away from the PEG chain, while the methyl group does not. This creates an overall stronger dipole moment for the methyl terminated guest than the hydroxyl terminated guest which explains the difference in water solubility.

3.3 Synthesis of Thiol Modified Poly(ethylene-glycol) (PEG-diSH)

Thiol terminated linear PEG molecules (PEGdiSH) [7a-f] were synthesized according to Scheme 5 at various molecular weights (ie. 1000, 2000, 3400, 4000, 10000, and 20000 g/mol), and characterized via ^{1}H NMR to confirm that linear crosslinking molecules were synthesized as expected.

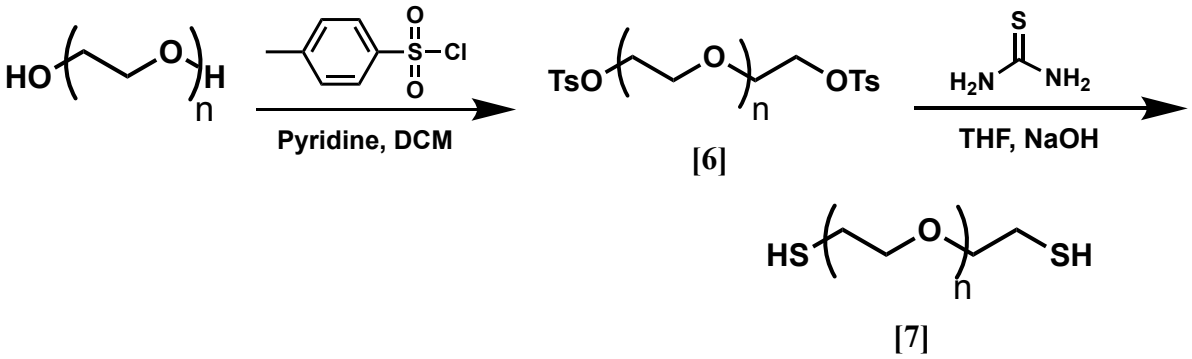

Scheme 4: Synthesis of **[6]** Poly(ethylene glycol)-di(p-toluenesulfonic acid) (PEGdiOTs), and **[7]** Poly(ethylene glycol)-dithiol (PEGdiSH) (n = 22 **[7a]**, 45 **[7b]**, 77 **[7c]**, 227 **[7e]**, 454 **[7f]**)

The ditosylation of PEG yielded excess unreacted TsCl that was very difficult to remove via aqueous workup. Instead, cellulose based filter paper was used to remove the excess TsCl. Here, the free hydroxyl groups in the cellulose structure are able to react with the excess TsCl when base is present to facilitate the substitution reaction in order to covalently bind the TsCl to the filter paper.[76] Therefore, the excess TsCl is able to be removed manually along with the filter paper. This method has proven to be extremely reliable and useful in obtaining a pure final product for use in the next synthetic step. The tosyl group provides a good leaving group for the nucleophilic S_N2 double substitution reaction in the next step, where both sides of the PEG chain covalently bind to the thiol. Addition of base then creates urea as a side product as the final product of dithiolated PEG (PEGdiSH [7]) is formed.

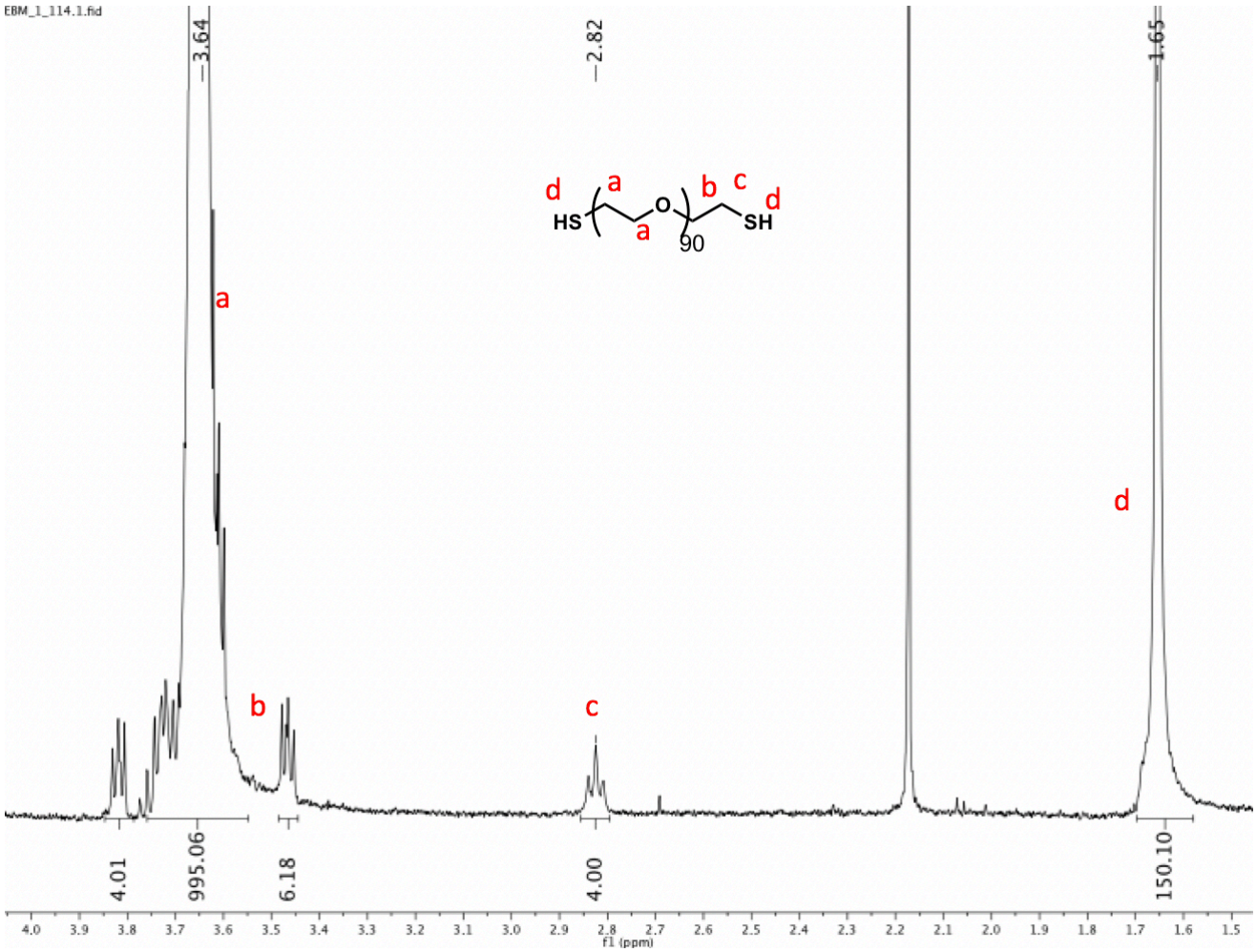

Figure 36: ^{1}H NMR of PEGdiSH (n = 90 **[7d]**, 4000 g/mol) in deuterated chloroform ($CDCl_3$)

The proton NMR in Figure 36 corresponds to PEGdiSH (n = 90 [7d]). Proton NMRs for PEGdiSH (n = 22 [7a], 45 [7b], 77 [7c], 227 [7e], 454 [7f]) can be found in the appendix. Here, peaks labeled a correspond to the ethylene glycol protons in the repeat unit. It is likely that there are varying amounts of free unreacted PEG from the first step of this two-step synthesis, as the integrations are much more than would be expected for each of these polymers. However, NMR is not the most optimal way to characterize polymers, so it is also possible that electrostatic effects from the polymer chains are overlapping and hence interfering with the peak

intensities to cause the discrepancy in integration values. Peaks labeled b and c correspond to the protons bonded to the two carbons closest to the terminal thiol group on each side of the polymer. Peak c is slightly more upfield than peak b because the thiol group is more shielding than the oxygen group nearby. Peaks labeled d may correspond to the terminal thiol protons. These integrations are also not what we would expect because thiol protons, like hydroxyl protons, are known to have broad and unreliable peaks in ^{1}H NMRs, if they show up at all. Additionally, peak d may also correspond to some type of grease, as this is also known to show up in the range of 1 ppm. Hence, the disappearance of tosyl proton peaks around 7-8 ppm and the appearance of peak c at 2.8 ppm were used to confirm the formation of the final PEGdiSH [7] products.

PEGdiSH (n = 90 [7d], 227 [7e], and 454 [7f]) molecules are the purest comparatively, with only trace solvent peaks remaining from DMF and acetone. PEGdiSH (n = 22 [7a], 45 [7b], and 77 [7c]) had some other trace impurities present, but the molecules were deemed pure enough to use in subsequent reactions since these impurities had relatively small signals compared to the signals from the final product. Overall, PEGdiSH [7a-f] molecules were synthesized successfully. Yields from this synthetic pathway (27-48%) were not as high as we would typically like them to be for organic substitution reactions, but since all the starting materials are so inexpensive and widely available, the reactions did not need to be further optimized for our purposes.

3.4 Inclusion Complex Formation

Inclusion complexes were formed according to the method described in section 2.7, which is also demonstrated in Figure 37, by taking advantage of the hydrophobic effect through combining host and guest molecules in an aqueous environment. Here, the thioalkyl modified βCDs [2a, 2b] have very poor water solubility, so it is necessary to sonicate to help them go into solution so that host: guest inclusion complexes could be formed.

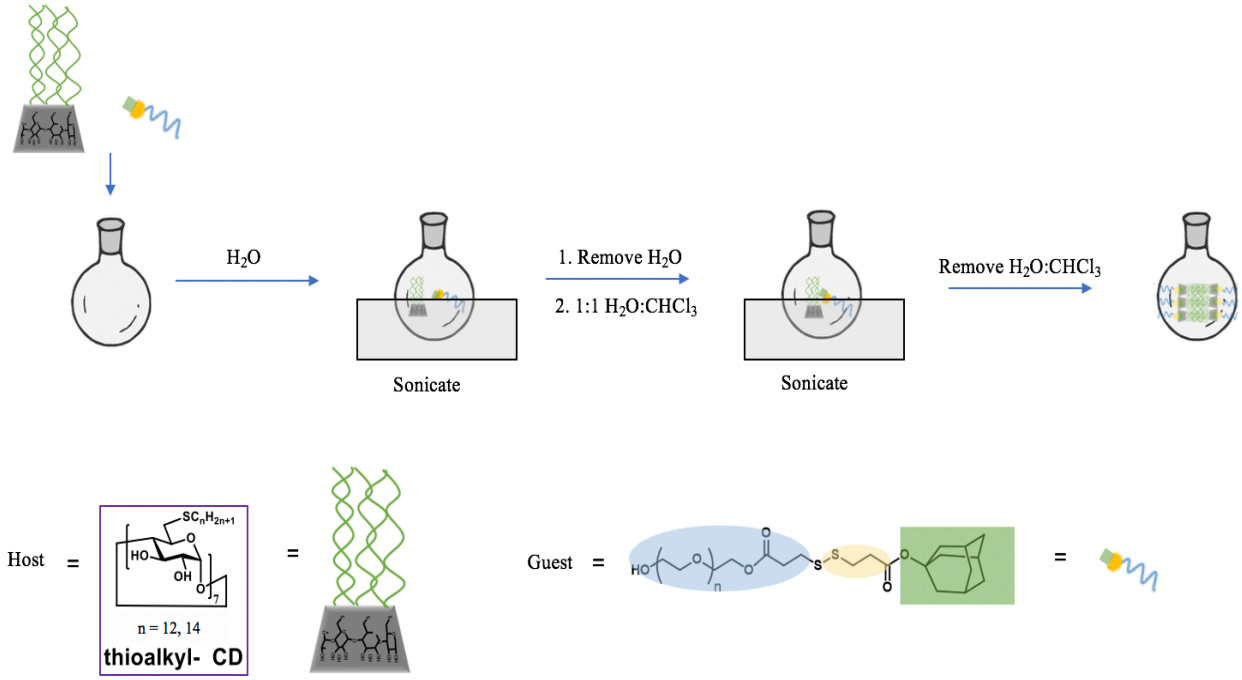

Figure 37: Supramolecular amphiphile inclusion complex formation method with thioalkyl modified βCD **[2a, 2b]** host, and adamantyl-dithiopropionic acid modified PEG / PEGOMe **[5a, 5b]** guest. The hydrophobic effects drives inclusion when combining host and guest molecules in aqueous media, which affords a thin film inclusion complex to be used in future vesicle formation methods

Four different host: guest combinations were made and tested- βCD-C12:AdSSPEGOMe, βCD-C12:AdSSPEG, βCD-C14:AdSSPEGOMe, and βCD-

C14:AdSSPEG. Here, C12 and C14 indicate the thioalkyl chain length attached to position 6 of the βCD. In this preparation method, sonication is an important step which helps bring the host and guest molecules into solution in order to drive inclusion complex formation. The process is repeated twice to give a higher probability that the inclusion complex will have formed. There are several methods commonly used to test for inclusion complex formation which often include examining the host and guest molecules on their own, a physical mixture of the host and guest molecules, and the inclusion complex. Among these are NMR, differential scanning calorimetry (DSC), and thermogravimetric analysis (TGA). NMR is not a particularly reliable method especially with non-ionic inclusion complexes, because it is likely that the chemical shifts will not show a distinct change with inclusion complexation. Here, the βCD inclusion complexes are not very water soluble, so obtaining comparable NMR data from hosts and guests on their own is also very difficult because the spectra appear broad and it is difficult to discern chemical shifts in peaks of interest. DSC and TGA measurements measure differences in phase transition and degradation temperatures, respectively. These methods are not useful in this case because we are not interested in these properties of our inclusion complexes, as they are designed to be used under physiological conditions, there is simply no need to test them at extreme conditions. Here, inclusion complex formation was confirmed through CMC testing with host and guest on their own compared to inclusion complexes, as described in sections 2.10.2 and 3.5. This is because the CMC is an important parameter for amphiphilic self-assembly as it gives the minimum concentration required to form aggregates

with a particular supramolecular amphiphile in aqueous solutions. All four supramolecular amphiphile inclusion complexes efficaciously and consistently form, as further discussed in section 3.5.

3.5 Critical Aggregation Concentration (CMC) via Fluorimetry

Nile red was chosen as a fluorescent probe for determining CMC because of its unique behavior in aqueous versus organic solutions. As demonstrated by Figure 38, nile red exhibits different emission wavelengths depending on whether it exists in a hydrophilic or a lipophilic environment.[75]

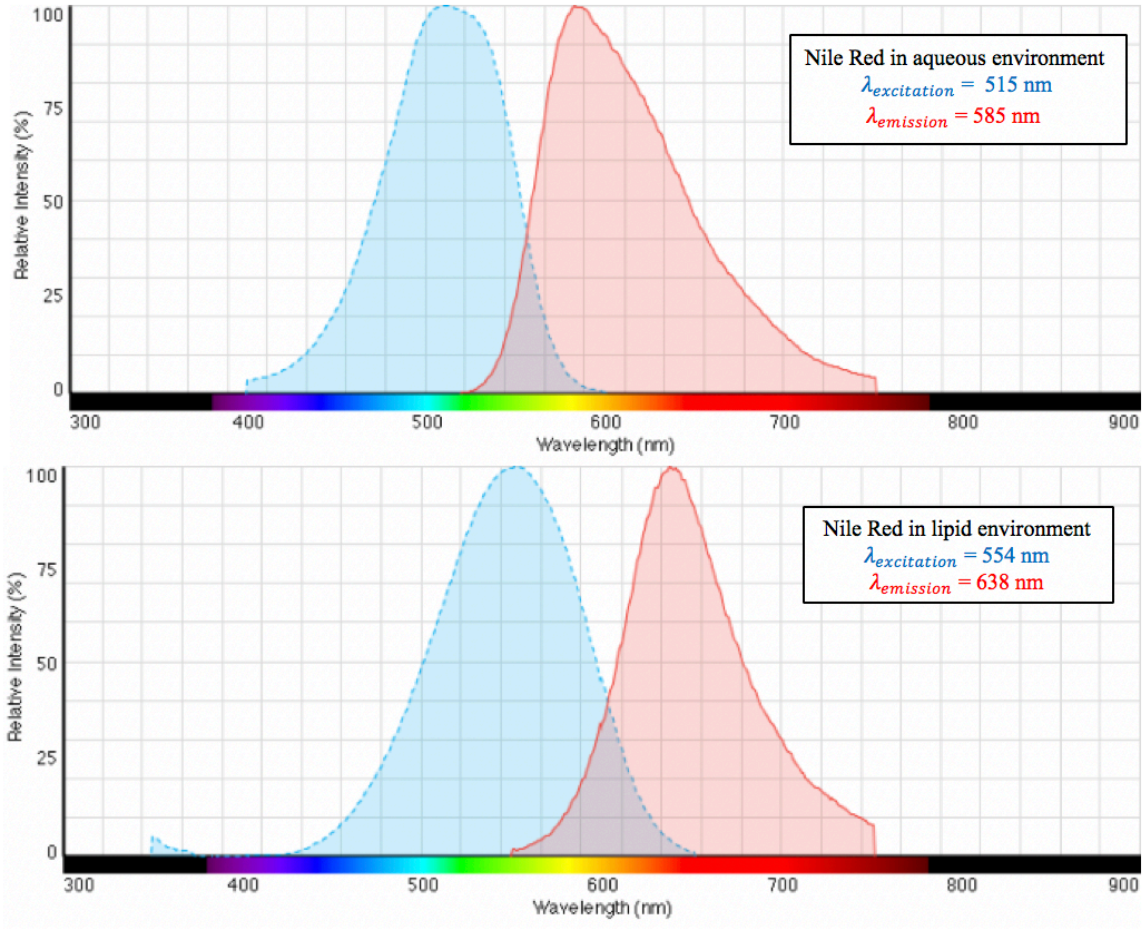

Figure 38: Nile red emission spectra in aqueous environments ($\lambda_{excitation}$ = *515 nm,* $\lambda_{emission}$ = *585 nm*) compared to lipid environments ($\lambda_{excitation}$ = *554 nm,* $\lambda_{emission}$ = *638 nm*) shows a notable shift in wavelength

The stokes shift, or the difference in energy between excitation and emission bands, is slightly larger for the lipophilic environment which makes it easier to detect with emission spectroscopy. Experimentally, a broad emission from approximately 530-640 nm was observed for amphiphile concentrations below the CMC, while a sharp emission at 638 nm was observed at amphiphile concentrations above the CMC.

Nile red on its own is practically insoluble in water, so it tends to migrate to the air-water interface of aqueous solutions. When amphiphile is added to this solution, the nile red will be attracted to the hydrophobic moieties. As concentration of amphiphile is increased amphiphile will begin to self-assemble into a monolayer, and eventually a micelle due to the hydrophobic effect, as previously mentioned in section 1.3.2. Since the nile red is attracted to the hydrophobic moieties, it becomes encapsulated in the lipophilic interior of the micelle once formed, which then alters its fluorescence behavior. This process is summarized in Figure 39.

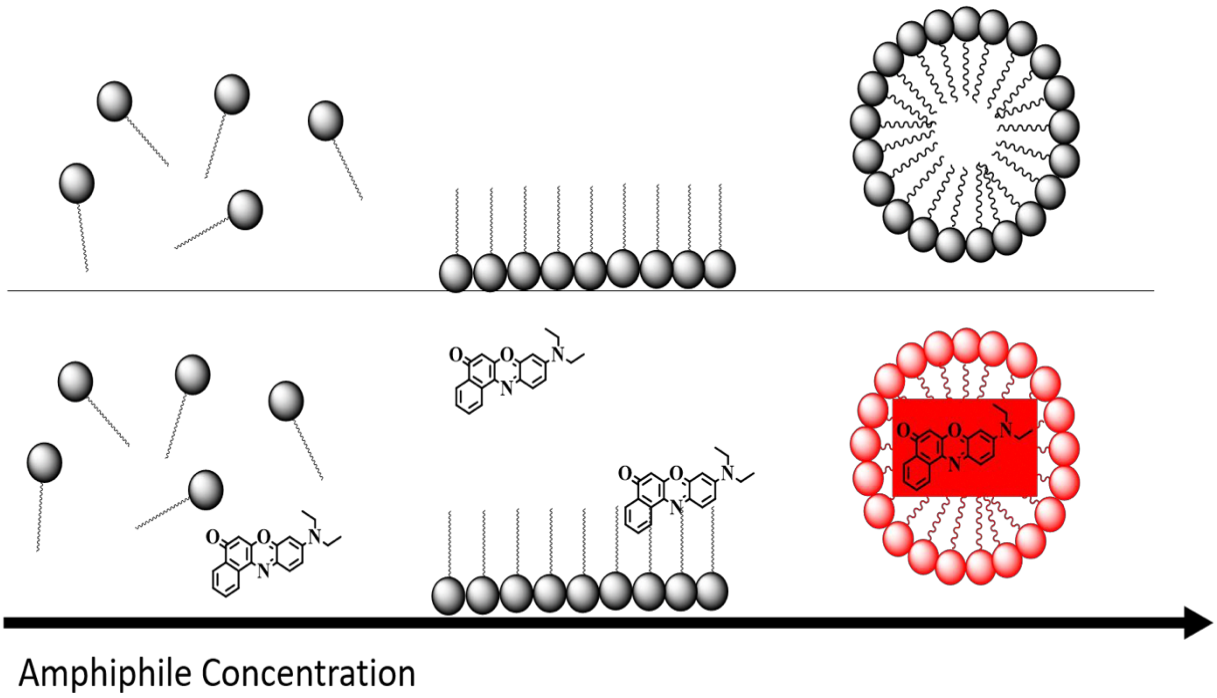

Figure 39: As amphiphile concentration is increased in aqueous solutions, amphiphilic molecules are driven to self-assemble into monolayers and eventually micelles due to the hydrophobic effect. Nile red becomes encapsulated in the lipophilic interior of the micelle as it is attracted to its hydrophobicity

Fluorescence spectroscopy was ran according to the method described in section 2.10.2 with each inclusion complex (ie. βCD-C12:AdSSPEGOMe, βCD-C12:AdSSPEG, βCD-C14:AdSSPEGOMe, and βCD-C14:AdSSPEG), as well as the linear AdSSPEGOMe [5b] guest molecule on its own. The guest molecule was tested on its own to confirm that the inclusion complexes are forming unique supramolecular amphiphiles, and that we were not just observing the self-assembly of the guest molecule. Macrocyclic βCD-C12 [2a] and βCD-C14 [2b] hosts were not tested on their own due to their poor water solubility. Because of this, it is highly impractical that they would self-assemble on their own. Overall, this method

yielded consistent results, and for each sample there was a note-able difference in λ_{em} maximum before and after the CMC, which was as expected since nile red emits at higher wavelengths in lipophilic environments, such as the interior of a micelle. Raw data in Figure 40 demonstrates this difference for one sample before and after the CMC.

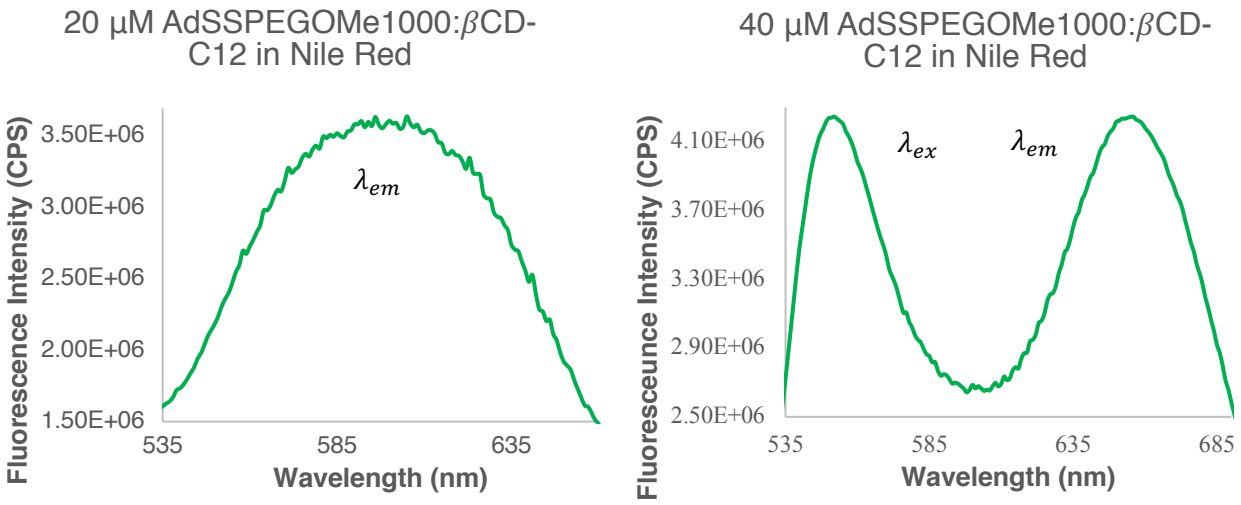

Figure 40: Fluorescence emission spectrum of supramolecular amphiphile AdSSPEGOMe:βCD-C12 before the CMC at 585 nm (left) and after the CMC at 638 nm (right). Initial excitation at 515 nm before the CMC (left) is not shown because wavelengths were only monitored in the range of 530 – 670 nm. Excitation was at 554 nm after the CMC (right)

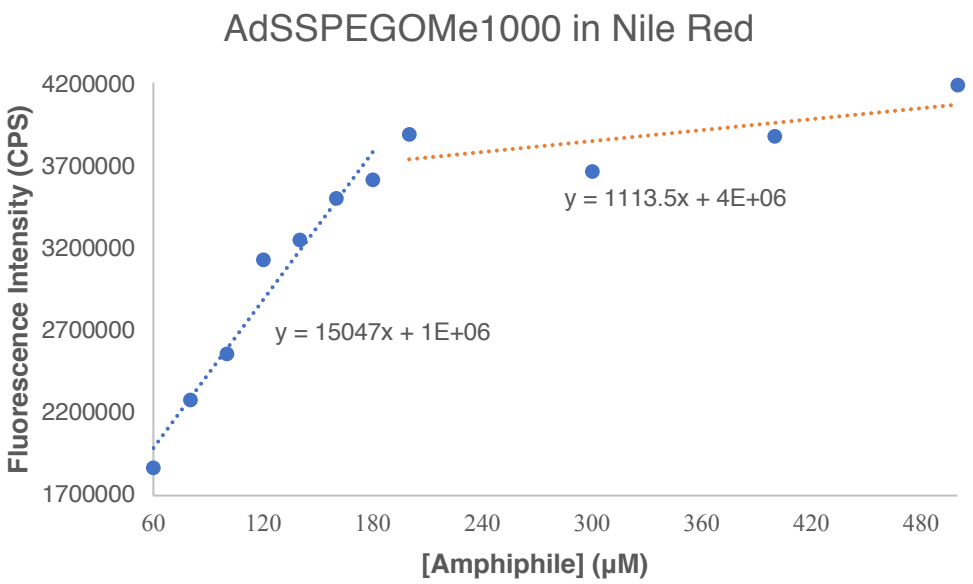

Figure 41: AdSSPEGOMe **[5b]** linear guest molecule CMC measured via fluorescence emission spectroscopy at approximately 638 nm and various concentrations of amphiphile and nile red held constant at 0.156 μg/mL. CMC was found to be 200.54 μM

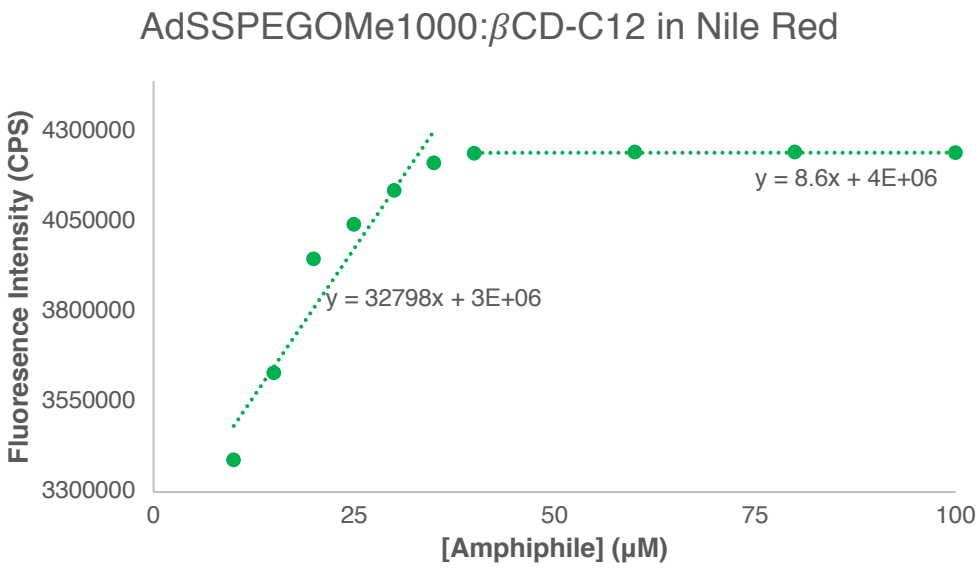

Figure 42: AdSSPEGOMe:βCD-C12 inclusion complex CMC measured via fluorescence emission spectroscopy at approximately 638 nm and various concentrations of amphiphile and nile red held constant at 0.156 μg/mL. CMC was found to be 30.50 μM

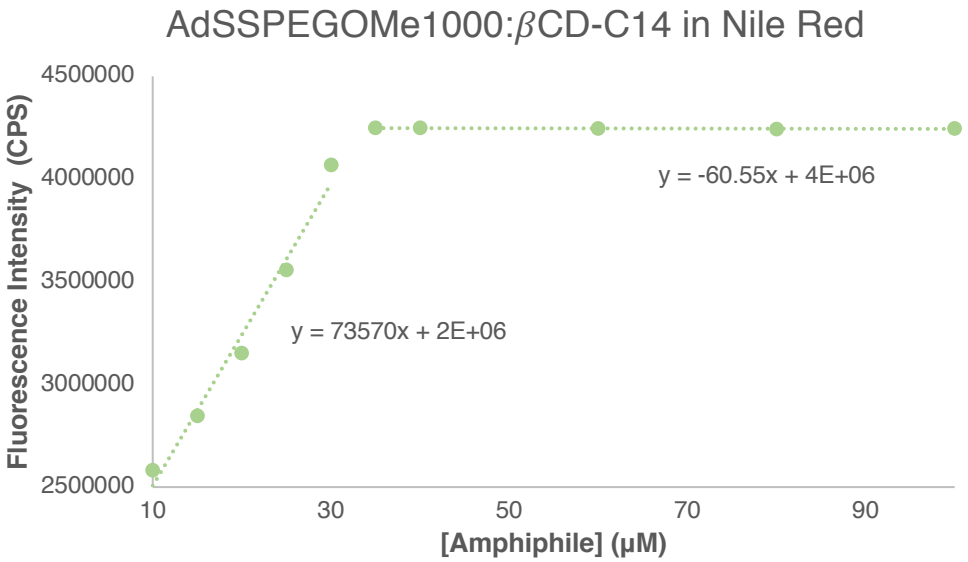

Figure 43: AdSSPEGOMe:βCD-C14 inclusion complex CMC measured via fluorescence emission spectroscopy at approximately 638 nm and various concentrations of amphiphile and nile red held constant at 0.156 μg/mL. CMC was found to be 27.16 μM

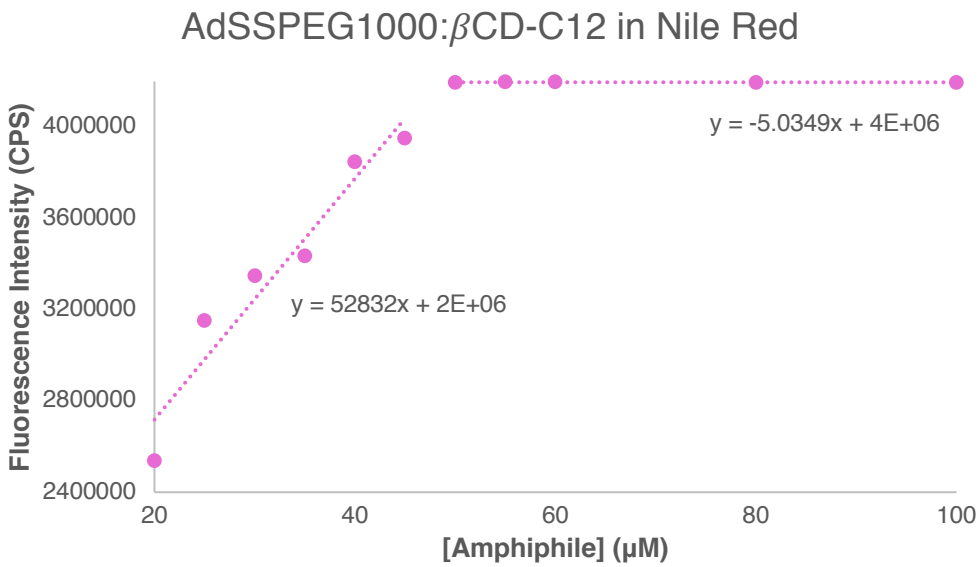

Figure 44: AdSSPEG:βCD-C12 inclusion complex CMC measured via fluorescence emission spectroscopy at approximately 638 nm and various concentrations of amphiphile and nile red held constant at 0.156 μg/mL. CMC was found to be 37.85 μM

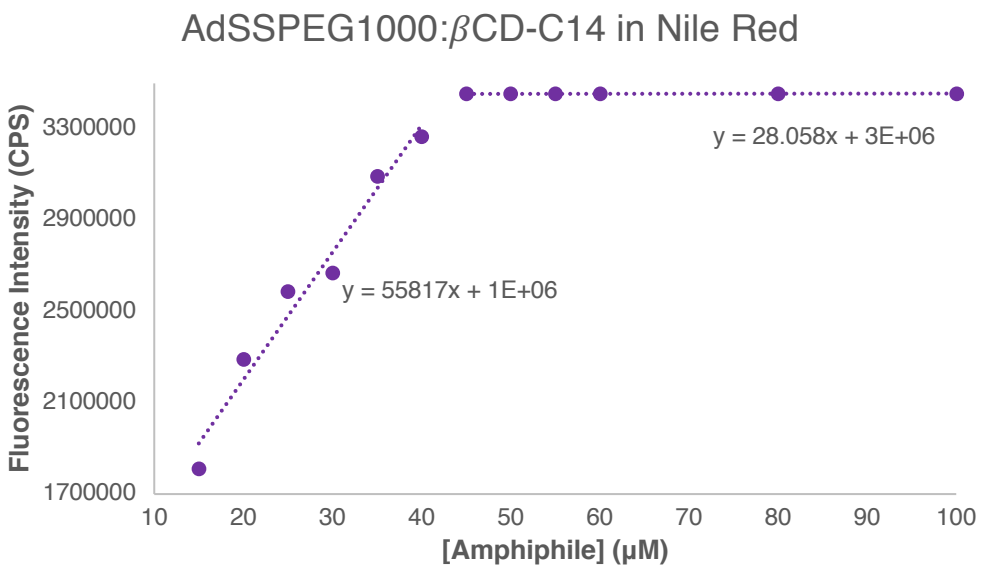

Figure 45: AdSSPEG:βCD-C14 inclusion complex CMC measured via fluorescence emission spectroscopy at approximately 638 nm and various concentrations of amphiphile and nile red held constant at 0.156 μg/mL. CMC was found to be 35.97 μM

Table 2: CMC results for all inclusion complexes and AdSSPEGOMe guest molecule on its own confirm inclusion complex formation, and give the minimum aggregation concentrations required for self-assembly

Sample	CMC (μM)
AdSSPEGOMe1000:βCD-C12	30.50
AdSSPEGOMe1000: βCD-C14	27.16
AdSSPEG1000: βCD-C12	37.85
AdSSPEG1000: βCD-C14	35.97
AdSSPEGOMe1000	200.54

Figures 41-45 and Table 2 summarize these results. For each sample, we see a stark difference in slope before and after the CMC, which was as expected. Here, the AdSSPEGOMe [5b] guest molecule (Figure 41) was shown to exhibit a CMC at more than five times that of all the inclusion complexes (Figures 42-45),

as it is more soluble in water on its own than it is when it is included in the thioalkyl modified βCD host. Additionally, thioalkyl βCD inclusion complexes with longer alkyl chains (ie. C14) have lower CMCs, which is also consistent with the principles of the hydrophobic effect and micellization; longer alkyl chains are less soluble in aqueous solutions and therefore tend to aggregate at lower concentrations than molecules with shorter alkyl chains. Similarly, AdSSPEG [5a] inclusion complexes have slightly higher CMCs than AdSSPEGOMe [5b] inclusion complexes, which could be due to the terminal hydroxyl group of AdSSPEG [5a] having more hydrogen bonding ability than the methyl ether group and hence increasing water solubility. These results were useful for subsequent vesicle formation reactions as the minimum aggregation concentration was increased to form vesicles, and the minimum amount of materials was used.

3.6 Vesicle Formation

Vesicles were formed according to the method described in section 2.8, which is also demonstrated in Figure 46. Here, thin film inclusion complexes, as demonstrated by Figure 47, are suitable for rehydration to form vesicles via this method.

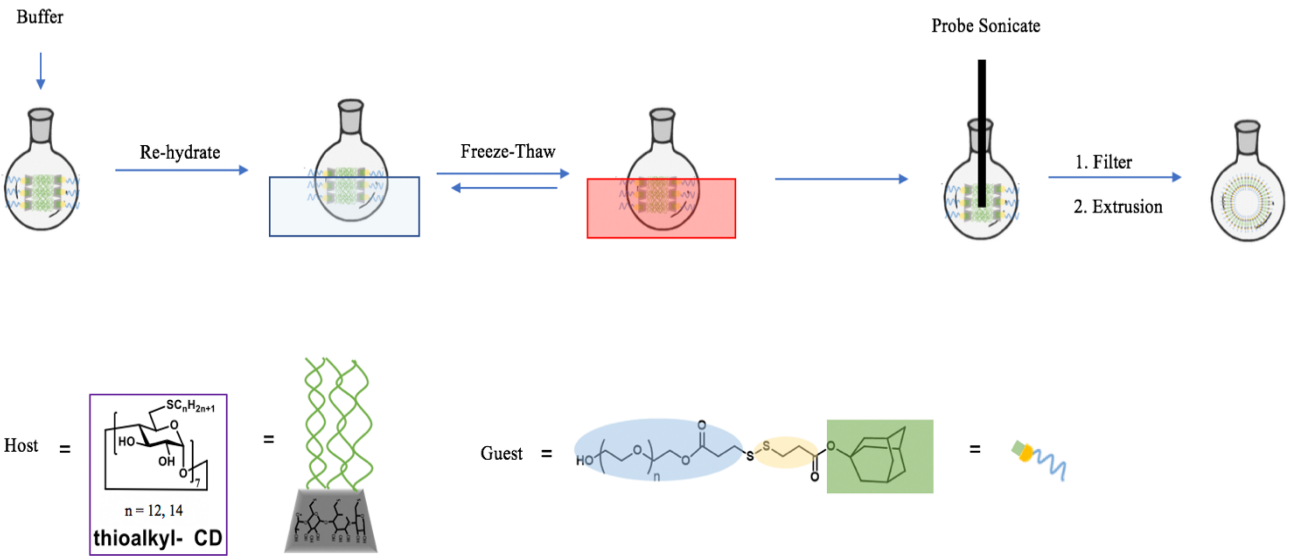

Figure 46: Thin film inclusion complex with thioalkyl modified βCD **[2a, 2b]** host, and adamantyl-dithiopropionic acid modified PEG / PEGOMe **[5a, 5b]** guest is rehydrated with Tris buffer and subjected to five freeze-thaw cycles to afford vesicles. The solution is probe sonicated to break up any larger aggregates, filtered, and extruded to obtain pure monodisperse vesicles

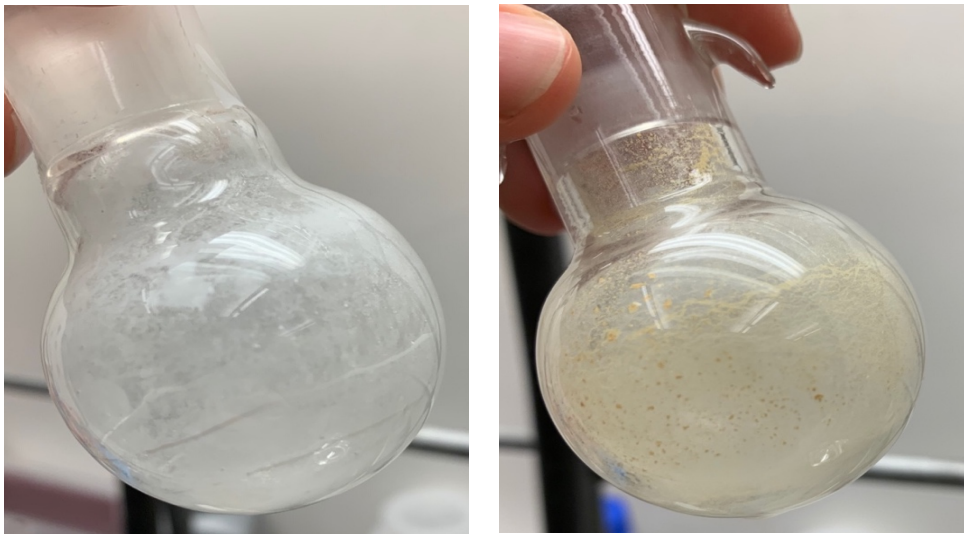

Figure 47: Inclusion complexes βCD-C12:AdSSPEG (left), and βCD-C14:AdSSPEGOMe (right) form thin films in round bottom flasks that are suitable for rehydration to form vesicles

Four different inclusion complexes were used to make vesicles- βCD-C12:AdSSPEGOMe, βCD-C12:AdSSPEG, βCD-C14:AdSSPEGOMe, and βCD-C14:AdSSPEG. Controls with AdSSPEGOMe [5b], AdSSPEG [5a], βCD-C12 [2a], and βCD-C14 [2b] on their own were also tested to further confirm that only the inclusion complexes self-assemble to bilayered vesicles. Freeze-thaw cycles "shock" the supramolecular amphiphiles and helps drive their self-assembly, while probe sonication breaks up larger aggregates that may have formed during this process. Filtering removes these larger particles, and extrusion further purifies the vesicle solution to obtain a more monodisperse sample. Probe sonication and extrusion methods were used to together as this method yielded the most consistent and stable vesicles as compared to just extrusion or just probe sonication as an isolation method, which will be further discussed in section 3.9. Vesicle solutions in Tris buffer were made at pH 7.4 and 8.5.

For this project we did not have access to high resolution microscopy such as SEM to confirm vesicle formation, so in order to confirm that vesicles were forming as expected, we encapsulated a fluorescent dye in the vesicle interior and destroyed them, as described in section 2.10.1 and discussed in section 3.8, and measured their particle size using dynamic light scattering to see if they were consistent with literature references, as described in section 2.11.1 and discussed in section 3.9. Overall, none of the control samples formed vesicles. All inclusion complexes formed vesicles consistently, and their particle sizes were consistent with literature values (100-250 nm diameter),[61-74] and were stable for several weeks

up to approximately one month before degradation and/or aggregating into larger particles.

3.7 Fluorescent Vesicle Formation

Fluorescent vesicles were formed according to the method described in section 2.9, which is also demonstrated in Figure 48.

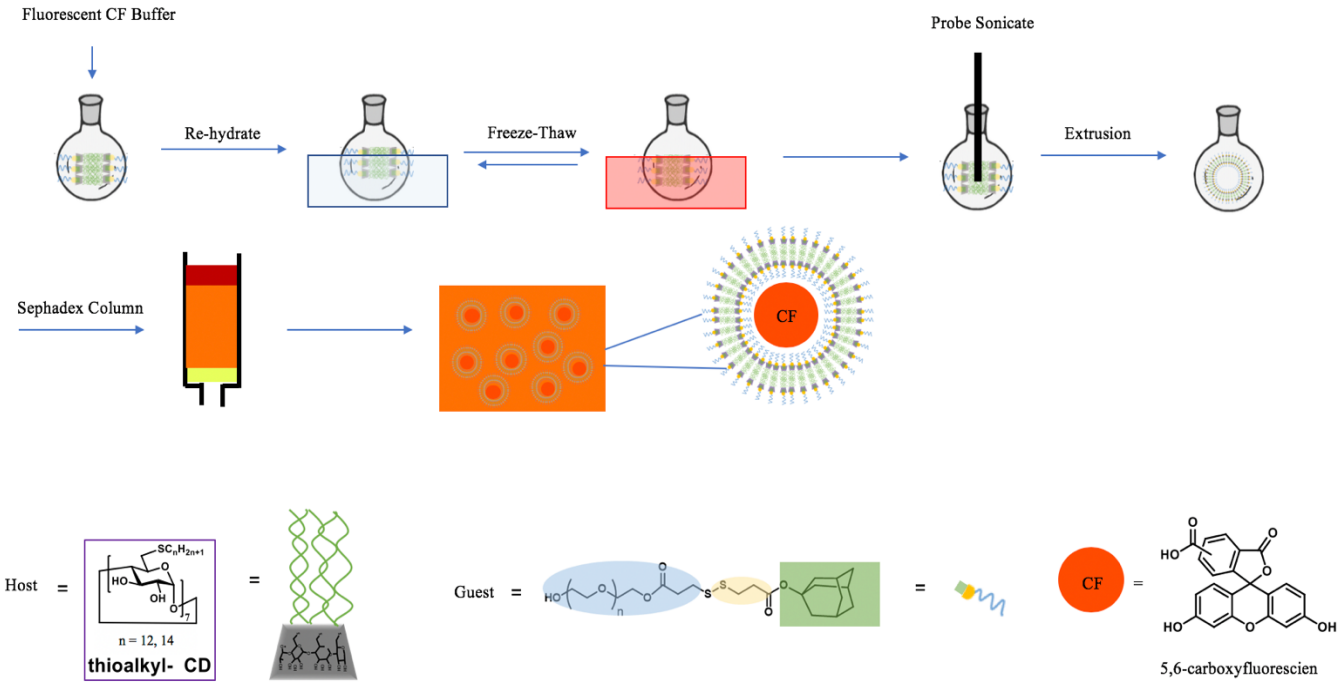

Figure 48: Thin film inclusion complex with thioalkyl modified βCD **[2a, 2b]** host, and adamantyl-dithiopropionic acid modified PEG / PEGOMe **[5a, 5b]** guest is rehydrated with CF buffer and subjected to five freeze thaw cycles to afford vesicles. The solution is probe sonicated to break up any larger aggregates, filtered, and extruded. The resulting vesicle containing solution is further purified with a sephadex G-50 column to obtain pure monodisperse vesicles with encapsulated CF

Four different inclusion complexes were used to make fluorescent vesicles- βCD-C12:AdSSPEGOMe, βCD-C12:AdSSPEG, βCD-C14:AdSSPEGOMe, and βCD-

C14:AdSSPEG. Controls with AdSSPEGOMe, AdSSPEG, βCD-C12, and βCD-C14 on their own were also tested to further confirm that only the inclusion complexes self-assemble to bilayered vesicles. This method is similar to the previously discussed vesicle formation method in section 3.6, with the modification of a fluorescently labeled CF buffer, and a sephadex G-50 column to remove free CF that was not encapsulated in the vesicle interior and any smaller aggregates that may have survived extrusion.

This sephadex G-50 column is a size exclusion chromatography method which elutes larger particles first as they are not absorbed into the porous medium like smaller particles are. This method allows for the isolation of pure monodisperse vesicles with encapsulated fluorescent CF, as demonstrated by Figure 49. By encapsulating a fluorescent small molecule during vesicle formation, we were able to determine if vesicles are forming as expected, and if they are capable of encapsulating small molecules. These parameters are tested via methods described in section 2.10.1 and discussed in section 3.8. Overall, all inclusion complexes formed vesicles and encapsulated the small molecule CF consistently, while controls did not show any signs of vesicle formation or subsequent encapsulation of CF.

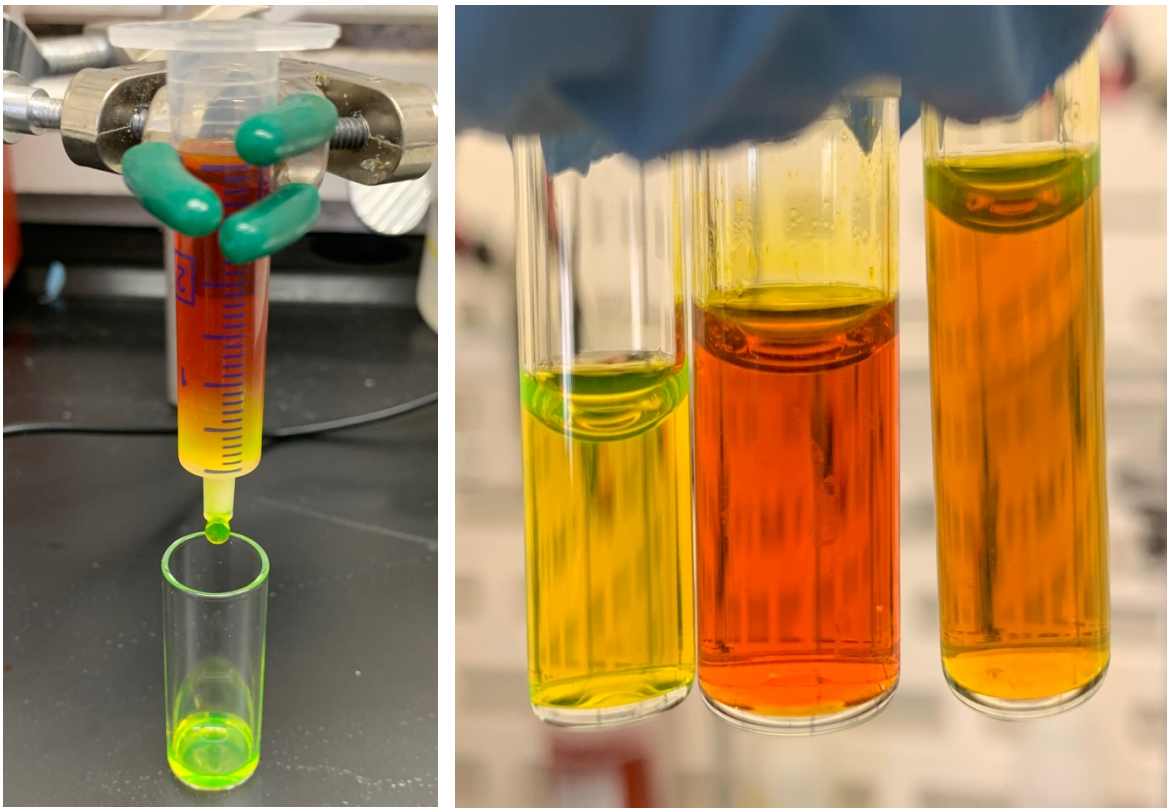

Figure 49: Sephadex G-50 column (left) elutes free CF, vesicles, and then smaller aggregates such as micelles. Fractions 1-3 (right) are bright yellow, orange, and brown (left-right) where the bright yellow fraction contains free CF, the orange fraction contains vesicles, and the brown fraction contains smaller aggregates

3.8 Fluorescent Vesicle Encapsulation and Lysing via Fluorimetry

Fluorescent vesicles and controls were prepared according to the methods described in section 2.9, and discussed in section 3.7. Fluorescence spectroscopy was ran according to the methods described in section 2.10.1 to probe the behavior of the vesicles to see if they formed and encapsulated fluorescent probe CF as expected. This method relies on the principles of the quenching of fluorescence, which is a process in which a fluorophore comes into contact with a quencher by either a static or dynamic mechanism to effectively decrease the fluorescence

intensity of a sample.[77] In the case of CF, it acts as both the fluorophore and the quencher through a static mechanism as it forms non-fluorescent dimers with itself at high concentrations.[78] For these experiments, CF was encapsulated in the interior of supramolecular vesicles at a concentration of 50 mM, which is well above the self-quenching concentration.[78] Therefore, when encapsulated in the vesicles, CF is non-fluorescent. When the vesicles are lysed, encapsulated CF is released to the surrounding environment and substantially diluted with regain of fluorescence.

This process was monitored via fluorescence spectroscopy with diluted vesicle samples, so if vesicles formed and encapsulated CF a large change in the fluorescence intensity is observed when lysed with 10% Triton X-100 detergent. If vesicles did not form, a small change in fluorescence intensity is observed when lysed with 10% Triton X-100 as a result of the dilution of any free CF already in solution, or the breaking up of other aggregates that may contain small amounts of CF. As demonstrated by Figure 50, all inclusion complex samples demonstrate a large increase in fluorescence compared to controls (ie. host and guest molecules on their own).

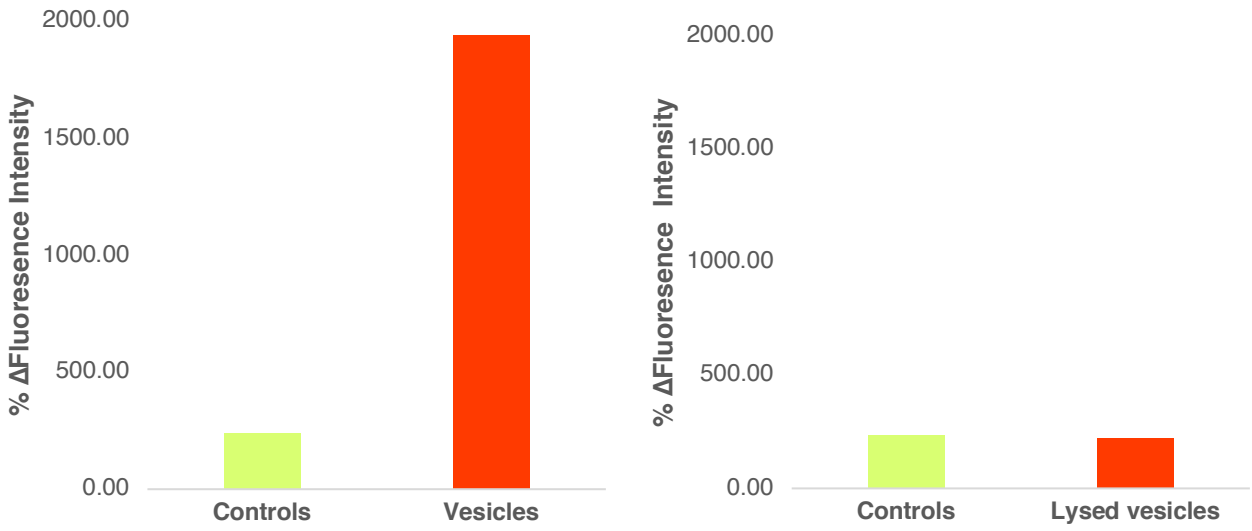

Figure 50: Initial vesicle lysing %ΔFluorescence Intensity (left) of inclusion complexes βCD-C12:AdSSPEGOMe, βCD-C12:AdSSPEG, βCD-C14:AdSSPEGOMe, and βCD-C14:AdSSPEG and controls AdSSPEGOMe, AdSSPEG, βCD-C12, and βCD-C14 shows a much higher average %ΔFluorescence Intensity for inclusion complex samples (ie. vesicles) than it does for controls (ie. host and guest molecules on their own), which indicates vesicle formation and CF encapsulation for inclusion complexes, while controls do not form vesicles or encapsulate CF. Two-week vesicle lysing %ΔFluorescence Intensity (right) shows the same average %ΔFluorescence Intensity for inclusion complex samples (ie. lysed vesicles) and controls, which indicates that the vesicles formed from inclusion complex samples have self-degraded

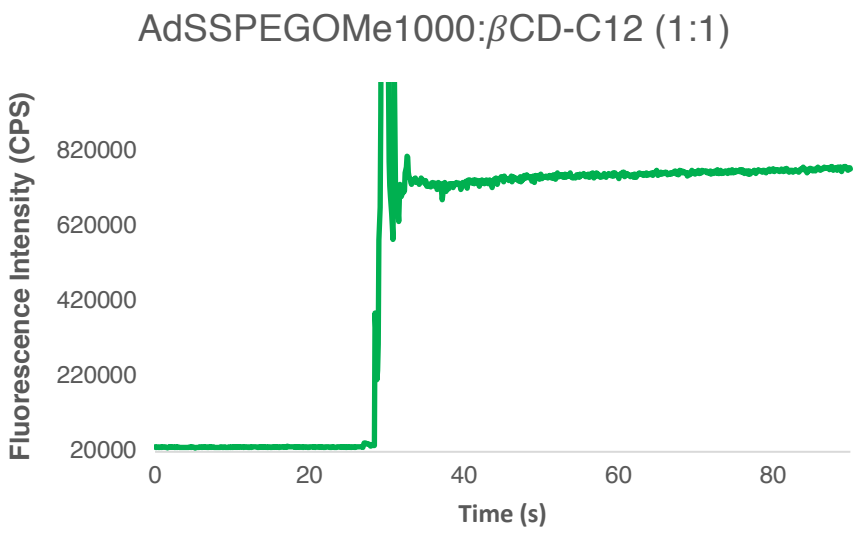

Figure 51: AdSSPEGOMe:βCD-C12 inclusion complex formed vesicles with encapsulated CF. When lysed with 250 μL 10% Triton X-100 there is a large increase in fluorescence intensity because CF is released and diluted below the self-quenching concentration range

These unique properties of the host and guest molecules confirm that the supramolecular amphiphiles are formed, self-assemble into vesicles, and encapsulate CF, while controls do not form vesicles on their own. All samples were measured over time to monitor self-degradation behavior, and it was found that the vesicles degraded on their own after approximately two weeks, as evident by the uniform increase in fluorescence compared to controls. All measurements used to calculate average values shown in Figure 50 are listed in Table 3, and a sample raw fluorescence measurement is demonstrated by Figure 51 (all other fluorescence measurements can be found in the appendix).

Table 3: % ΔFluorescence Intensity of vesicle forming inclusion complexes with encapsulated CF, and controls when lysed with 250 μL 10% Triton X-100 over time. After two weeks, the vesicles with encapsulated CF have degraded, which is evident by the decrease in % ΔFluorescence Intensity compared to previous measurements

Time	Sample	% ΔFluorescence Intensity
Initial	AdSSPEG1000	328.57
	βCD-C12	209.52
	βCD-C14	369.70
	AdSSPEGOMe1000	96.08
	AdSSPEG1000: βCD-C12	2071.43
	AdSSPEG1000: βCD-C14	1768.42
	AdSSPEG1000OMe: βCD-C12	2203.03
	AdSSPEG1000OMe: βCD-C14	1875.00
1 week	AdSSPEG1000	254.17
	βCD-C12	150.88
	βCD-C14	272.55
	AdSSPEGOMe1000	135.29
	AdSSPEG1000: βCD-C12	2070.00
	AdSSPEG1000: βCD-C14	1548.15
	AdSSPEG1000OMe: βCD-C12	2185.71
	AdSSPEG1000OMe: βCD-C14	1821.05
2 week	AdSSPEG1000	409.68
	βCD-C12	267.65
	βCD-C14	248.57
	AdSSPEGOMe1000	110.00
	AdSSPEG1000: βCD-C12	156.41
	AdSSPEG1000: βCD-C14	156.76
	AdSSPEG1000OMe: βCD-C12	408.57
	AdSSPEG1000OMe: βCD-C14	175.00

3.9 Vesicle Particle Size via DLS

Samples that were demonstrated to form vesicles, as discussed in section 3.8, (ie. inclusion complexes βCD-C12:AdSSPEGOMe, βCD-C12:AdSSPEG, βCD-C14:AdSSPEGOMe, and βCD-C14:AdSSPEG) were prepared via the

method described in section 2.8, and initially discussed in section 3.6, for measuring particle size via DLS.

Table 4: Particle size of vesicle samples comparing isolation methods of probe sonication and extrusion, wherein extrusion yields more consistent hydrodynamic radii and lowers polydispersity

Sample	Isolation Method	# of peaks	Hydrodynamic Radius (nm)*	%Intensity*	%PD*
AdSSPEG1000: βCD-C12	Probe Sonication	3	107.13	90.4	58.9
	Extruder	2	64.36	98.7	32.3
AdSSPEG1000: βCD-C14	Probe Sonication	3	97.53	71.7	52.4
	Extruder	3	64.34	94.5	28.2
AdSSPEGOMe1000: βCD-C12	Probe Sonication	3	128.43	92.6	98.3
	Extruder	2	64.12	93.1	32.4
AdSSPEGOMe1000: βCD-C14	Probe Sonication	3	94.23	92.3	23.6
	Extruder	2	48.21	93.4	21.2

*of the highest intensity peak

As demonstrated by data in Table 4, when comparing vesicle isolation methods of probe sonication and extrusion, extrusion yields much more consistent hydrodynamic radii of vesicles (which are consistent with previously mentioned literature values in section 3.6) with lower polydispersity than probe sonication. Both of these characteristics are highly desirable for vesicle nanocarriers as their behavior is more predictable and consistent.

All vesicle containing samples isolated via extrusion were monitored over the course of ten weeks to determine a time range of when degradation and/or

further aggregation into much larger particles occurs for vesicles without any encapsulated payloads. It was previously established that vesicles with encapsulated CF have a shelf life of approximately two weeks. Here, vesicles without any encapsulated agent have a shelf life of approximately 3 to 5 weeks. Interestingly, the particle size distribution of these vesicles became more uniform over time before degradation/further aggregation occurred, as demonstrated by Figures 52 and 53. This is likely due to a more stable thermodynamic equilibrium being established over time after vesicle formation.

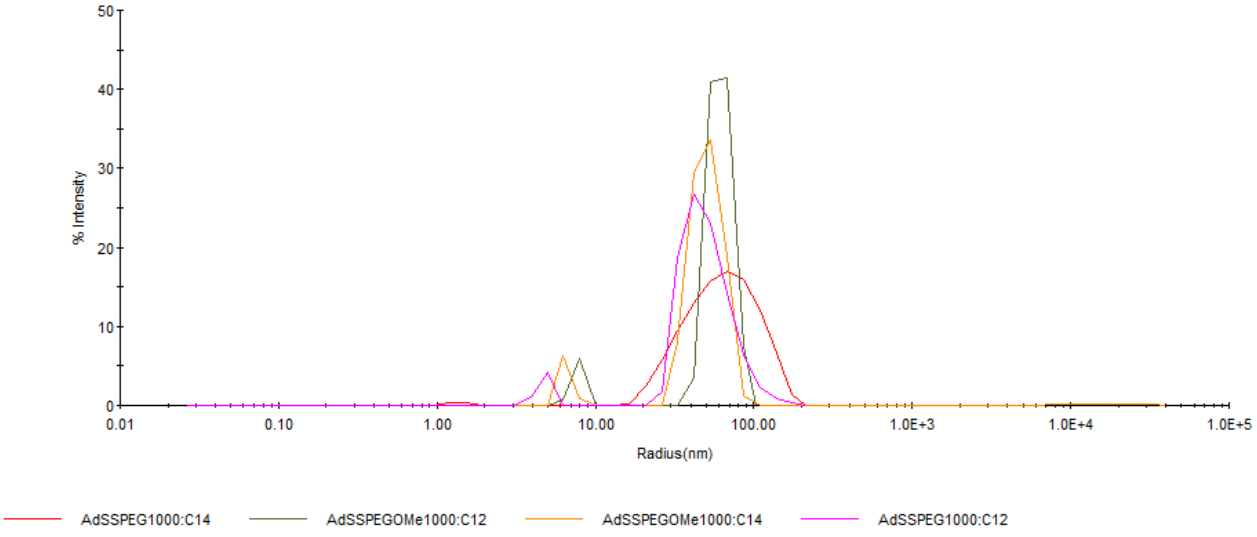

Figure 52: Initial % Intensity v. Hydrodynamic Radius (nm) of vesicle samples derived from inclusion complexes βCD-C12:AdSSPEGOMe, βCD-C12:AdSSPEG, βCD-C14:AdSSPEGOMe, and βCD-C14:AdSSPEG demonstrates uniform radii with low polydispersity. Note that the legend C12 indicates βCD-C12 and C14 indicates βCD-C14

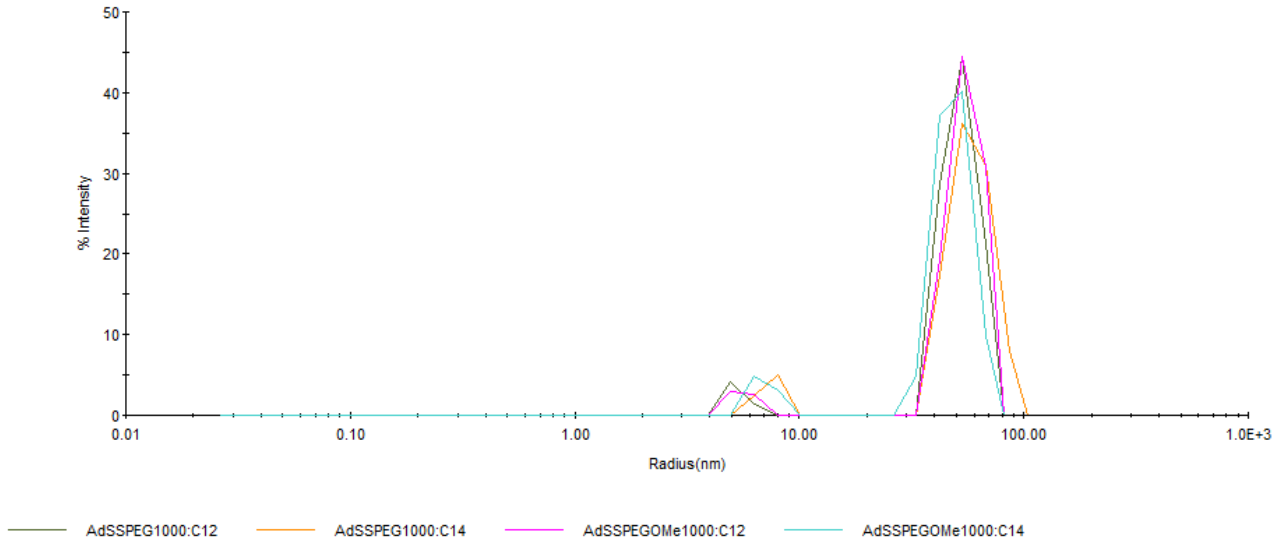

Figure 53: 1 week % Intensity v. Hydrodynamic Radius (nm) of vesicle samples derived from inclusion complexes βCD-C12:AdSSPEGOMe, βCD-C12:AdSSPEG, βCD-C14:AdSSPEGOMe, and βCD-C14:AdSSPEG demonstrates even more uniform radii with lower polydispersity than initial measurements. Note that the legend C12 indicates βCD-C12 and C14 indicates βCD-C14

3.10 Vesicle Glutathione (GSH) Degradation via DLS

Samples that were demonstrated to form vesicles, as discussed in section 3.8 and 3.9, (ie. inclusion complexes βCD-C12:AdSSPEGOMe, βCD-C12:AdSSPEG, βCD-C14:AdSSPEGOMe, and βCD-C14:AdSSPEG) were prepared via the method described in section 2.8 for measuring vesicle degradation in the presence of both intracellular and extracellular glutathione (GSH), as well as 10% Triton X-100 via DLS. As previously mentioned in section 1.4.1, GSH is a naturally occurring antioxidant found at higher concentrations inside cells than outside. The thiol group in GSH degrades the vesicles through a dynamic disulfide exchange reaction with the disulfide group embedded in the linear guest molecule

of the vesicles' bilayer membrane. This reaction will alter the HLB of the vesicles' bilayer membrane and cause it to degrade and release any encapsulated payload due to the degree of polarity and small size of GSH. Hence, GSH was used to mimic these physiological conditions in vitro. Here, it is desirable for vesicles to degrade under intracellular concentrations of GSH but remain intact under extracellular conditions. These experiments were ran according to the method described in section 2.11.2 with 12 mM GSH to mimic the intracellular environment, and 20 μM GSH to mimic the extracellular environment. Initial vesicle particle size distributions for these experiments is shown in Figure 53. An aliquot from each vesicle sample 1 week after formation was incubated overnight in both intra and extracellular GSH and particle size distribution was measured the next day.

When comparing initial vesicle particle size measurements with vesicle particle size in 10% Triton X-100 containing environments, all vesicle samples were reduced to a hydrodynamic radius of approximately 5 nm. This indicates that all aggregates have been broken up, and is consistent with fluorescent vesicle lysing results that demonstrate this detergent's ability to lyse vesicles.

When comparing initial vesicle particle size measurements with vesicle particle size in GSH containing environments, it can be concluded that there is much more of a chemical change with the intracellular GSH containing samples than with the extracellular GSH containing samples. Here, it is evident that the polydispersity and particle size of the intracellular GSH containing samples changed dramatically, while the extracellular GSH containing samples still demonstrate hydrodynamic radii within the expected range for all samples. This

could indicate that vesicles are more stable in extracellular environments than intracellular environments, which is ideal for drug delivery systems as it is desirable for the drug to be released from the vesicle nanocarrier intracellularly and remain stable extracellularly. Figures 54 and 55 demonstrate this difference in particle size distribution of vesicles between intracellular and extracellular environments, respectively, while Figures 56 and 57 demonstrate direct comparisons of vesicle samples before and after GSH incubation.

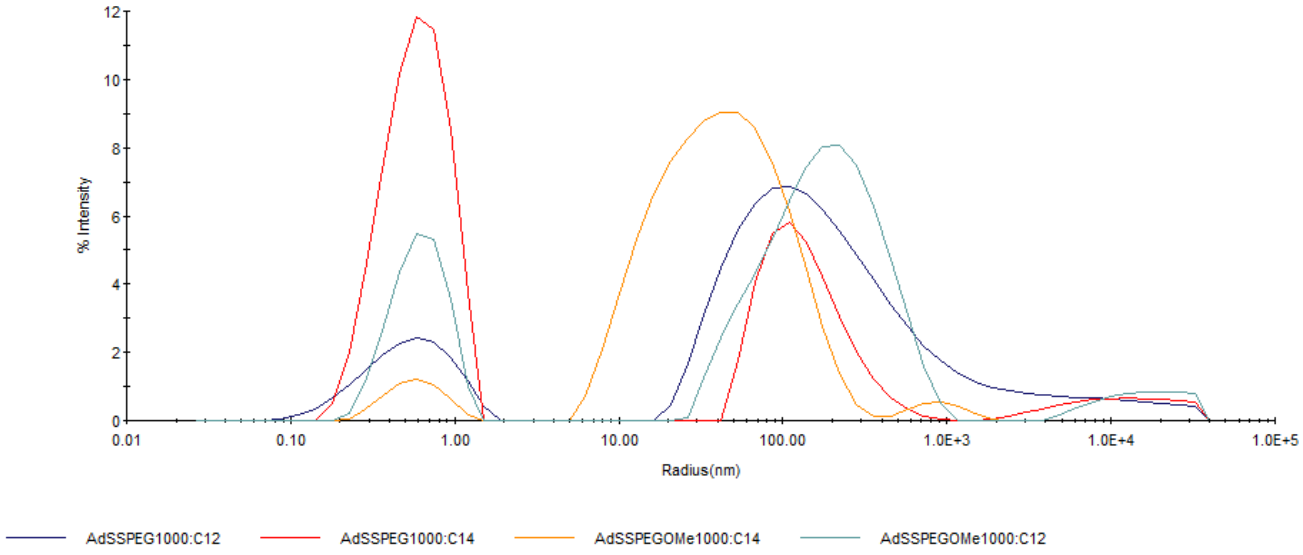

Figure 54: 12 mM GSH, pH 8.5, reaction time overnight % Intensity v. Hydrodynamic Radius (nm) of vesicle samples derived from inclusion complexes βCD-C12:AdSSPEGOMe, βCD-C12:AdSSPEG, βCD-C14:AdSSPEGOMe, and βCD-C14:AdSSPEG demonstrates an dramatic increase in polydispersity and a change in overall particle size, which may indicate vesicle degradation in intracellular environments. Note that the legend C12 indicates βCD-C12 and C14 indicates βCD-C14

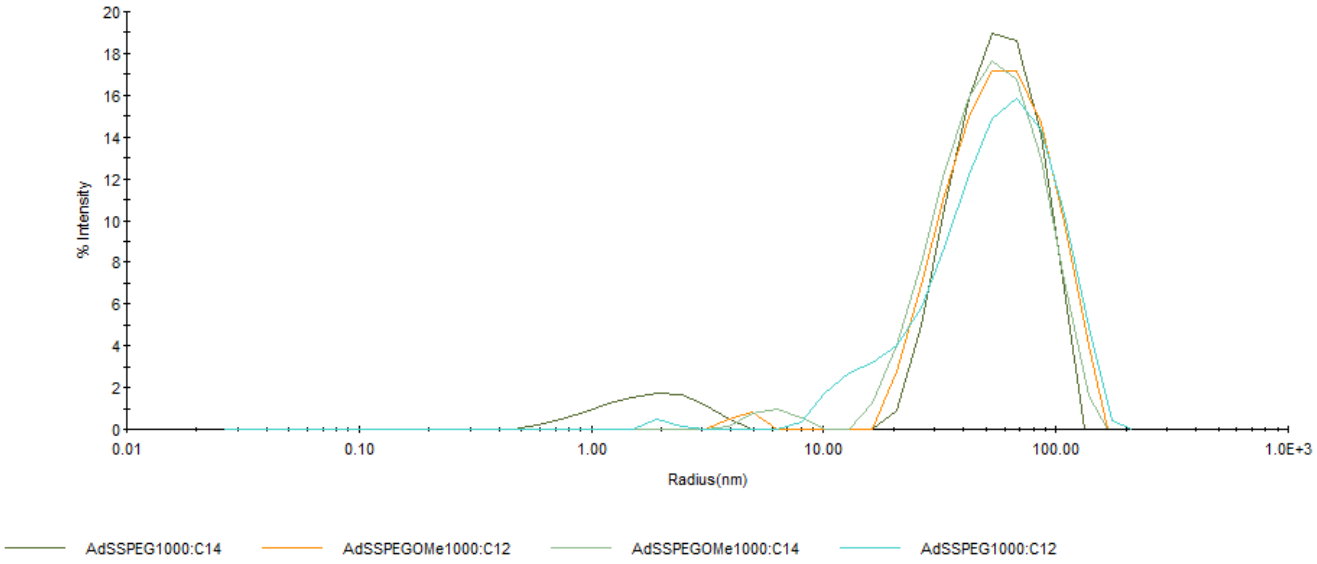

Figure 55: 20 μM GSH, pH 8.5, reaction time overnight % Intensity v. Hydrodynamic Radius (nm) of vesicle samples derived from inclusion complexes βCD-C12:AdSSPEGOMe, βCD-C12:AdSSPEG, βCD-C14:AdSSPEGOMe, and βCD-C14:AdSSPEG demonstrates a slight increase in polydispersity, but no change in overall particle size, which may indicate vesicle stability in extracellular environments. Note that the legend C12 indicates βCD-C12 and C14 indicates βCD-C14

For intracellular GSH containing samples, new peaks at less than 1 nm and greater than 1000 nm in radii are observed. This could indicate that the vesicles are either being broken down into smaller aggregates such as micelles or the individual inclusion complex building blocks (ie. less than 1 nm), or are forming even larger aggregates (ie. greater than 1000 nm) once the highly ordered vesicle structure is destroyed by intracellular GSH. This is because, contrary to 10% Triton X-100, GSH will only disrupt vesicles, while the detergent disrupts all aggregates.

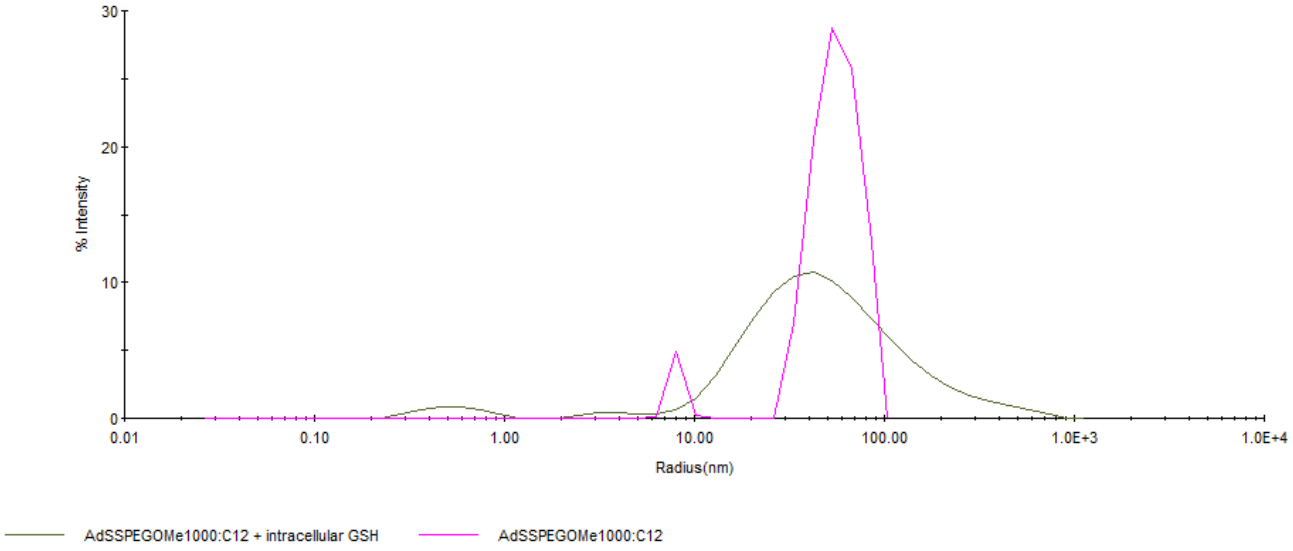

Figure 56: 12 mM GSH, pH 8.5, reaction time overnight compared to initial % Intensity v. Hydrodynamic Radius (nm) of vesicle samples derived from inclusion complex βCD-C12:AdSSPEGOMe demonstrate a dramatic increase in polydispersity and a very wide broadening of overall particle size distribution, which may indicate vesicle degradation in intracellular environments. Note that the legend C12 indicates βCD-C12

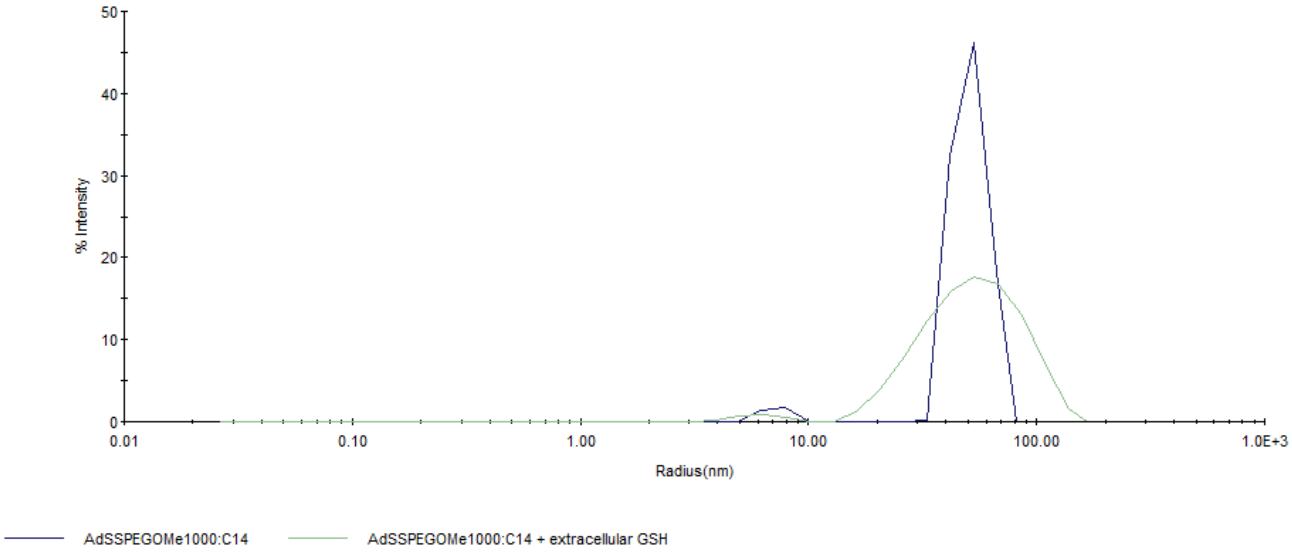

Figure 57: 20 μM GSH, pH 8.5, reaction time overnight compared to initial % Intensity v. Hydrodynamic Radius (nm) of vesicle samples derived from inclusion complex βCD-C14:AdSSPEGOMe demonstrate an increase in polydispersity and a slight broadening of overall particle size distribution, which may indicate vesicle stability in extracellular environments. Note that the legend C14 indicates βCD-C14

It is important to note that these experiments only indicate whether or not a reaction is happening with GSH in extracellular and intracellular environments, and does not definitively confirm, but rather may indicate, whether or not vesicles are degrading. This is because DLS only measures hydrodynamic radius, which is by definition dynamic, and may change as a result of external environment with or without vesicle degradation. Dialysis experiments that measure the concentration of encapsulated payload release over time are currently underway to determine definitively if vesicles are degrading in extracellular or intracellular environments or not, as well as the rate of release of encapsulated drugs.

3.11 Hydrogel Formation

Hydrogel formation was attempted with each vesicle sample that was demonstrated to form vesicles, as discussed in section 3.8-3.10, (ie. inclusion complexes βCD-C12:AdSSPEGOMe, βCD-C12:AdSSPEG, βCD-C14:AdSSPEGOMe, and βCD-C14:AdSSPEG). As previously mentioned in section 1.5.1, it is desirable to combine vesicle and hydrogel drug delivery platforms to mitigate their individual drawbacks (ie. burst release of encapsulated drug with hydrogels, and poor stability of vesicles), and create an optimized hybrid drug delivery system. Here, vesicles were prepared via the method described in section 2.8, and hydrogel gelation reactions were attempted via the method described in section 2.12. Although a variety of pHs (7.4, 8.5), temperatures (25, 30, 35, 40, 45, 50, 55 ℃), and amounts of PEGdiSH [7a-f] and vesicles were tested, all samples demonstrated liquid flow behavior and were not able to hold their own weight, which is not consistent with hydrogel formation. Samples with PEGdiSH [7e, 7f] molecular weight of 10000 or 20000 g/mol demonstrated a visual increase in viscosity at pH 8.5 and all temperatures and $\geq$ 10 wt/wt% PEGdiSH, which indicates that a reaction is occurring.

In theory, the disulfide exchange between the thiol group in the hydrophilic crosslinker (PEGdiSH) and the disulfide group in the vesicles should not lyse the vesicles, as the exterior HLB is maintained with a hydrophilic crosslinker. This theory was confirmed via DLS particle size measurements (ran according to the method described in section 2.11.1) with the PEGdiSH [7e] containing vesicle solutions (20 wt/wt% PEGdiSH calculated according to Equation 4, pH 8.5,

reaction time 1 hr at room temperature). Particle size distribution demonstrated by Figures 58 indicate that the vesicles are stable with crosslinker addition, as the particle size was only slightly increased, and polydispersity was shown to be unchanged compared to initial measurements demonstrated by Figure 53. Figure 59 shows a direct comparison between a neat vesicle sample, and a PEGdiSH containing vesicle sample which confirm the aforementioned observations. Additionally, it is evident that a reaction is occurring and eliciting a chemical change in the solution by the slight increase in particle size, but this reaction was not enough to crosslink the vesicles into a hydrogel.

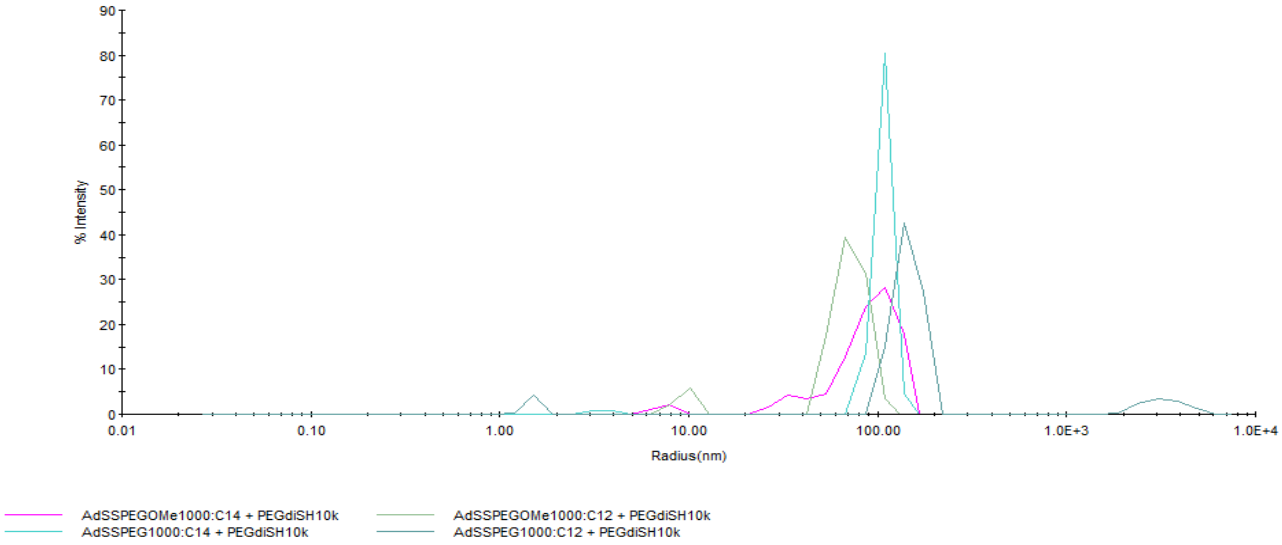

Figure 58: 20 wt/wt% PEGdiSH **[7e]**, pH 8.5, reaction time 1 hour % Intensity v. Hydrodynamic Radius (nm) of vesicle samples derived from inclusion complexes βCD-C12:AdSSPEGOMe, βCD-C12:AdSSPEG, βCD-C14:AdSSPEGOMe, and βCD-C14:AdSSPEG demonstrates no change in polydispersity, and a slight increase in overall particle size, which may indicate vesicle stability with a hydrophilic crosslinker. Note that the legend C12 indicates βCD-C12 and C14 indicates βCD-C14, and PEGdiSH10k indicates **[7e]**

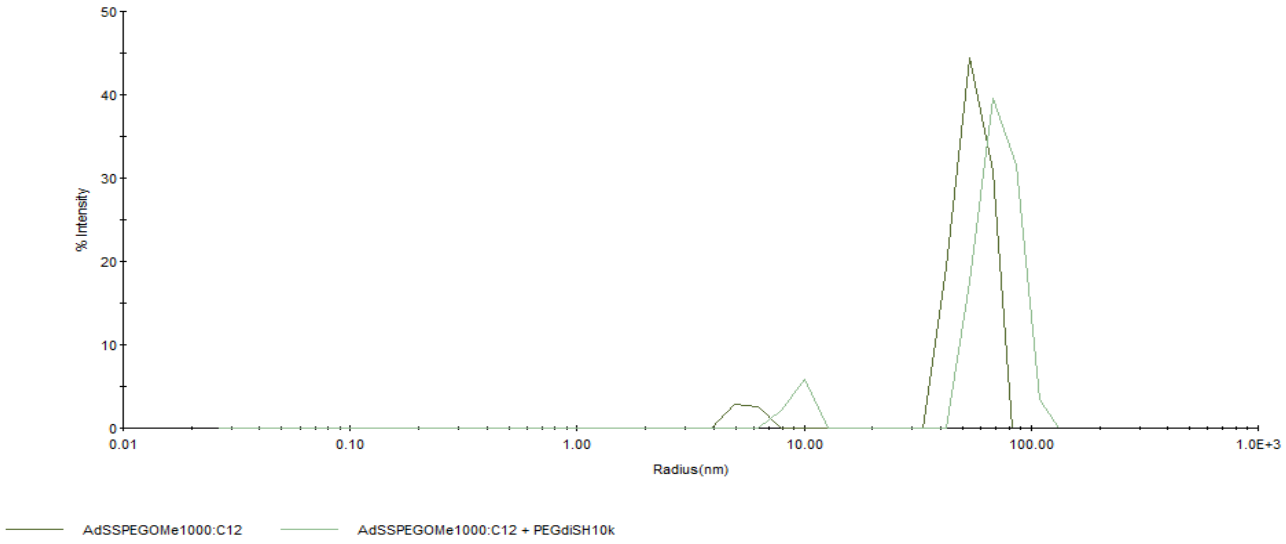

Figure 59: 20 wt/wt% PEGdiSH **[7e]**, pH 8.5, reaction time 1 hour % Intensity v. Hydrodynamic Radius (nm) of vesicle samples derived from inclusion complexes βCD-C12:AdSSPEGOMe demonstrates no change in polydispersity, and a slight increase in overall particle size, which may indicate vesicle stability with a hydrophilic crosslinker. Note that the legend C12 indicates βCD-C12 and PEGdiSH10k indicates **[7e]**

Results from previous experiments testing vesicle stability in intracellular and extracellular GSH environments (discussed in section 3.10) indicate that the disulfide bond embedded in the exterior of the vesicle membrane is indeed accessible, as some vesicle degradation was indicated in intracellular GSH environments. Hence, it can be further confirmed that a reaction is happening, but that the overall crosslinking density is not enough to form a hydrogel. Future experiments with multi-arm PEGdiSH crosslinkers would likely increase the crosslinking density enough to form a hydrogel.

4. CONCLUSION

In summary, thioalkyl modified βCD-C12 [2a] and βCD-C14 [2b] were successfully synthesized as macrocyclic hosts for novel AdSSPEGOMe [5b] and AdSSPEG [5a] linear guest molecules. All host and guest combinations were demonstrated to form inclusion complexes with critical aggregation concentrations in the range of 30-40 μM. These inclusion complexes were used to form bilayered vesicles with hydrodynamic diameters ranging from 100-150 nm and were stable for over a month. This shelf life is much longer than is typical of phospholipid based liposomes of this nature, which indicates enhanced stability from this novel host: guest combination. All vesicles were also able to encapsulate a small organic molecule within their core during vesicle formation, with triggered release in the presence of detergent. Vesicles with a disulfide bond covalent embedded in the bilayer membrane were shown to be more sensitive to intracellular concentrations of GSH than extracellular through a dynamic disulfide exchange reaction, which could serve as a stimuli induced release mechanism for encapsulated payloads once vesicles are taken up into cells.

Linear PEGdiSH [7a-f] of varying molecular weights from 1000-20000 g/mol were also successfully synthesized as crosslinking molecules to link the three-dimensional vesicles as multivalent junctions and form a hydrogel coating. However, although a variety of pHs, temperatures, and ratios of SH/SS were tested, hydrogels did not form under any conditions. A visual increase in viscosity was observed with crosslinkers with molecular weights $\geq$ 10000 g/mol, so there was

evidence that a reaction was occurring. It can be concluded that the crosslinking density with the linear crosslinkers was not enough to form a hydrogel.

Overall, vesicles formed from this novel host: guest combination are extremely promising for achieving a hybrid vesicle-hydrogel drug delivery system that can be applied as a coating or injected directly to a target site. The biocompatibility, stimuli responsivity, enhanced stability, and ease of preparation and modification of these materials is highly desirable for this purpose. Future work is needed to bring this novel drug delivery system from in vitro studies to in vivo studies for commercial applicability.

5. FUTURE WORK

Future work on this project should include more quantitative release studies with all vesicle samples. These studies should include the use of a model drug molecule such as curcumin, α-tocopherol, or doxorubicin. Vesicles with encapsulated drug payload should be isolated so that there is no free drug in solution, and then treated with both extracellular and intracellular concentrations of GSH to monitor % Drug Release over time. This method will give information on the kinetic release rates from these novel vesicles, as well as drug loading capacity and more quantitative measurements of degradation in the presence of GSH.

Additionally, hydrogel formation studies with a multi-arm thiol terminated PEG with molecular weight ≥ 10000 g/mol in order to increase the crosslinking density enough to form a hydrogel should be performed. A 4-arm thiol terminated PEG with a pentraethythritol core structure, as shown in Figure 60, would be a suitable material for this purpose.

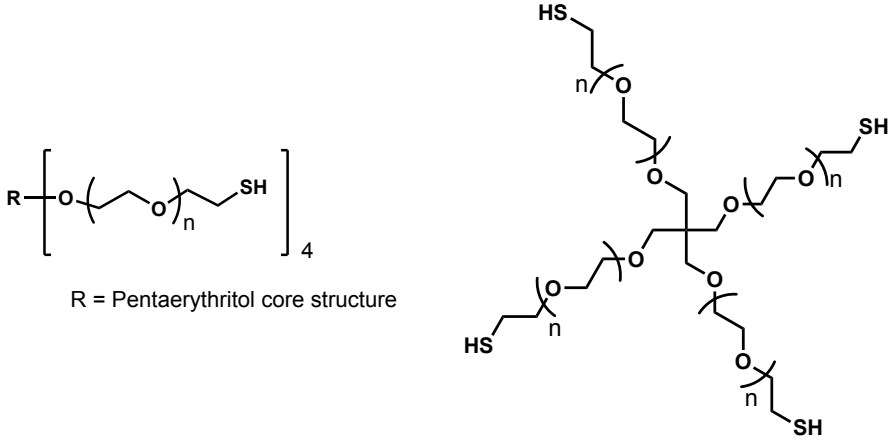

Figure 60: Condensed (left) and expanded (left) chemical structures of 4-arm thiol terminated PEG

Once hydrogels are formed, they should be characterized for mechanical and rheological properties, as well as swelling behavior and adhesion to various materials commonly used in medical devices. The crosslinking molecule should then be modified with an acid labile siyl-ether bond in its core structure to embed an acid sensitive degradation mechanism. Hydrogels, similarly to the vesicles, should also be studied for the encapsulation and release of model drugs with environments of varying acidity to probe the triggered degradation, drug loading capacity, and release rates of the material.

It may also be of interest to modify the host and guest molecules with varying functionalities to probe their behavior for other drug delivery related applications. All suggestions for future work are summarized in Figure 61.

Additionally, once all future work pathways described in Figure 61 have been explored, this material should undergo additional multidisciplinary characterizations by biologists and/or biomedical engineers to determine the viability of this novel drug delivery system for commercial applications as antibacterial coatings. Among others, these studies should include in vitro cell viability and drug delivery tests under physiological conditions, as well as broad spectrum bactericidal studies with encapsulated antibiotics to determine their safety in the presence of healthy eukaryotic cells versus bacteria-infected cells, as well as their effectiveness against a variety of different types of bacteria, respectively. Once in vitro studies have been thoroughly explored and the material has been further optimized to demonstrate viability, in vivo studies should be conducted according to FDA standards.

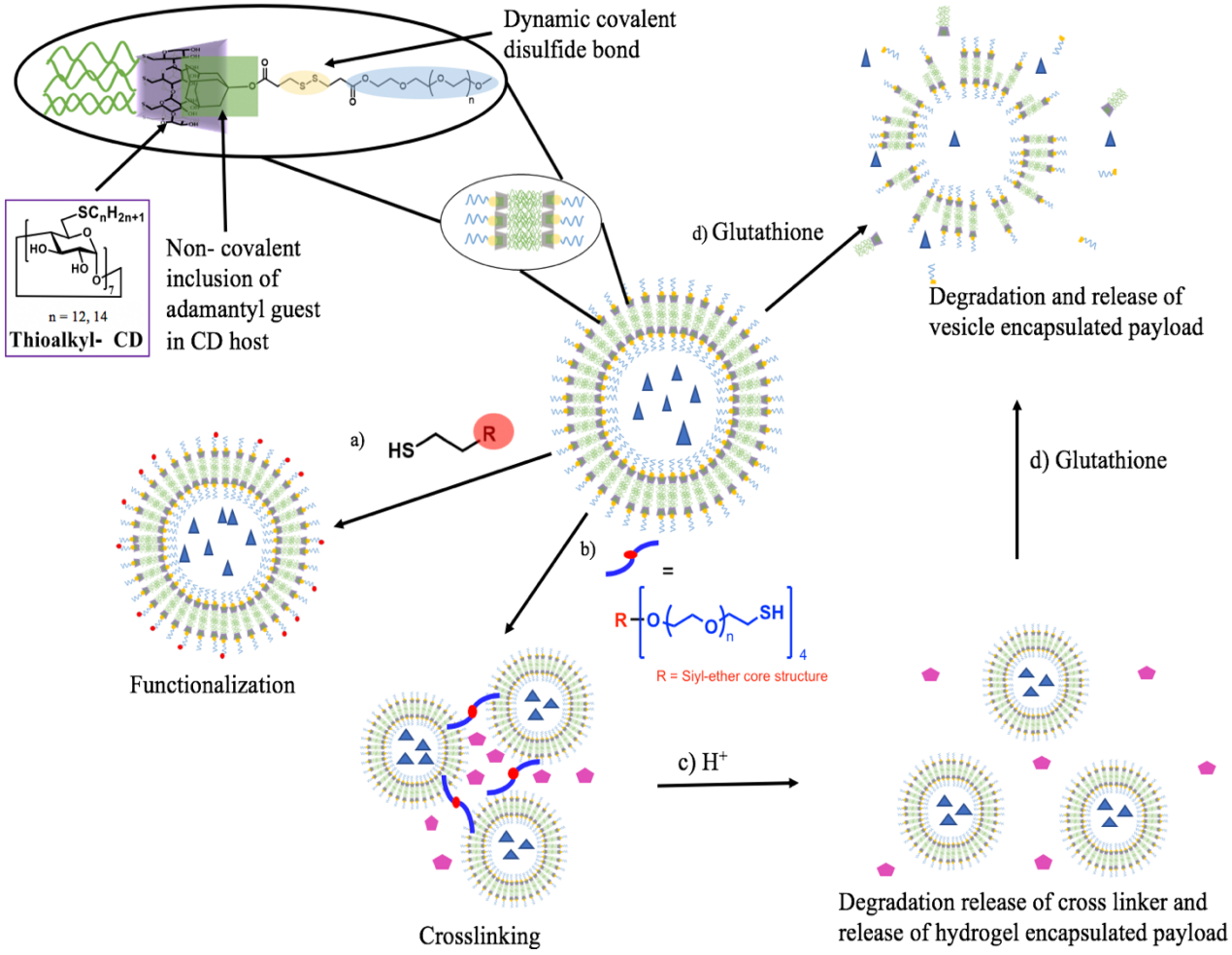

Figure 61: Summary of future work includes a) functionalization of vesicles b) crosslinking to form a hydrogel with thiol terminated 4-arm PEG with a siyl-ether core structure c) acid triggered degradation and release of hydrogel encapsulated payload and d) GSH triggered degradation and release of vesicle encapsulated payload

BIBLIOGRAPHY

1. Wicks, Z; Jones, F; Pappas, S; Wicks, D. Organic Coatings: Science and Technology, Third Edition. **2007,** *1,* 1-6.
2. Li, S.; Dong, S.; Xu, W.; Tu, S.; Yan, L.; Zhao, C.; Ding, J.; Chen, X. Antibacterial Hydrogels. *Cell Press* **2018**, *1700527*.
3. Mauri, E.; Naso, D.; Rossetti, A.; Borghi, E.; Ottaviano, E.; Gri, G.; Masi, M.; Sacchetti, A.; Rossi, F. Design of Polymer-Based Antimicrobial Hydrogels through Physico-Chemical Transition. *Mat. Sci. and Eng.* **2019**, No. February.
4. Fischer, M.; Vahdatzadeh, M.; Konradi, R.; Friedrichs, J.; Maitz, M. F.; Freudenberg, U.; Werner, C. Multilayer Hydrogel Coatings to Combine Hemocompatibility and Antimicrobial Activity. *Biomaterials* **2015**, *56*, 198–205.
5. Cloutier, M.; Mantovani, D.; Rosei, F. Antibacterial Coatings : Challenges , Perspectives , and Opportunities. *Trends Biotechnol.* **2015**, *xx*, 1–16.
6. Swartjes, J.; International, B.; Sharma, P. K.; Kooten, T. G. Van; Mei, H. C. Van Der. Current Developments in Antimicrobial Surface Coatings for Biomedical Applications. *J. Med. Chem.* **2014**, *22* (1), 1-14.
7. Taheri, S.; Cavallaro, A.; Christo, S. N.; Smith, L. E.; Majewski, P.; Barton, M.; Hayball, J. D.; Vasilev, K. Substrate Independent Silver Nanoparticle Based Antibacterial Coatings. *Biomaterials* **2014**, *35* (16), 4601–4609.
8. Tan, S. Y.; Tatsumura, Y. Alexander Fleming (1881–1955): Discoverer of Penicillin. **2015**, *56* (7), 366–367.
9. Schierholz, J. M.; Beuth, J. Implant Infections : A Haven for Opportunistic Bacteria. *J. Hospital Infections* **2001**, 87–93.

10. Tuson, H. H.; Weibel, D. B. Bacteria-Surface Interactions. *Soft Matter* **2013**, 4368–4380.

11. Missirlis, Y. F.; Katsikogianni, M.; Missirlis, Y. F. CONCISE REVIEW OF MECHANISMS OF BACTERIAL ADHESION TO BIOMATERIALS AND OF TECHNIQUES USED IN ESTIMATING BACTERIA- MATERIAL INTERACTIONS. *Euro. Cells and Mat.* **2004**, *8*, 37–57.

12. Subbiahdoss, G.; Joana, F.; Domingues, S.; Kuijer, R.; Mei, H. C. Van Der; Busscher, H. J. Bridging the Gap Between In Vitro and In Vivo Evaluation of Biomaterial-Associated Infections. *Biomaterials Associated Infection: Immunilogical Aspects and Antimicrobial Strategies* **2013**, 107–117.

13. Darouiche, R. O. Device-Associated Infections : A Macroproblem That Starts with Microadherence. *Healthcare Epidemiology* **2001**, *33*, 1567–1572.

14. Gupta, P.; Vermani, K.; Garg, S. Hydrogels: From Controlled Release to PH-Responsive Drug Delivery. *Drug Discov. Today* **2002**, *7* (10), 569–579.

15. Thatiparti, T. R.; Shoffstall, A. J.; von Recum, H. A. Cyclodextrin-Based Device Coatings for Affinity-Based Release of Antibiotics. *Biomaterials* **2010**, *31* (8), 2335–2347.

16. Yang, W., Tao, X., Zhao, T., Weng, L., Kang, E., Wang, L. Antifouling and Antimicrobial Hydrogel Coatings with Self-Healing Properties Based on Dynamic Disulfide Exchange Reaction. *Polym. Chem.* **2015***, 39,* 7027-7035.

17. Tiwari, G.; Tiwari, R.; Bannerjee, S.; Bhati, L.; Pandey, S.; Pandey, P.; Sriwastawa, B. Drug Delivery Systems: An Updated Review. *Int. J. Pharm. Investig.* **2012**, *2* (1), 2.

18. Patra, J. K.; Das, G.; Fraceto, L. F.; Campos, E. V. R.; Rodriguez-Torres, M. D. P.; Acosta-Torres, L. S.; Diaz-Torres, L. A.; Grillo, R.; Swamy, M. K.; Sharma, S.; et al. Nano Based Drug Delivery Systems: Recent Developments and Future Prospects. *Nanobiotechnology* **2018**, *16* (1), 1–33.

19. Savjani, K.; Gajjar, A.;Savjani, J. Drug Solubility: Importance and Enhancement Techniques. *ISRN Pharmaceutics*. **2012,** *2012* (195727), 1-10.

20. Kakkar, A.; Traverso, G.; Farokhzad, O. C.; Weissleder, R.; Langer, R. Evolution of Macromolecular Complexity in Drug Delivery Systems. *Nat. Rev. Chem.* **2017**, *1* (0063), 1–18.

21. Singh, N.; Joshi, A.; Toor, A. P.; Verma, G. Drug Delivery: Advancements and Challenges. *J. Biomat. and Nanobiotech*. **2017**, *27* (1), 865-886.

22. Singh, N.; Joshi, A.; Toor, A. P.; Verma, G. Drug Delivery: Advancements and Challenges. *J. Biomat. and Nanobiotech*. **2017**, *27* (1), 865-886.

23. Zylberberg, C.; Matosevic, S. Pharmaceutical Liposomal Drug Delivery: A Review of New Delivery Systems and a Look at the Regulatory Landscape. *Drug Deliv.* **2016**, *23* (9), 1-11.

24. Fedeli, E.; Lancelot, A.; Dominguez, J. M.; Serrano, J. L.; Calvo, P.; Sierra, T. Self-Assembling Hybrid Linear-Dendritic Block Copolymers: The Design of Nano-Carriers for Lipophilic Antitumoral Drugs. *Nanomaterials* **2019**, *9* (2).

25. Rashmi; Singh, A. K.; Achazi, K.; Schade, B.; Böttcher, C.; Haag, R.; Sharma, S. K. Synthesis of Non-Ionic Bolaamphiphiles and Study of Their Self-Assembly and Transport Behaviour for Drug Delivery Applications. *RSC Adv.* **2018**, *8* (55), 31777–31782.

26. Gao, J.; Xu, Y.; Zheng, Y.; Wang, X.; Li, S.; Yan, G.; Wang, J.; Tang, R. pH-Sensitive Carboxymethyl Chitosan Hydrogels Via Acid-Labile Ortho Ester Linkage as an Implantable Drug Delivery System. *Carbohydr. Polym.* **2019**, *225* (July), 115237.

27. Gu, D.; Tan, S.; O'Connor, A. J.; Qiao, G. G. On-Demand Cascade Release of Hydrophobic Chemotherapeutics from a Multicomponent Hydrogel System. *ACS Biomater. Sci. Eng.* **2018**, *4* (5), 1696–1707.

28. Lee, S. M.; Nguyen, S. T. Smart Nanoscale Drug Delivery Platforms from Stimuli-Responsive Polymers and Liposomes. *Macromolecules* **2013**, *46* (23), 9169–9180.

29. Schmaljohann, D. Thermo- and PH-Responsive Polymers in Drug Delivery. **2006**, *58*, 1655-1670.

30. Reinhoudt, D. N.; Crego-Calama, M. Synthesis beyond the Molecule. *Science (80).* **2002**, *295* (5564), 2403–2407.

31. Savyasachi, A. J.; Kotova, O.; Shanmugaraju, S.; Bradberry, S. J.; Ó'Máille, G. M.; Gunnlaugsson, T. Supramolecular Chemistry: A Toolkit for Soft Functional Materials and Organic Particles. *Chem* **2017**, *3* (5), 764–811.

32. Lehn, J. M. Toward Self-Organization and Complex Matter. *Science (80).* **2002**, *295* (5564), 2400–2403.

33. Whitesides, G. M.; Boncheva, M. Supramolecular Chemistry And Self-Assembly Special Feature: Beyond Molecules: Self-Assembly of Mesoscopic and Macroscopic Components. *Proc. Natl. Acad. Sci. U. S. A.* **2002**, *99* (8), 4769.

34. Jie, K.; Zhou, Y.; Yao, Y.; Huang, F. Macrocyclic Amphiphiles. *Chem. Soc. Rev.* **2015**, 1-20.

35. Zhang, X.; Wang, C. Supramolecular Amphiphiles. *Chem. Soc. Rev.* **2011**, *40* (1), 94–101.

36. Wang, C.; Wang, Z.; Zhang, X. Amphiphilic Building Blocks for Self-Assembly: From Amphiphiles to Supra-Amphiphiles. *Acc. Chem. Res.* **2012**, *45* (4), 608–618.

37. Stupp, S. I.; Palmer, L. C. Supramolecular Chemistry and Self-Assembly in Organic Materials Design. *Chem. of Mat.* **2013,** (25) A-L.

38. Chen, L.; Xiang, J.; Zhao, Y.; Yan, Q. Reversible Self-Assembly of Supramolecular Vesicles and Nanofibers Driven by Chalcogen-Bonding Interactions. *J. Am. Chem. Soc.* **2018**, *140* (23), 7079–7082.

39. Brinker, C. J.; Lu, Y.; Sellinger, A.; Fan, H. ChemInform Abstract: Evaporation-Induced Self-Assembly: Nanostructures Made Easy. *ChemInform* **2010**, *30* (28), 579-585.

40. Butt, H.; Graf, K.; Kappl, M. Physics and Chemistry of Interfaces, Third Revised and Enlarged Edition. *Wiley-VCH.* **2013**, 323-360.

41. Tanford, C. The Hydrophobic Effect: Formation of Micelles and Biological Membranes. *John Wiley & Sons Inc., New York.* **1980,** 233.

42. Widom, B.; Bhimalapuram, P.; Koga, K. The Hydrophobic Effect. *Phys. Chem. Chem. Phys.* **2003**, *5* (15), 3085–3093.

43. Southall, N. T.; Dill, K. A.; Haymet, A. D. J. A View of the Hydrophobic Effect. *J. Phys. Chem. B* **2002**, *106* (3), 521–533.

44. Chen, G.; Jiang, M. Cyclodextrin-Based Inclusion Complexation Bridging Supramolecular Chemistry and Macromolecular Self-Assembly. *Chem Soc Rev* **2011**, 2254–2266.

45. Zhang, J.; Ma, P. X. Cyclodextrin-Based Supramolecular Systems for Drug Delivery: Recent Progress and Future Perspective. *Adv. Drug Deliv. Rev.* **2013**, *65* (9), 1215–1233.

46. Liu, H.; Zhang, Y.; Hu, J.; Li, C.; Liu, S. Multi-Responsive Supramolecular Double Hydrophilic Diblock Copolymer Driven by Host-Guest Inclusion Complexation between β-Cyclodextrin and Adamantyl Moieties. *Macromol. Chem. Phys.* **2010**, *210* (24), 2125–2137.

47. Antonietti, M.; Förster, S. Vesicles and Liposomes: A Self-Assembly Principle Beyond Lipids. *Adv. Mater.* **2003**, *15* (16), 1323–1333.

48. Chen, I. A.; Walde, P. From Self-Assembled Vesicles to Protocells. *Cold Spring Harb. Perspect. Biol.* **2010**, *2* (7), 1–14.

49. Sevink, G. J. A.; Zvelindovsky. Self Assembly of Complex Vesicles. *Macromol.* **2005**, 7502–7513.

50. Ulrich, S. Growing Prospects of Dynamic Covalent Chemistry in Delivery Applications. *Acc. Chem. Res.* **2019,** A-J.

51. Jin, Y.; Wang, Q.; Taynton, P.; Zhang, W. Dynamic Covalent Chemistry Approaches Toward Macrocycles, Molecular Cages, and Polymers. *Acc. Chem. Res.* **2014**, *47* (5), 1575–1586.

52. Jin, Y.; Yu, C.; Denman, R. J.; Zhang, W. Recent Advances in Dynamic Covalent Chemistry. *Chem. Soc. Rev.* **2013**, *42* (16), 6634–6654.

53. Aida, T., Meijer, E. W., & Stupp, S. I. Functional Supramolecular Polymers. *Science.* **2012,** *335(6070), 813–817.*

54. Nagy, P. Kinetics and Mechanisms of Thiol-Disulfide Exchange Covering Direct Substitution and Thiol Oxidation-Mediated Pathways. *Antioxidants Redox Signal.* **2013**, *18* (13), 1623–1641.

55. Black, S. P.; Sanders, J. K. M.; Stefankiewicz, A. R. Disulfide Exchange: Exposing Supramolecular Reactivity through Dynamic Covalent Chemistry. *Chem. Soc. Rev.* **2014**, *43* (6), 1861–1872.

56. Yan, X.; Yang, X.; Tong, X.; Huang, Y. A Method to Accelerate the Gelation of Disulfide-Crosslinked Hydrogels. *Chinese J. Polym. Sci. (English Ed.* **2015**, *33* (1), 118–127.

57. Maiti, B.; Kumar, K.; Moitra, P.; Kondaiah, P.; Bhattacharya, S. Reduction Responsive Nanovesicles Derived from Novel α-Tocopheryl-Lipoic Acid Conjugates for Efficacious Drug Delivery to Sensitive and Drug Resistant Cancer Cells. *Bioconjug. Chem.* **2018**, *29* (2), 255–266.

58. Kumar, K.; Yadav, L.; Kondaiah, P.; Chaudhary, S. Efficacious Doxorubicin Delivery Using Glutathione-Responsive Hollow Non-Phospholipid Vesicles Bearing Lipoyl Cholesterols. *ChemMedChem* **2019**, *14* (18), 1633–1640.

59. Sligo, T.; Lane, A.; Yw, S. F. Toxicity of Nanomaterials: Exposure, Pathways, Assessment, and Recent Advances. *ACS Biomater. Sci. Eng.* **2018**, *4*, 2237–2275.

60. Fernando, Raymond H. Sung, L.-P. Nanotechnology Applications in Coatings. *ACS Symposium Series.* **2009**, *1008,* (1-5).

61. Wickremasinghe, N. C.; Kumar, V. A.; Hartgerink, D. Two-Step Self-Assembly of Liposome-Multidomain Peptide Nano Fi Ber Hydrogel for Time-Controlled Release. *Bio Macromol.* **2014**, *15* (3587-3595).

62. Qu, Y.; Tang, J.; Liu, L.; Song, L. L.; Chen, S.; Gao, Y. α-Tocopherol Liposome Loaded Chitosan Hydrogel to Suppress Oxidative Stress Injury in Cardiomyocytes. *Int. J. Biol. Macromol.* **2019**, *125* (xxxx), 1192–1202.

63. Popescu, M. T.; Mourtas, S.; Pampalakis, G.; Antimisiaris, S. G.; Tsitsilianis, C. PH-Responsive Hydrogel/Liposome Soft Nanocomposites for Tuning Drug Release. *Biomacromolecules* **2011**, *12* (8), 3023–3030.

64. Lv, J.; Wu, G.; Liu, Y.; Li, C.; Huang, F.; Zhang, Y.; Liu, J.; An, Y.; Ma, R.; Shi, L. Injectable Dual Glucose-Responsive Hydrogel-Micelle Composite for Mimicking Physiological Basal and Prandial Insulin Delivery. *Sci. China Chem.* **2019**, *62* (5), 637–648.

65. Xu, S.; An, X. Preparation, Microstructure and Function for Injectable Liposome-Hydrogels. *Colloids Surfaces A Physicochem. Eng. Asp.* **2019**, *560*, 20–25.

66. Tsai, H. C.; Chou, H. Y.; Chuang, S. H.; Lai, J. Y.; Chen, Y. S.; Wen, Y. H.; Yu, L. Y.; Lo, C. L. Preparation of Immunotherapy Liposomal-Loaded Thermal-Responsive Hydrogel Carrier in the Local Treatment of Breast Cancer. *Polymers (Basel)*. **2019**, *11* (10).

67. Torres-Martínez, A.; Angulo-Pachón, C. A.; Galindo, F.; Miravet, J. F. Liposome-Enveloped Molecular Nanogels. *Langmuir* **2019**, *35* (41), 13375–13381.

68. O'Neill, H. S.; Herron, C. C.; Hastings, C. L.; Deckers, R.; Lopez Noriega, A.; Kelly, H. M.; Hennink, W. E.; McDonnell, C. O.; O'Brien, F. J.; Ruiz-Hernández, E.; et al. A Stimuli Responsive Liposome Loaded Hydrogel Provides Flexible On-Demand Release of Therapeutic Agents. *Acta Biomater.* **2017**, *48*, 110–119.

69. Lyu, D.; Chen, S.; Guo, W. Liposome Crosslinked Polyacrylamide/DNA Hydrogel: A Smart Controlled-Release System for Small Molecular Payloads. *Smal.l* **2018**, *14* (15), 1–8.

70. Liu, P.; Guo, B.; Wang, S.; Ding, J.; Zhou, W. A Thermo-Responsive and Self-Healing Liposome-in-Hydrogel System as an Antitubercular Drug Carrier for Localized Bone Tuberculosis Therapy. *Int. J. Pharm.* **2019**, *558* (January), 101–109.

71. Hosta-Rigau, L.; Chandrawati, R.; Saveriades, E.; Odermatt, P. D.; Postma, A.; Ercole, F.; Breheney, K.; Wark, K. L.; Städler, B.; Caruso, F. Noncovalent Liposome Linkage and Miniaturization of Capsosomes for Drug Delivery. *Biomacromolecules.* **2010**, *11* (12), 3548–3555.

72. Himmelein, S.; Lewe, V.; Stuart, M. C. A.; Ravoo, B. J. A Carbohydrate-Based Hydrogel Containing Vesicles as Responsive Non-Covalent Cross-Linkers. *Chem. Sci.* **2014**, *5* (3), 1054–1058.

73. Cheng, R.; Yan, Y.; Liu, H.; Chen, H.; Pan, G.; Deng, L.; Cui, W. Mechanically Enhanced Lipo-Hydrogel with Controlled Release of Multi-Type Drugs for Bone Regeneration. *Appl. Mater. Today.* **2018**, *12*, 294–308.

74. Billard, A.; Pourchet, L.; Malaise, S.; Alcouffe, P.; Montembault, A.; Ladavière, C. Liposome-Loaded Chitosan Physical Hydrogel: Toward a Promising Delayed-Release Biosystem. *Carbohydr. Polym.* **2015**, *115*, 651–657.

75. Thermo Fisher Scientific. Cell Stains: Nile Red. https://www.thermofisher.com/order/catalog/product/N1142#/N1142. (accessed Aug 11, 2020).

76. Schoonover, D.; Gibson, H. Facile Removal of Tosyl Chloride from Tosylates

Using Cellulosic Materials, e.g., Filter Paper. *Tetrah. Let.* **2009**, *58* (3), 242-244.

77. Lakowicz, J. R. Quenching of Fluorescence. *Princ. Fluoresc. Spectrosc.* **2006**, *3*, 277–330.

78. Chen, R. F.; Knutson, J. R. Mechanism of Fluorescence Concentration Quenching of Carboxyfluorescein in Liposomes: Energy Transfer to Nonfluorescent Dimers. *Anal. Biochem.* **1988**, *172* (1), 61–77.

APPENDICES

A. Supporting Information

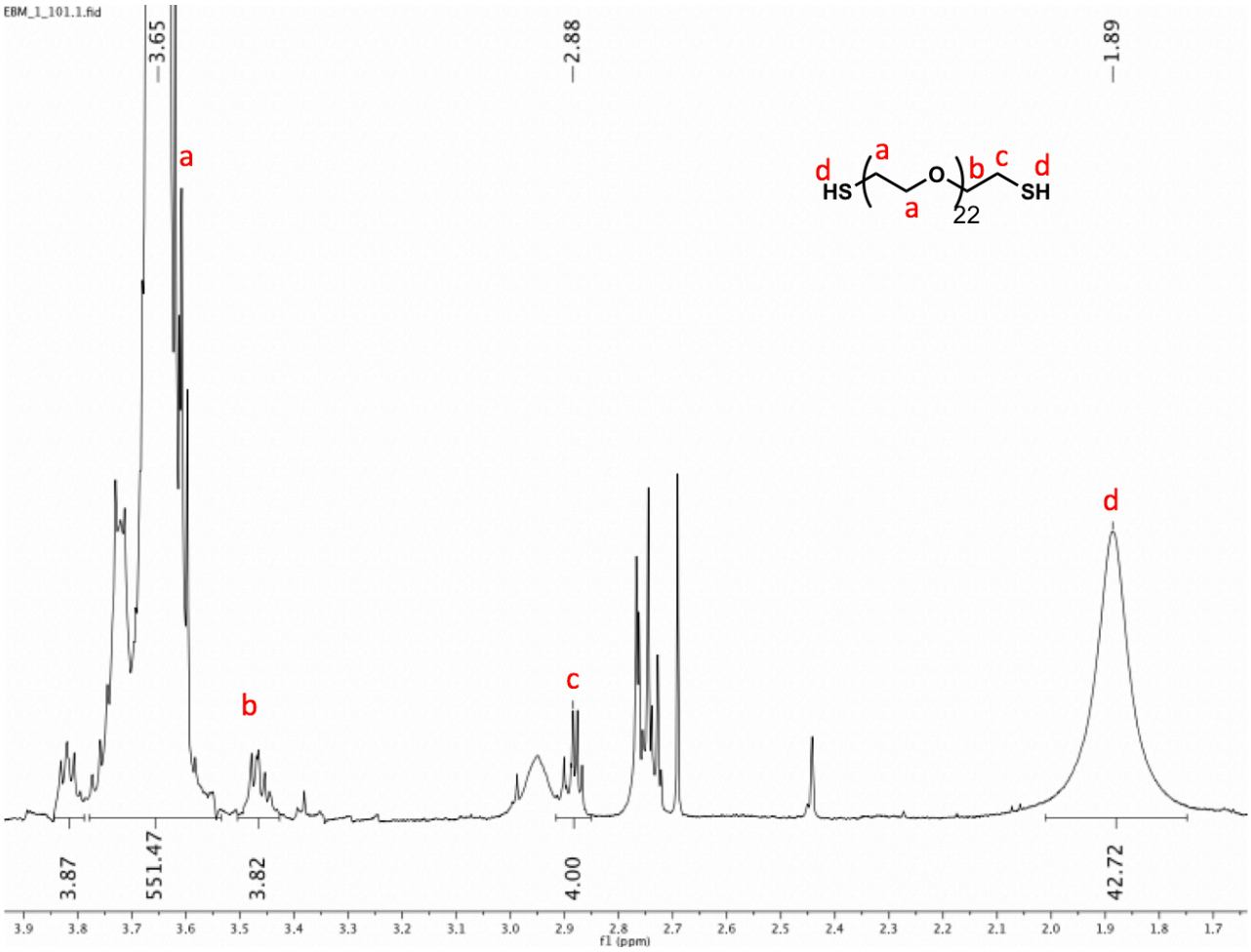

Figure 1A: ^{1}H NMR of PEGdiSH (n = 22 **[7a]**, 1000 g/mol) in deuterated chloroform ($CDCl_3$)

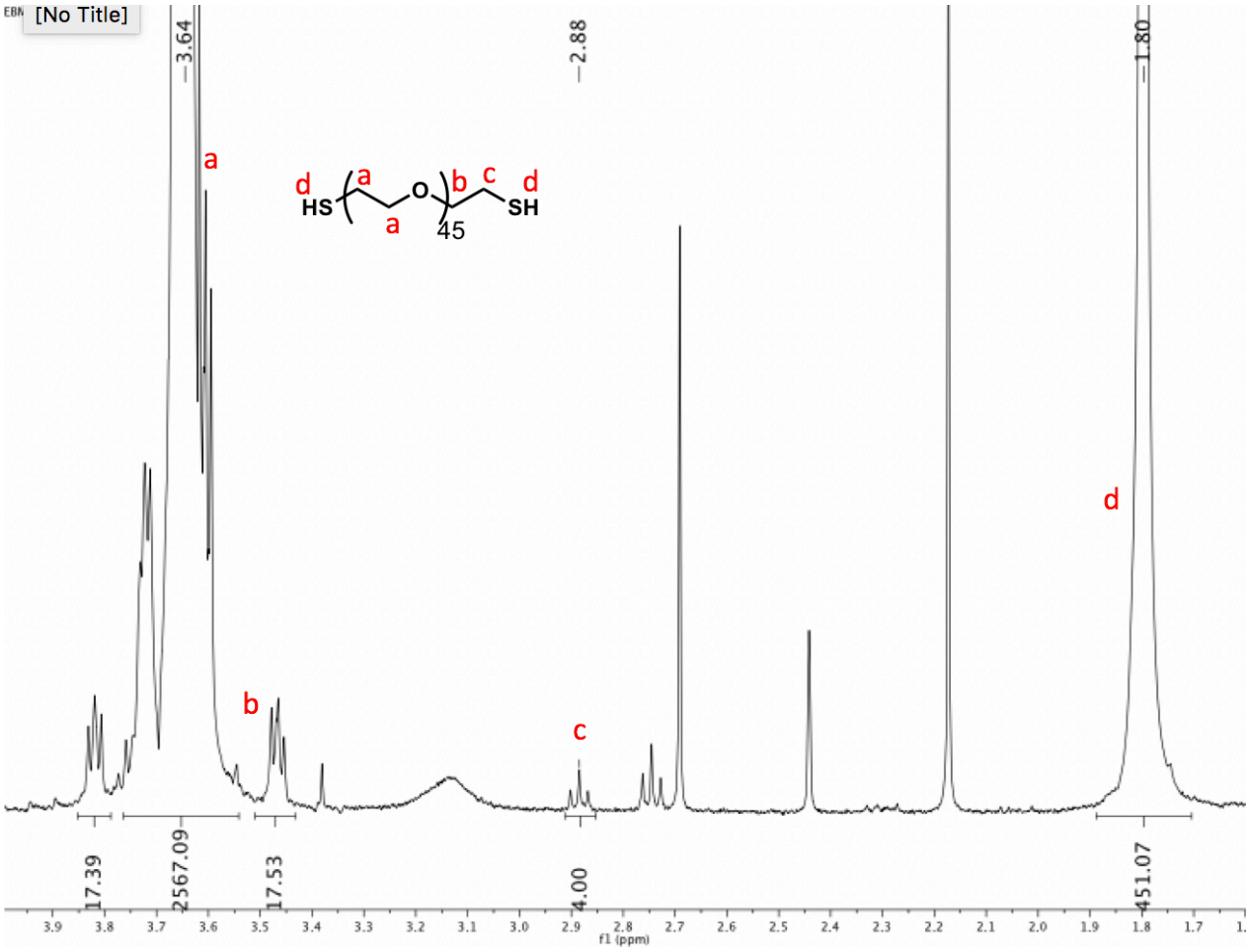

Figure 2A: ^{1}H NMR of PEGdiSH (n = 45 **[7b]**, 2000 g/mol) in deuterated chloroform ($CDCl_3$)

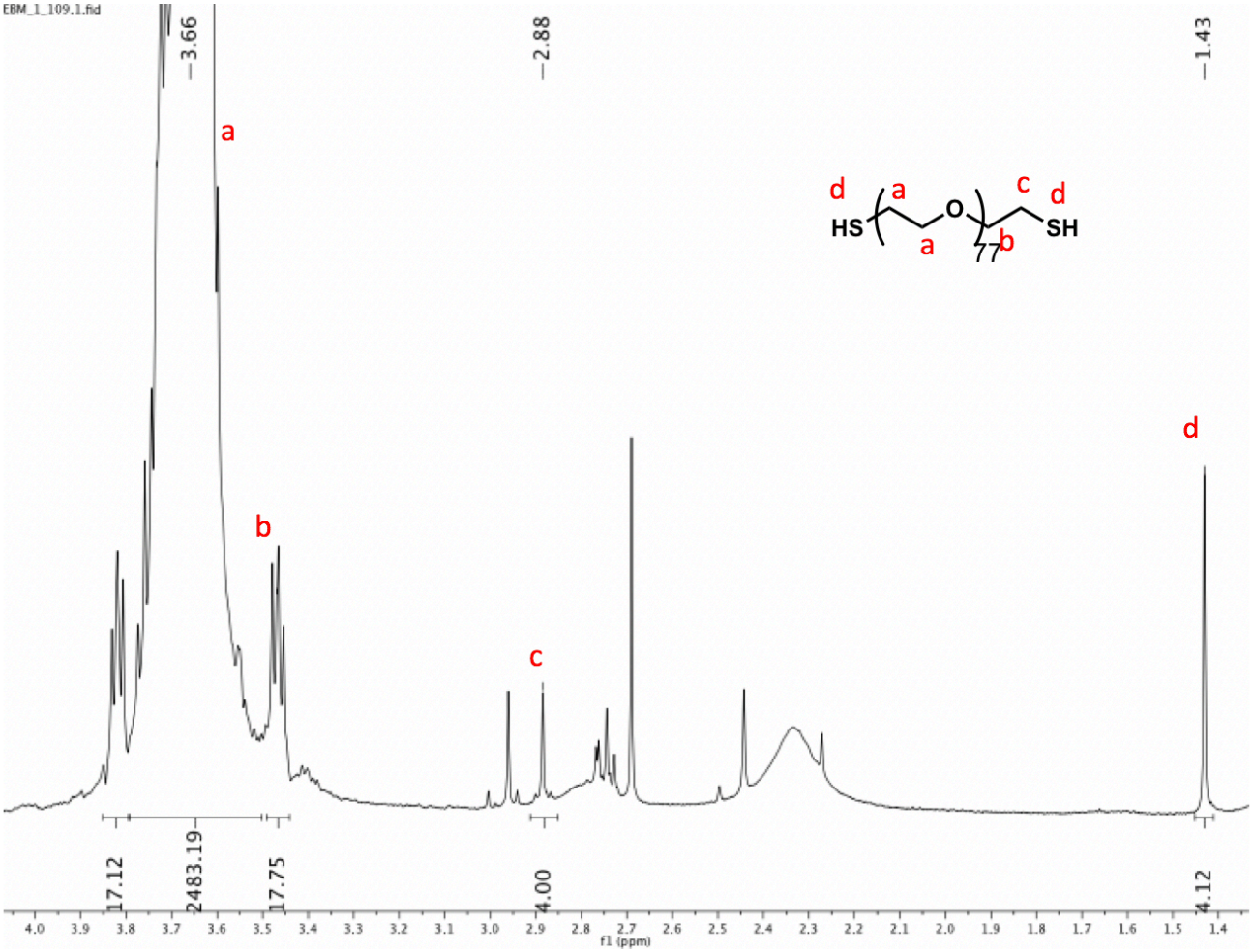

Figure 3A: ^{1}H NMR of PEGdiSH (n = 77 **[7c]**, 3400 g/mol) in deuterated chloroform ($CDCl_3$)

*Note- ^{1}H NMR for PEGdiSH (n = 90 **[7d]**, 4000 g/mol) can be found on page 89

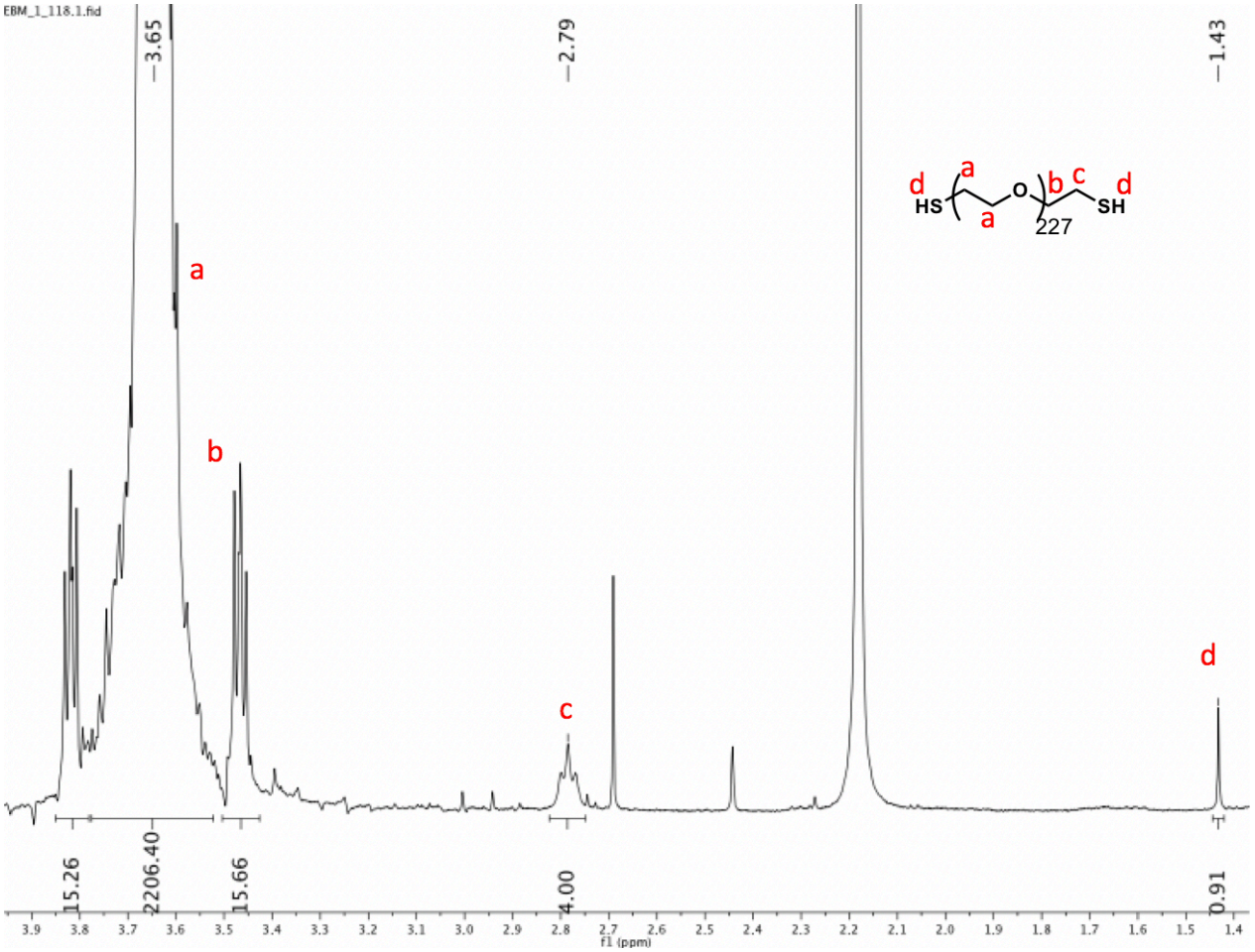

Figure 4A: ^{1}H NMR of PEGdiSH (n = 227 **[7e]**, 10000 g/mol) in deuterated chloroform ($CDCl_3$)

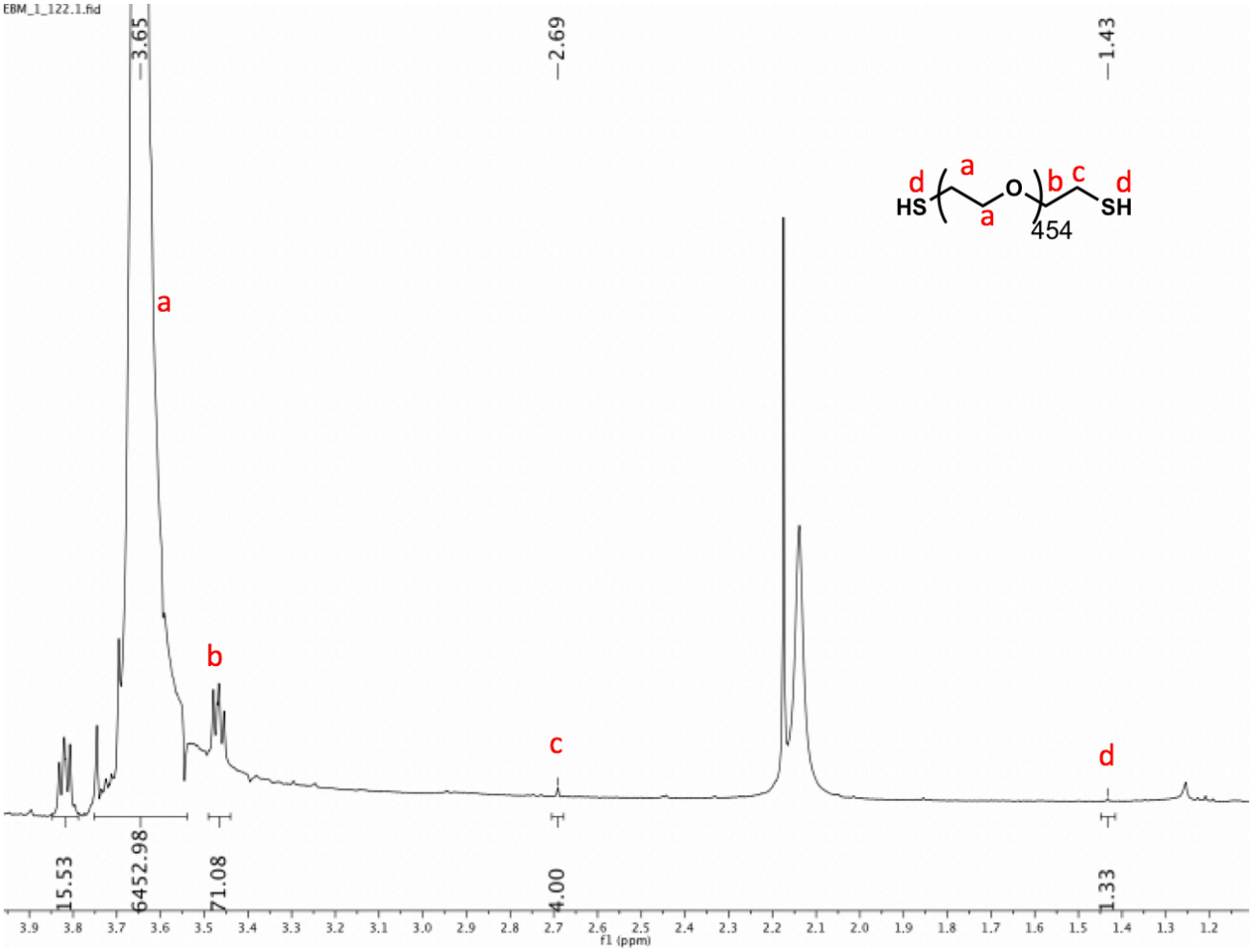

Figure 5A: ^{1}H NMR of PEGdiSH (n = 454 **[7f]**, 20000 g/mol) in deuterated chloroform ($CDCl_3$)

Table 1A: AdSSPEGOMe fluorescence measurements with varying concentration of amphiphile and 0.156 $\mu g/mL$ nile red

[Amphiphile] (μM)	Trial #	$\lambda_{em\,max}$ (nm)	Intensity (CPS)	Avg $\lambda_{em\,max}$ (nm)	Avg Intensity (CPS)
60	1	618	1916830	618	1867717
	2	617	1833120		
	3	619	1853200		
80	1	616	2497720	617	2284580
	2	618	1919240		
	3	616	2436780		
100	1	611	2622970	613	2563893
	2	616	2487530		
	3	612	2581180		
120	1	605	3231220	609	3137913
	2	611	3078210		
	3	611	3104310		
140	1	613	3280050	611	3257833
	2	611	3274040		
	3	610	3219410		
160	1	608	3538580	608	3514243
	2	608	3516570		
	3	609	3487580		
180	1	606	3769400	606	3625443
	2	609	3513960		
	3	603	3592970		
200	1	606	3879300	609	3904533
	2	609	3938560		
	3	612	3895740		
300	1	611	3756220	612	3676017
	2	612	3667560		
	3	612	3604270		
400	1	610	3899340	611	3892133
	2	611	3866450		
	3	611	3910610		
500	1	613	4212220	612	4203663
	2	612	4196020		
	3	612	4202750		

Table 2A: AdSSPEG:βCD-C12 fluorescence measurements with varying concentration of amphiphile and 0.156 $\mu g/mL$ nile red

[Amphiphile] (μM)	Trial #	$\lambda_{em\,max}$ (nm)	Intensity (CPS)	Avg $\lambda_{em\,max}$ (nm)	Avg Intensity (CPS)
20	1	589	2692380	585	2537227
	2	583	2495070		
	3	582	2424230		
25	1	592	3132520	589	3151507
	2	588	3195730		
	3	586	3126270		
30	1	592	3365420	588	3347943
	2	585	3353890		
	3	588	3324520		
35	1	596	3471490	597	3436180
	2	598	3433940		
	3	597	3403110		
40	1	605	3802830	608	3848590
	2	608	3885400		
	3	610	3857540		
45	1	594	3928990	595	3950447
	2	592	3978470		
	3	598	3943880		
50	1	620	4194430	623	4194377
	2	623	4192320		
	3	625	4196380		
55	1	623	4196350	625	4198460
	2	623	4199820		
	3	630	4199210		
60	1	622	4203100	625	4198200
	2	627	4195670		
	3	625	4195830		
80	1	629	4191630	629	4195527
	2	629	4196600		
	3	628	4198350		
100	1	632	4196930	634	4196643
	2	635	4195210		
	3	636	4197790		

Table 3A: AdSSPEG:βCD-C14 fluorescence measurements with varying concentration of amphiphile and 0.156 $\mu g/mL$ nile red

[Amphiphile] (μM)	Trial #	$\lambda_{em\,max}$ (nm)	Intensity (CPS)	Avg $\lambda_{em\,max}$ (nm)	Avg Intensity (CPS)
15	1	596	1773950	596	1810597
	2	599	1816450		
	3	594	1841390		
20	1	599	2330300	594	2290830
	2	598	2314230		
	3	585	2227960		
25	1	600	2683510	598	2587940
	2	595	2538300		
	3	600	2542010		
30	1	606	2673540	607	2669550
	2	609	2650390		
	3	607	2684720		
35	1	610	3187780	611	3093063
	2	614	3049850		
	3	609	3041560		
40	1	611	3219960	615	3266520
	2	619	3371220		
	3	615	3208380		
45	1	626	3454260	628	3453957
	2	628	3457990		
	3	630	3449620		
50	1	629	3457040	628	3454150
	2	631	3452230		
	3	625	3453180		
55	1	632	3455214	631	3454216
	2	630	3452103		
	3	630	3455330		
60	1	628	3455560	627	3453950
	2	629	3450350		
	3	625	3455940		
80	1	630	3454190	629	3455363
	2	632	3455020		
	3	626	3456880		
100	1	628	3456460	629	3455273
	2	626	3453220		
	3	632	3456140		

Table 4A: AdSSPEGOMe:βCD-C12 fluorescence measurements with varying concentration of amphiphile and 0.156 $\mu g/mL$ nile red

[Amphiphile] (μM)	Trial #	$\lambda_{em\,max}$ (nm)	Intensity (CPS)	Avg $\lambda_{em\,max}$ (nm)	Avg Intensity (CPS)
10	1	602	3408420	602	3388790
	2	601	3427360		
	3	602	3330590		
15	1	605	3639430	601	3630130
	2	600	3655010		
	3	598	3595950		
20	1	614	3991630	614	3947913
	2	617	3921670		
	3	612	3930440		
25	1	604	4021960	607	4043417
	2	608	4070560		
	3	608	4037730		
30	1	602	4175370	603	4136443
	2	600	4129650		
	3	607	4104310		
35	1	612	4218940	614	4213830
	2	616	4212240		
	3	615	4210310		
40	1	617	4236910	615	4240427
	2	614	4240600		
	3	615	4243770		
60	1	646	4238920	644	4243220
	2	644	4245160		
	3	643	4245580		
80	1	655	4247980	655	4242870
	2	655	4244910		
	3	655	4235720		
100	1	649	4240510	648	4241117
	2	647	4240730		
	3	647	4242110		

Table 5A: AdSSPEGOMe:βCD-C14 fluorescence measurements with varying concentration of amphiphile and 0.156 $\mu g/mL$ nile red

[Amphiphile] (μM)	Trial #	$\lambda_{em\ max}$ (nm)	Intensity (CPS)	Avg $\lambda_{em\ max}$ (nm)	Avg Intensity (CPS)
10	1	604	2542740	605	2583310
	2	605	2564350		
	3	606	2642840		
15	1	607	2839610	607	2847270
	2	609	2850090		
	3	605	2852110		
20	1	608	3178680	610	3152350
	2	611	3168110		
	3	611	3110260		
25	1	614	3504140	612	3557280
	2	612	3637400		
	3	611	3530300		
30	1	611	4095710	611	4067563
	2	612	4021950		
	3	611	4085030		
35	1	610	4248320	612	4248627
	2	614	4243780		
	3	611	4253780		
40	1	615	4246680	616	4248283
	2	618	4248340		
	3	616	4249830		
60	1	640	4245970	640	4245567
	2	640	4247670		
	3	641	4243060		
80	1	655	4243540	653	4244843
	2	653	4247530		
	3	652	4243460		
100	1	650	4246240	650	4245027
	2	652	4246670		
	3	648	4242170		

Table 6A: Particle size measurements for inclusion complexes and host and guest on their own prepared by probe sonication vesicle isolation method

Sample	Ratio (host:guest)	Time (days)	Hydrodynamic Radius (nm)	%Intensity	%PD
AdSSPEG1000	0 to 1	0	1.522	2.1	40.6
			95.123	97.9	44.2
		1	0.706	2.1	18.6
			11.236	2.2	15.7
AdSSPEG1000OMe	0 to 1	0	6.28	0.9	10.8
			106.642	99.1	106.8
		1	6.03	5.1	8.8
			42.443	60.9	17.6
			187.776	34	16.8
bCD-C12	1 to 0	0	7.097	2.8	11.9
			88.23	76	36.3
			1189.18	18.1	56.2
			19018.2	3.1	43.8
		1	6.827	1.6	11.5
			93.824	54.3	11.7
			503.546	44	12.1
bCD-C14	1 to 0	0	3.912	0.7	0
			9.791	0.7	7.9
			73.922	64.7	21.8
			384.427	33.9	16.3
		1	3.689	1	9.9
			161.629	93.5	85.2
AdSSPEG1000/bCD-C12	1 to 1	0	1.704	2.3	12.8
			107.131	90.4	58.9
			934.781	7.3	30.5
		1	2.239	1.6	19.7
			113.813	98.4	66.1
AdSSPEG1000/bCD-C14	1 to 1	0	1.648	1.8	13.8
			97.53	71.7	52.4
			518.176	26.5	43.9
		1	2.747	1.4	11.9
			33.446	9	17.3
			112.225	81.7	29.1
			1333.97	7.9	20.5
AdSSPEg1000OMe/bCD-C12	1 to 1	0	6.291	4.2	0
			128.431	92.6	98.3
			14920.5	3.2	57.1
		1	3.247	1.9	11.8
			39.506	34.5	37.2
			222.854	63.7	47.5
AdSSPEG1000OME/bCD- C14	1 to 1	0	5.059	2	6.9
			94.234	92.3	23.6
			535.093	5.7	19
		1	6.1	1.4	7.9
			119.979	98.6	18.5

Table 7A: Particle size measurements for inclusion complexes and host and guest on their own prepared by extrusion vesicle isolation method

Sample	Ratio (host:guest)	Time (days)	Hydrodynamic Radius (nm)	%Intensity	%PD
AdSSPEG1000	0 to 1	0	0.569	0.2	19.4
			5.383	0.7	15.6
			70.162	99.2	34.4
		1	5.472	1	11.8
			67.59	86.9	27.1
			296.919	12.1	16.8
AdSSPEG1000OMe	0 to 1	0	3.458	2.5	11.9
			20.406	18.8	16.6
			71.553	78.7	19.7
		1	11.236	11.8	11.9
			59.84	88.2	24
bCD-C12	1 to 0	0	4.29	0.7	11.7
			67.057	99.3	39.7
		1	1.724	0.1	11.8
			8.475	2	10.4
			62.095	94.9	12.6
			430.904	2.9	9.3
bCD-C14	1 to 0	0	1.397	0.1	11
			98.248	96.2	69
			817.548	3.6	29.1
		1	1.929	1.6	3.8
			88.27	91	42.6
			1300.87	7.4	70.9
AdSSPEG1000:bCD-C12	1 to 1	0	5.026	1.3	5.2
			64.357	98.7	32.3
		1	3.5	12	11.8
			95.98	88	11.9
AdSSPEG1000:bCD-C14	1 to 1	0	1.016	0.7	11.4
			13.692	4.9	15.5
			64.336	94.5	28.2
		1	1.349	0.7	12.7
			69.188	99.3	48.5
AdSSPEg1000OMe:bCD-C12	1 to 1	0	9.19	6.9	11.5
			64.121	93.1	32.4
		1	7.803	6.7	6.6
			61.905	93.3	16.8
AdSSPEG1000OMe:bCD- C14	1 to 1	0	5.814	6.6	11
			48.21	93.4	21.2
		1	6.515	7.3	8.8
			51.361	92.7	22.2

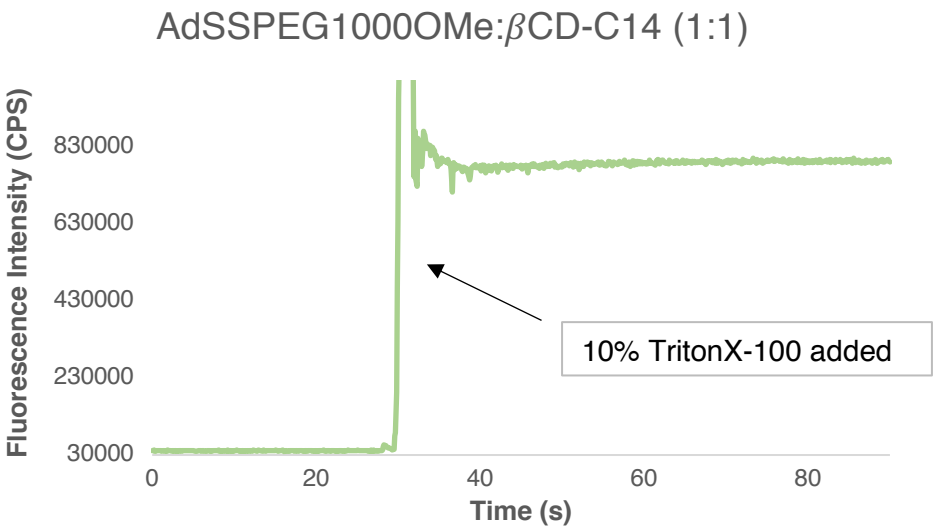

Figure 6A: Initial lysing of AdSSPEGOMe:βCD-C14 inclusion complex measured via fluorescence spectroscopy.. When lysed with 250 µL 10% Triton X-100 there is a large increase in fluorescence intensity which indicates vesicles formed with encapsulated CF

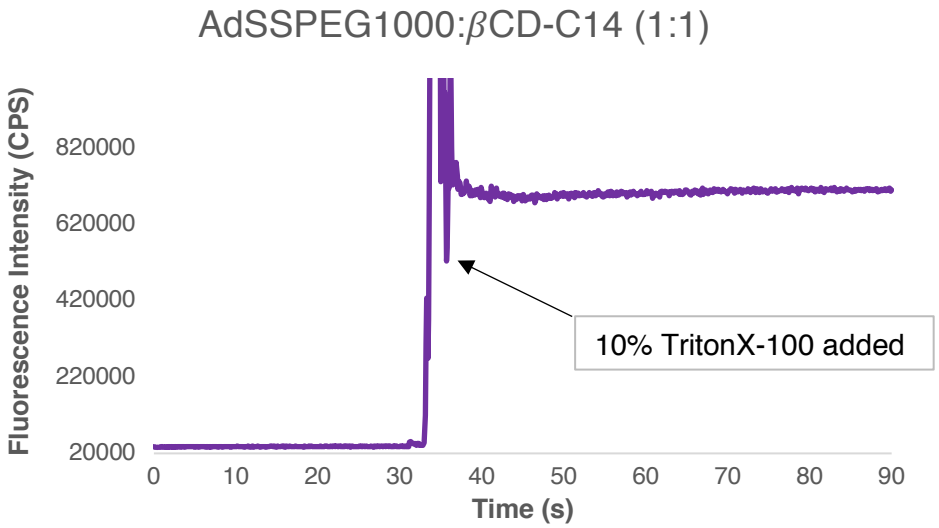

Figure 7A: Initial lysing of AdSSPEG:βCD-C14 inclusion complex measured via fluorescence spectroscopy. When lysed with 250 µL 10% Triton X-100 there is a large increase in fluorescence intensity which indicates vesicles formed with encapsulated CF

*Note – AdSSPEGOMe: βCD-C12 initial lysing measurements can be found on page 106

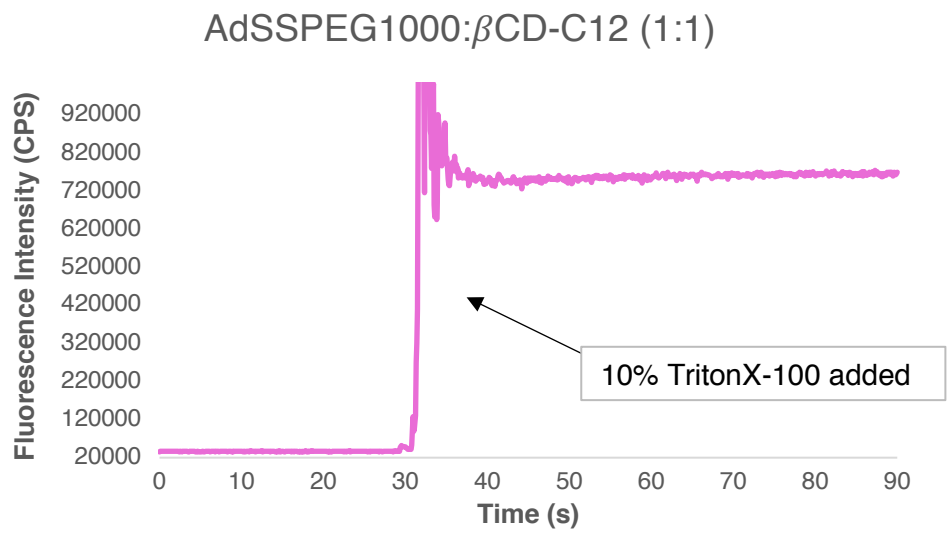

Figure 8A: Initial lysing of AdSSPEG:βCD-C12 inclusion complex measured via fluorescence spectroscopy. When lysed with 250 µL 10% Triton X-100 there is a large increase in fluorescence intensity which indicates vesicles formed with encapsulated CF

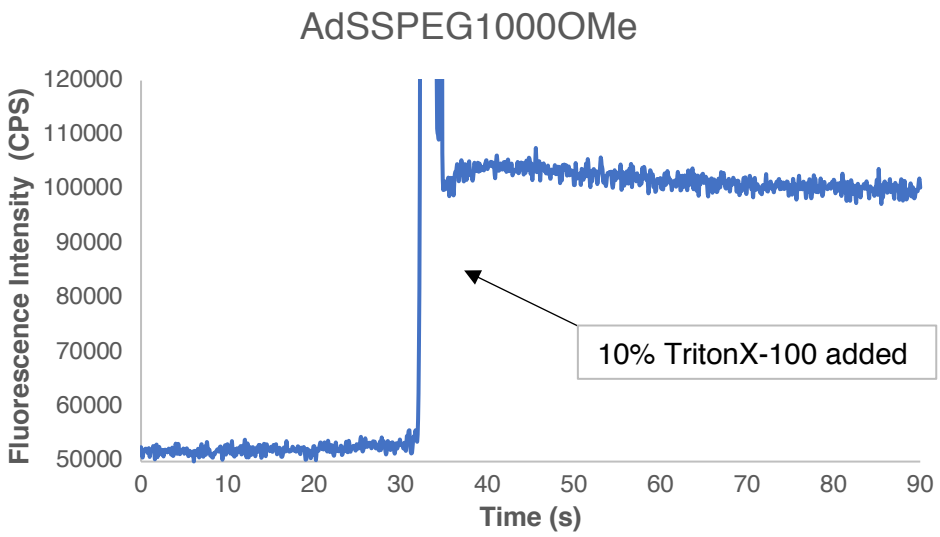

Figure 9A: Initial lysing of AdSSPEGOMe guest measured via fluorescence spectroscopy. When lysed with 250 µL 10% Triton X-100 there is a small increase in fluorescence intensity which indicates vesicles did not form

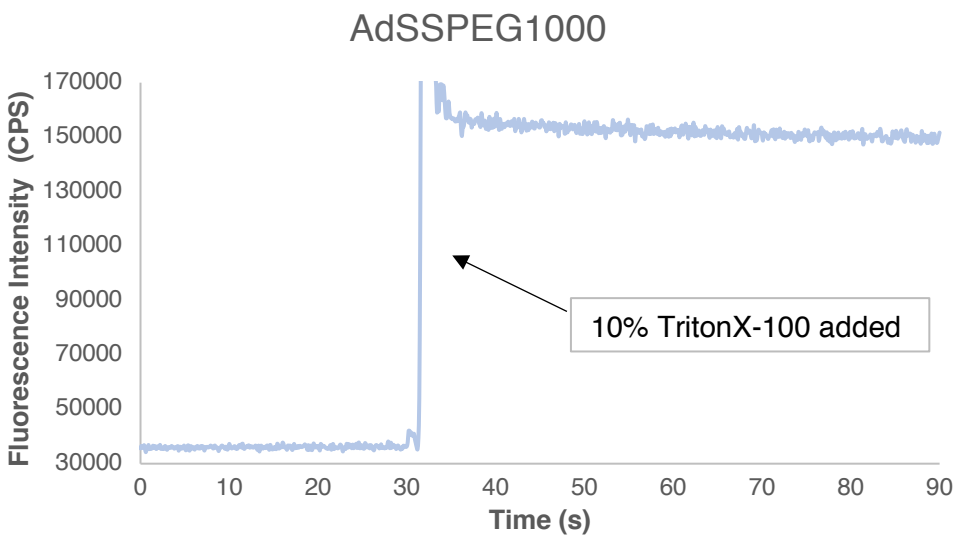

Figure 10A: Initial lysing of AdSSPEG guest measured via fluorescence spectroscopy. When lysed with 250 µL 10% Triton X-100 there is a small increase in fluorescence intensity which indicates vesicles did not form

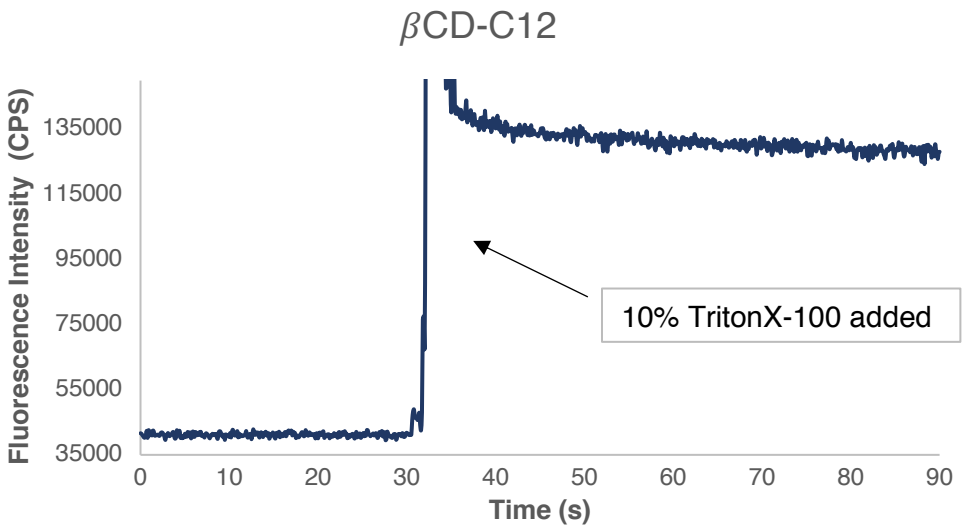

Figure 11A: Initial lysing of βCD-C12 host measured via fluorescence spectroscopy. When lysed with 250 µL 10% Triton X-100 there is a small increase in fluorescence intensity which indicates vesicles did not form

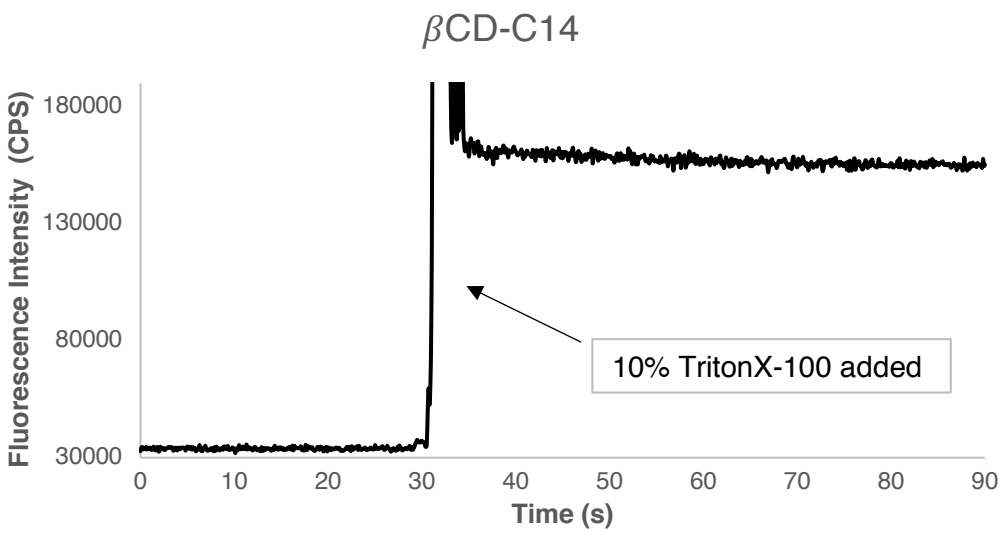

Figure 12A: Initial lysing of βCD-C14 host measured via fluorescence spectroscopy. When lysed with 250 µL 10% Triton X-100 there is a small increase in fluorescence intensity which indicates vesicles did not form

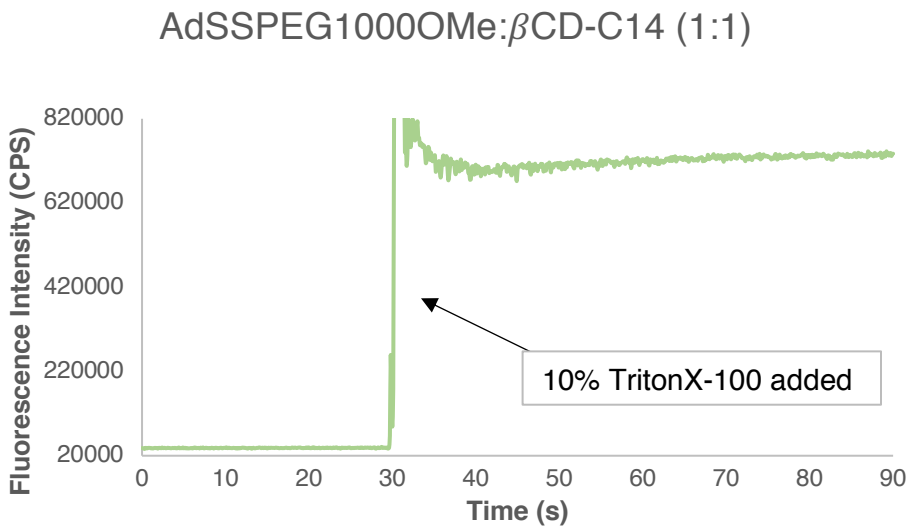

Figure 13A: 1 week lysing of AdSSPEGOMe:βCD-C14 inclusion complex measured via fluorescence spectroscopy is consistent with initial measurements

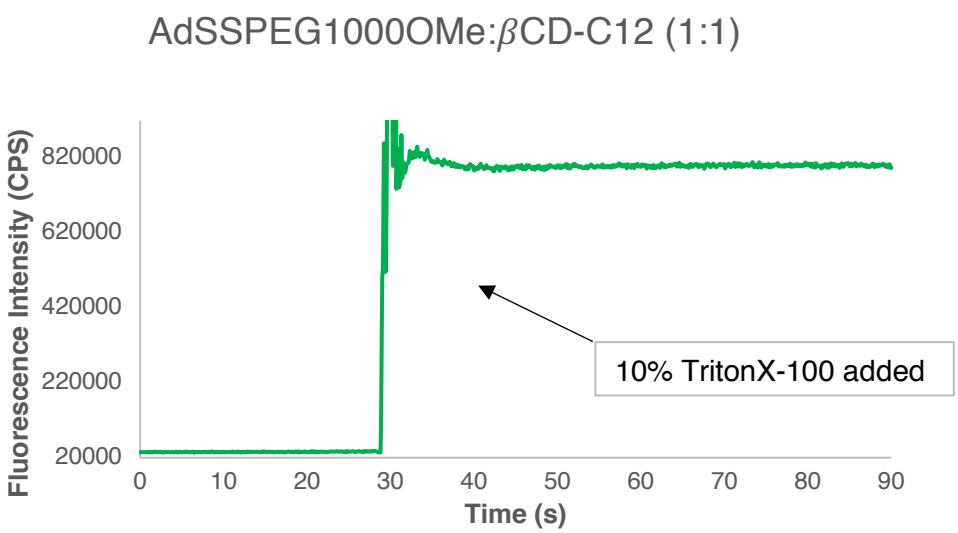

Figure 14A: 1 week lysing of AdSSPEGOMe:βCD-C12 inclusion complex measured via fluorescence spectroscopy is consistent with initial measurements

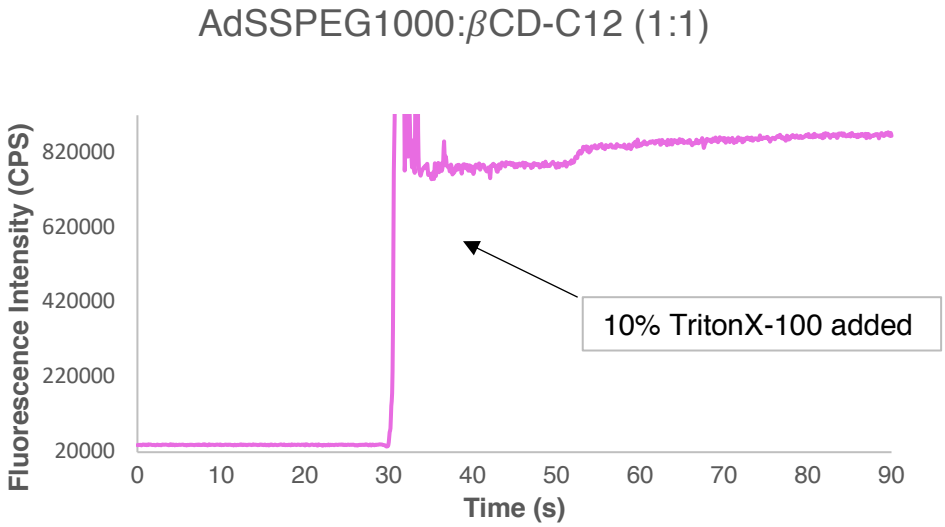

Figure 15A: 1 week lysing of AdSSPEG:βCD-C12 inclusion complex measured via fluorescence spectroscopy is consistent with initial measurements

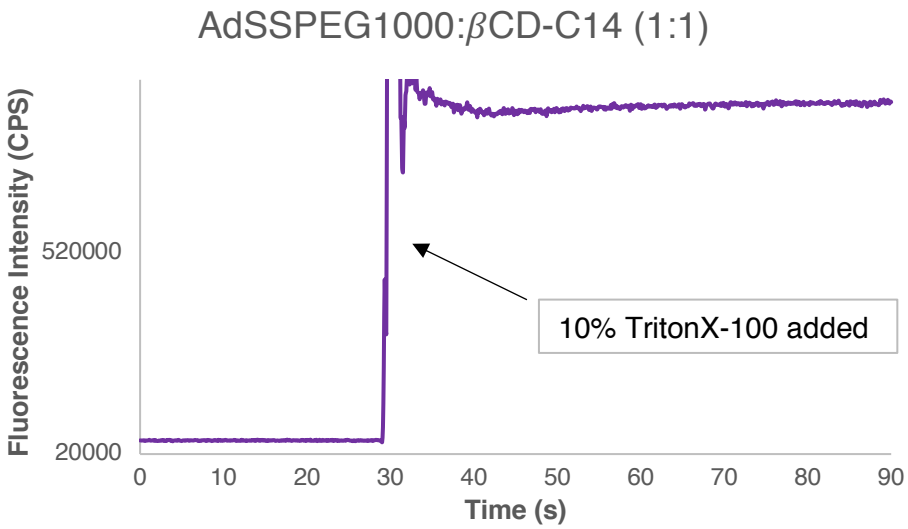

Figure 16A: 1 week lysing of AdSSPEG:βCD-C14 inclusion complex measured via fluorescence spectroscopy is consistent with initial measurements

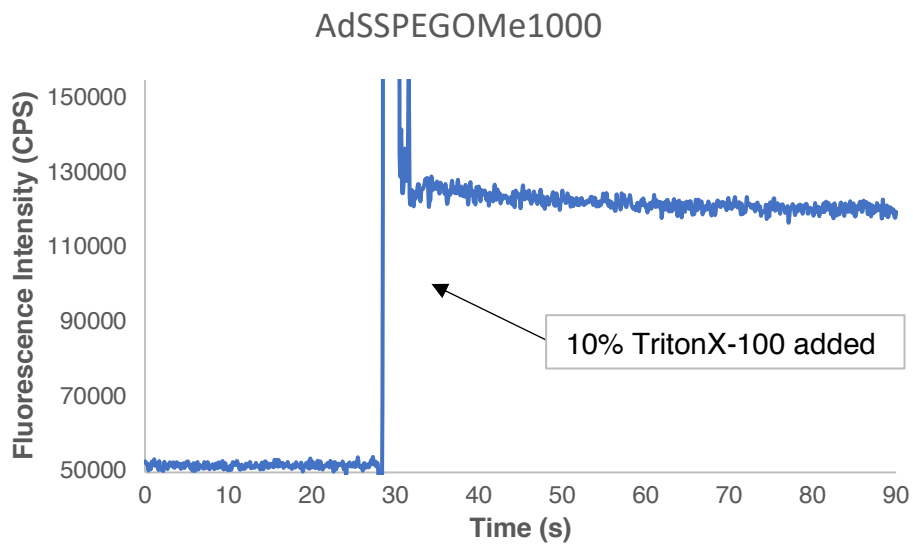

Figure 17A: 1 week lysing of AdSSPEGOMe guest measured via fluorescence spectroscopy is consistent with initial measurements

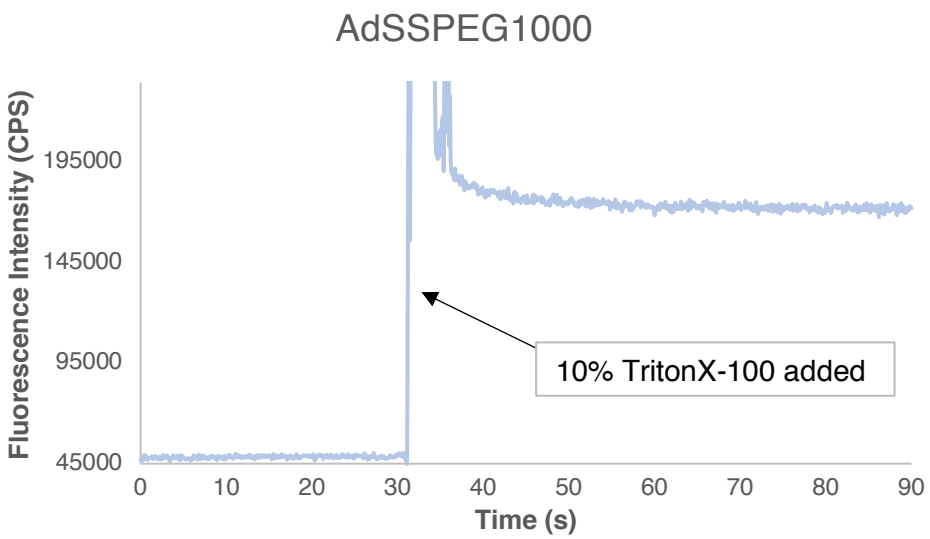

Figure 18A: 1 week lysing of AdSSPEG guest measured via fluorescence spectroscopy is consistent with initial measurements

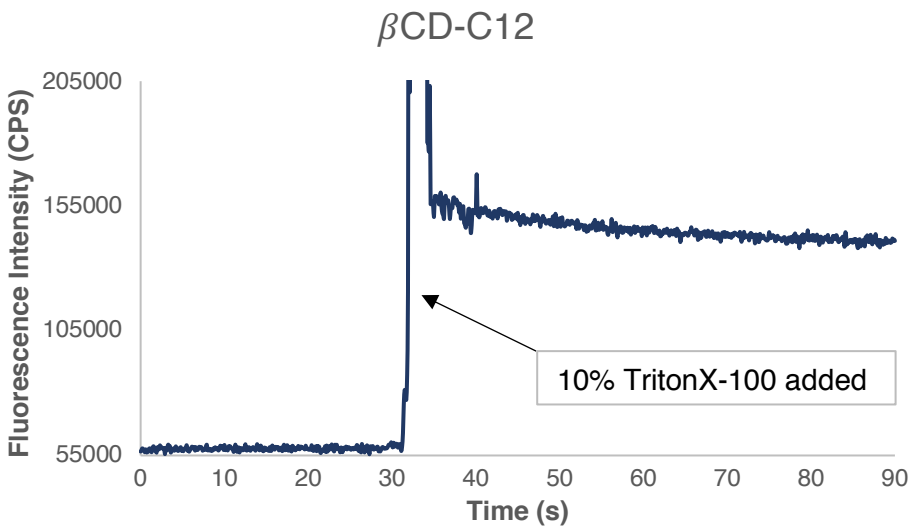

Figure 19A: 1 week lysing of βCD-C12 host measured via fluorescence spectroscopy is consistent with initial measurements

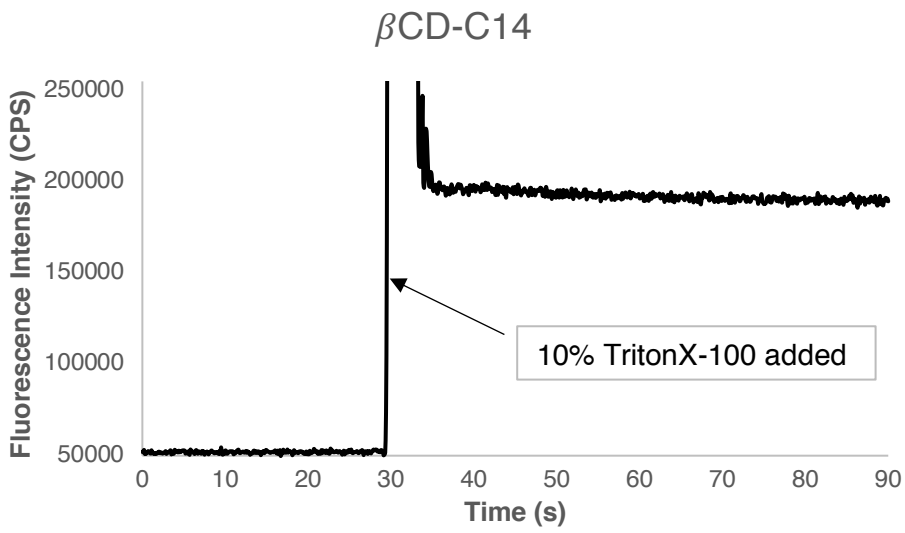

Figure 20A: 1 week lysing of βCD-C14 host measured via fluorescence spectroscopy is consistent with initial measurements

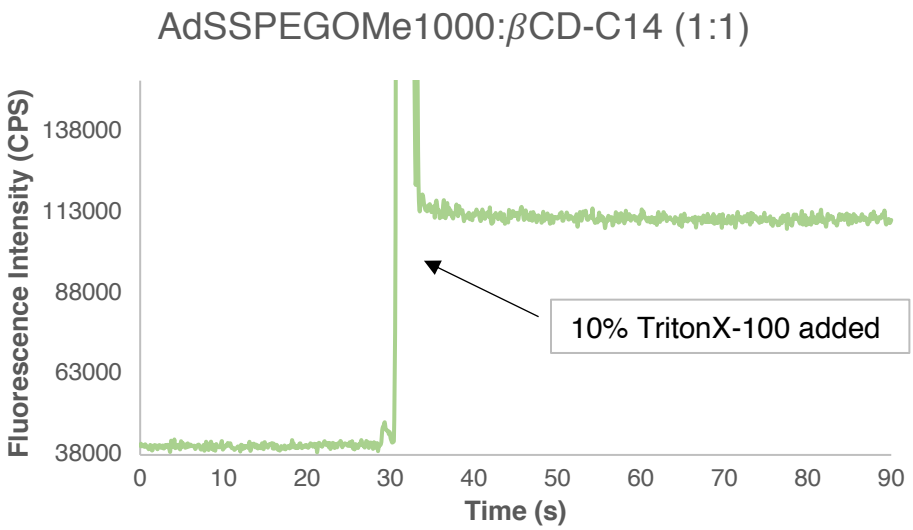

Figure 21A: 2 week lysing of AdSSPEGOMe:βCD-C14 inclusion complex measured via fluorescence spectroscopy. When lysed with 250 µL 10% Triton X-100 there is a small increase in fluorescence intensity which indicates vesicles have degraded

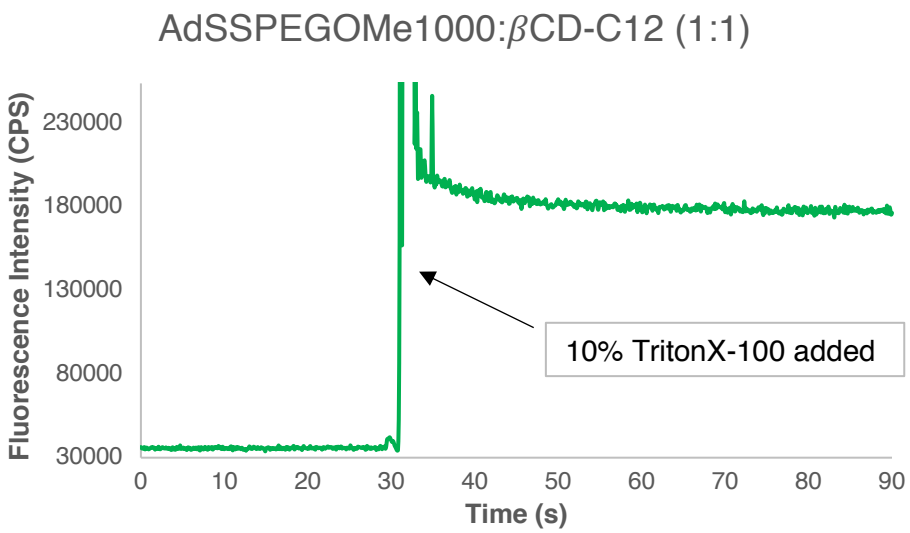

Figure 22A: 2 week lysing of AdSSPEGOMe:βCD-C12 inclusion complex measured via fluorescence spectroscopy. When lysed with 250 µL 10% Triton X-100 there is a small increase in fluorescence intensity which indicates vesicles have degraded

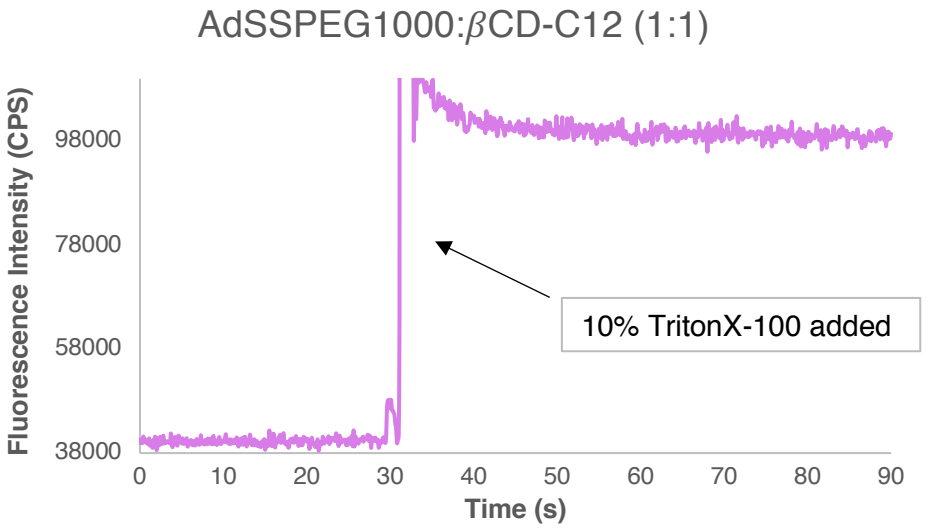

Figure 23A: 2 week lysing of AdSSPEG:βCD-C12 inclusion complex measured via fluorescence spectroscopy. When lysed with 250 µL 10% Triton X-100 there is a small increase in fluorescence intensity which indicates vesicles have degraded

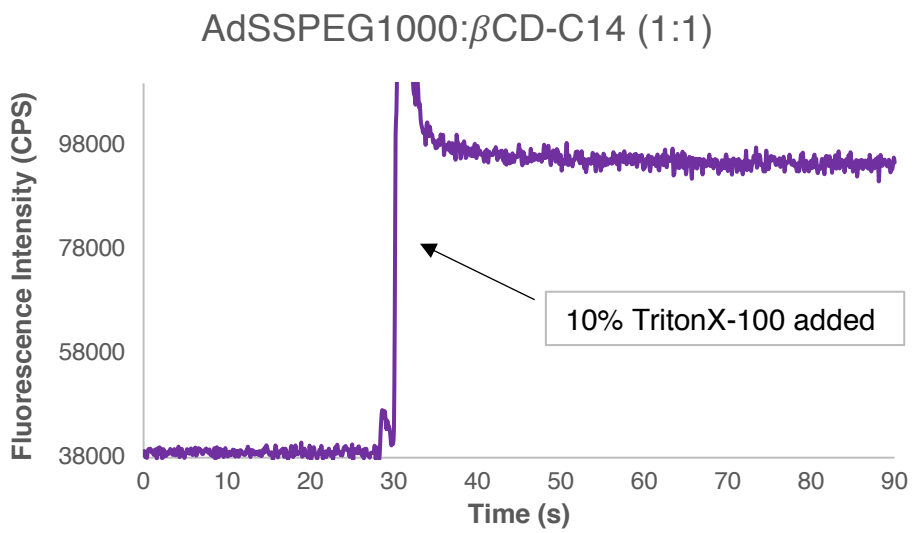

Figure 24A: 2 week lysing of AdSSPEG:βCD-C14 inclusion complex measured via fluorescence spectroscopy. When lysed with 250 µL 10% Triton X-100 there is a small increase in fluorescence intensity which indicates vesicles have degraded

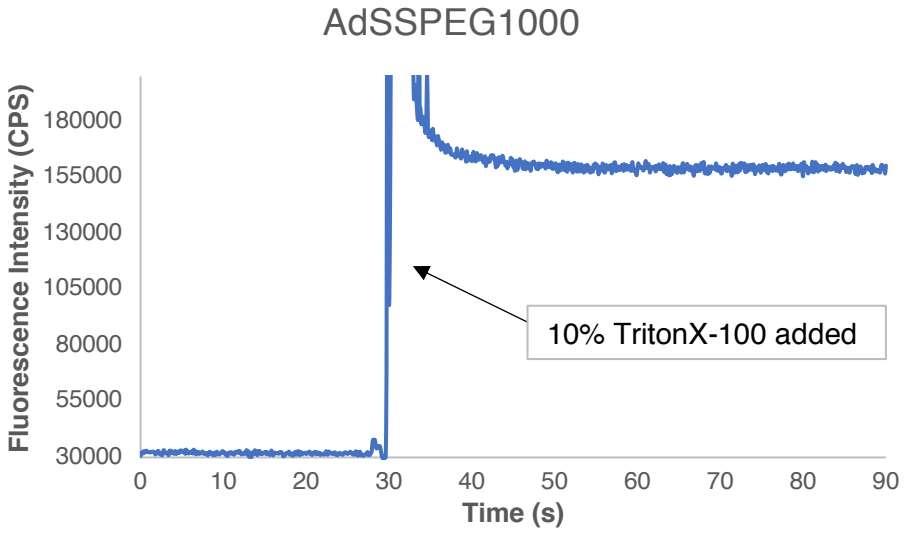

Figure 25A: 2 week lysing of AdSSPEG guest measured via fluorescence spectroscopy is consistent with initial measurements

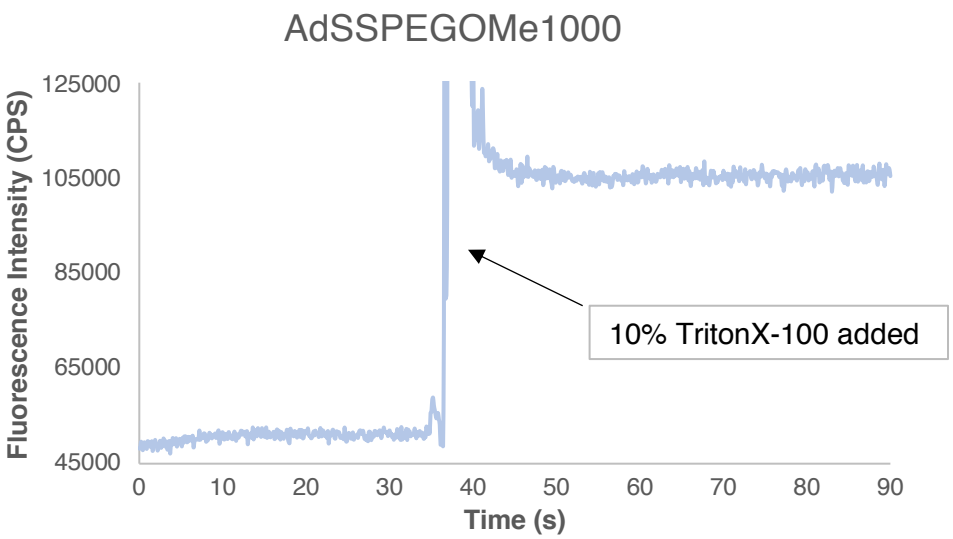

Figure 26A: 2 week lysing of AdSSPEGOMe guest measured via fluorescence spectroscopy is consistent with initial measurements

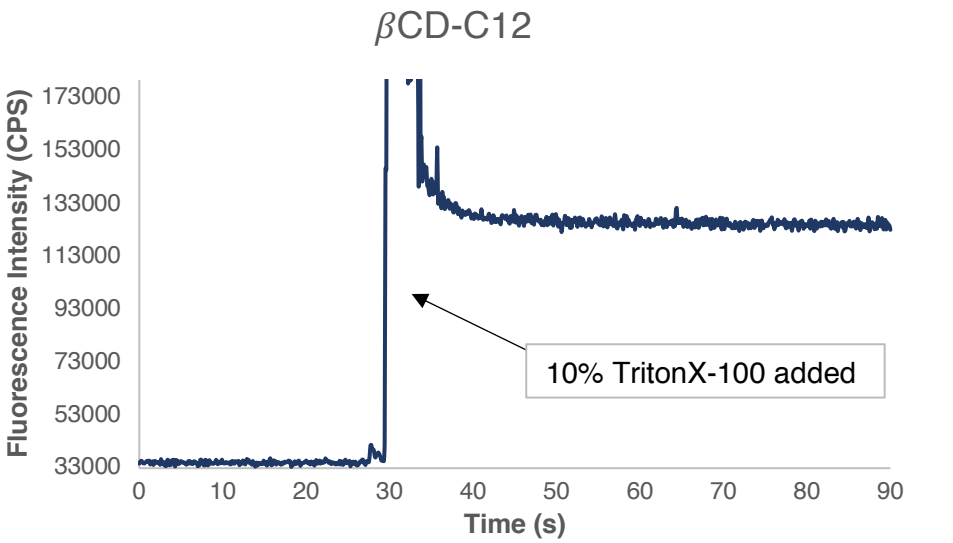

Figure 27A: 2 week lysing of βCD-C12 host measured via fluorescence spectroscopy is consistent with initial measurements

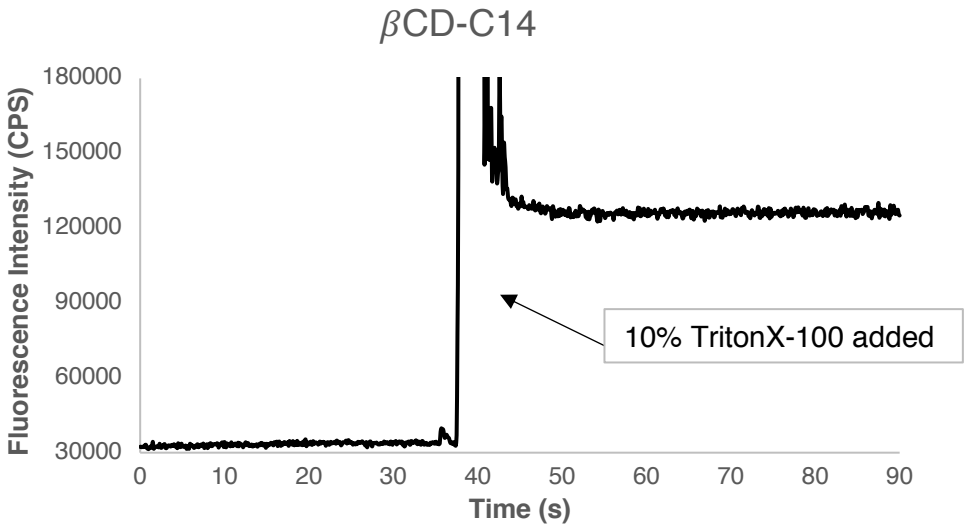

Figure 28A: 2 week lysing of βCD-C14 host measured via fluorescence spectroscopy is consistent with initial measurements

Table 8A: Particle size measurements of vesicles treated with 12 mM GSH to mimic intracellular environments

Sample	Ratio (host:guest)	Time Since GSH Added	Hydrodynamic Radius (nm)	%Intensity	%PD
AdSSPEG1000:βCD-C12	1 to 1	before	5.026	1.3	5.2
			64.357	98.7	32.3
		overnight	0.589	16	55.2
			1159.24	84	330.7
AdSSPEG1000:βCD-C14	1 to 1	before	1.016	0.7	11.4
			13.692	4.9	15.5
			64.336	94.5	28.2
		overnight	0.618	63.8	41.4
			153.649	36.2	67
AdSSPEg1000OMe:βCD-C12	1 to 1	before	9.19	6.9	11.5
			64.121	93.1	32.4
		overnight	2.432	0.7	0
			22.242	24.8	11.3
			77.074	69.8	18.7
			495.931	4.7	8.1
AdSSPEG1000OMe:βCD- C14	1 to 1	before	5.814	6.6	11
			48.21	93.4	21.2
		overnight	0.604	5.3	36.6
			56.458	92.6	87
			905.557	2.2	34.3

Table 9A: Particle size measurements of vesicles treated with 20 μM GSH to mimic extracellular environments

Sample	Ratio (host:guest)	Time Since GSH Added	Hydrodynamic Radius (nm)	%Intensity	%PD
AdSSPEG1000: βCD-C12	1 to 1	before	5.026	1.3	5.2
			64.357	98.7	32.3
		overnight	0.512	0.9	21.7
			95.004	99.1	57.3
AdSSPEG1000: βCD-C14	1 to 1	before	1.016	0.7	11.4
			13.692	4.9	15.5
			64.336	94.5	28.2
		overnight	1.902	9.4	44.3
			59.337	90.6	38.4
AdSSPEG1000OMe: βCD-C12	1 to 1	before	9.19	6.9	11.5
			64.121	93.1	32.4
		overnight	4.563	1.3	11.2
			62.883	98.7	46.3
AdSSPEG1000OMe: βCD-C14	1 to 1	before	5.814	6.6	11
			48.21	93.4	21.2
		overnight	6.09	2.4	20.4
			57.139	97.6	46.3

Table 10A: Particle size measurements of vesicles and PEGdiSH crosslinker [7e] with a molecular weight of 10000 g/mol

Sample	Ratio (host:guest)	Mol Ratio SH/SS	SH % wt	Time Since Crosslinker Added	Hydrodynamic Radius (nm)	%Intensity	%PD
AdSSPEG1000:βCD-C12	1 to 1	1 to 1	20	before	5.026	1.3	5.2
					64.357	98.7	32.3
				overnight	7.43	3.2	10.6
					35.243	9.3	16.2
					99.55	87.4	25.5
AdSSPEG1000:βCD-C14	1 to 1	1 to 1	20	before	1.016	0.7	11.4
					13.692	4.9	15.5
					64.336	94.5	28.2
				overnight	9.56	8	9.8
					72.737	92	19
AdSSPEg1000OMe:βCD-C12	1 to 1	1 to 1	20	before	9.19	6.9	11.5
					64.121	93.1	32.4
				overnight	3.496	1.7	11.8
					107.038	98.3	9.7
AdSSPEG1000OMe:βCD-C14	1 to 1	1 to 1	20	before	5.814	6.6	11
					48.21	93.4	21.2
				overnight	1.487	4.6	5.8
					144.648	85	16.2
					3304.26	10.4	25.4